Non-Invasive Imaging Techniques and Evaluation of Sensory Neuronal Protection by *N*-Acetylcysteine

A thesis submitted to The University of Manchester for the degree of Doctor of Medicine (MD) in the Faculty of Medical and Human Sciences

2011

Alexander E. Hamilton

School of Medicine

LIST OF CONTENTS

WORD COUNT: 51,457

LIST OF FIGURES

LIST OF TABLES

ABSTRACT

Abstract of thesis submitted by Alexander Euan Hamilton for the degree of Doctor of Medicine (MD) to the University of Manchester and entitled **Non-Invasive Imaging Techniques and Evaluation of Sensory Neuronal Protection by *N*-acetylcysteine**, September 2010.

Background & Objectives

The potential benefits of adjuvant pharmacotherapy with *N*-acetylcysteine and acetyl-*L*-carnitine to reduce the amount of primary sensory neurons in the dorsal root ganglion (DRG) which die by apoptosis after peripheral nerve injury has been previously established. However, the duration of NAC therapy sufficient to achieve neuroprotection is unknown. Establishment of clinical trials of NAC/ALCAR therapy is hindered by relatively poor existing methods of assessment of neuronal populations and nerve regeneration in human subjects. Magnetic Resonance Imaging (MRI), a non-invasive modality, has been demonstrated in a pilot study to provide volumetric analysis of rat L4 DRG after sciatic nerve transection; detecting DRG volume reductions which reflect neuronal loss. Further, MRI has been reported to detect changes occurring in peripheral nerves distal to the site of injury, corresponding to axonal degeneration and subsequent regeneration. High Frequency Ultrasound (HFUS) is a new, high resolution imaging modality, not previously applied to the study of animal or human peripheral nervous system.

Experiments were designed to test the duration of NAC treatment needed to achieve a neuroprotectant effect; to further evaluate the MRI DRG imaging protocol under interventional experimental conditions and *in vivo;* to investigate the ability of MRI and HFUS to visualise murine sciatic nerve and its response to injury and to assess the ability of HFUS to visualise human digital nerves in the hand. Further, a pilot study investigating the effect of NAC and ALCAR on primary sensory neurons in tissue culture was carried out to assess the neurotrophic effect of these agents *in vitro*.

Methods

1. Groups of rats underwent sciatic nerve transection, and NAC treatment for 7, 14, 30 or 60 days. At 60 days post injury neuron counts from L4 and L5 DRG were assessed histologically using a stereological optical fractionator analysis, and compared to the contralateral no*N-a*xotomised DRG.
2. Animals from treatment groups were MRI scanned after two months to measure the L4 DRG volume bilaterally. A single animal was also scanned under anæsthesia and after death.
3. Numerous MRI techniques were used to scan rats after sciatic nerve crush, division and intraneural injection of contrast, attempting to identify the nerve and its response to injury.
4. Normal and injured rat sciatic nerve and intact human digital nerve were assessed by HFUS.
5. Cultured DRG neurons were exposed to a range of ALCAR/NAC doses or NGF, with assessment of cell survival and neurite formation at 24h.

Results

1. Neuronal death was related to duration of NAC treatment; with losses of 20%, 9%, 4% & 0% after treatment for 7, 14, 30 and 60 days respectively.
2. MR measured L4 DRG volume reduction correlated well with neuron loss. *In vivo* MRI scanning is feasible; however images are subject to motion artefact distortion, precluding accurate quantification.
3. The rat sciatic nerve could not reliably and consistently be identified by MRI in this model.
4. High frequency ultrasound can image sciatic nerve and its branches and human digital nerve with good resolution and can detect neurotmesis and axonotmesis grade injurys.
5. Non-toxic *in vitro* NAC/ALCAR dosage regimens have been defined, but do not affect neuron survival or neuritogenesis in the absence of NGF.

Conclusions

1. One month treatment with NAC post neurotomy prevents death of the majority of axotomised neurons. Apoptosis is prevented rather than delayed for some neuronal populations by NAC treatment.
2. MRI is a valuable objective tool, and DRG volume serves as a proxy measure of neuronal loss, fit for translation to human studies.
3. *In vivo* MRI DRG imaging requires motion compensation techniques such as respiratory gaiting.
4. Further investigation is needed to facilitate murine sciatic nerve imaging with MRI in this model, but HFUS easily demonstrates two grades of peripheral nerve injury, and is proposed for investigation of human digital nerve trauma.
5. The neuroprotective and regenerative effects of NAC/ALCAR on primary sensory neurons *in vivo* can not be replicated by direct treatment of isolated neurons in culture.

AUTHOR DECLARATION

No portion of the work referred to in the thesis has been submitted in support of an application for another degree or qualification of this or any other university or other institute of learning.

Signed ……. Date…….

COPYRIGHT STATEMENT

i. The author of this thesis (including any appendices and/or schedules to this thesis) owns certain copyright or related rights in it (the "Copyright") and s/he has given The University of Manchester certain rights to use such Copyright, including for administrative purposes.

ii. Copies of this thesis, either in full or in extracts and whether in hard or electronic copy, may be made **only** in accordance with the Copyright, Designs and Patents Act 1988 (as amended) and regulations issued under it or, where appropriate, in accordance with licensing agreements which the University has from time to time. This page must form part of any such copies made.

iii. The ownership of certain Copyright, patents, designs, trademarks and other intellectual property (the "Intellectual Property") and any reproductions of copyright works in the thesis, for example graphs and tables ("Reproductions"), which may be described in this thesis, may not be owned by the author and may be owned by third parties. Such Intellectual Property and Reproductions cannot and must not be made available for use without the prior written permission of the owner(s) of the relevant Intellectual Property and/or Reproductions.

iv. Further information on the conditions under which disclosure, publication and commercialisation of this thesis, the Copyright and any Intellectual Property and/or Reproductions described in it may take place is available in the University IP Policy (seehttp://www.campus.manchester.ac.uk/medialibrary/policies/intellectual-property.pdf), in any relevant Thesis restriction declarations deposited in the University Library, The University Library's regulations (http://www.manchester.ac.uk/library/aboutus /regulations) and in The University's policy on presentation of Theses

ACKNOWLEDGEMENTS

All work presented in this thesis was carried out between the Blond-McIndoe Laboratories and the Department of Imaging Science & Biomedical Engineering at the University of Manchester, UK, the Department of Surgical and Perioperative Science (Section for Hand and Plastic Surgery) University Hospital, Umeå and the Department of Integrative Medical Biology (Section for Anatomy) Umeå University, Sweden.

I am grateful for the funding provided by the Foyle Foundation, the Swedish Medical Research Council, The County of Vasterbotten and Josef Aner's Foundation.

Thank you to my supervisors, Giorgio Terenghi and Mikael Wiberg and advisor, David Tomlinson, for their guidance, encouragement and patientce, and to Andy Hart for steering me towards this reseach. I am grateful to Steve Williams and Karen Davies for their technical advice and assistance in the MRI studies.

Thanks also to Christina Mantovani, Paul Kingham, Natalie Gardiner and everyone else in both the Manchester and Umeå labs for constantly being available and providing advice on every aspect of my research - teaching science to a surgeon. To Adam, Rob, Paul and Chris for their social support, to the kind folk of Umeå who both helped me 'furnish' the space beneath the microscope and tactfully ignored my singing; and to Alecz and Glenn for putting up with me for months in their flat.

Finally, thank you to my wife for her constant support, patience and making everything alright; and to my son, Aiden whose birth may have slowed this work, but who makes the world a better place (Dagga!).

LIST OF COMMON ABBREVIATIONS

2D	Two Dimensional
2PD	Two Point Discrimination
3D	Three Dimensional
AIF	Apoptosis Inhibitory Factor
ALCAR	Acetyl-*L*-carnitine
ANOVA	Analysis of variance.
APAF	apoptosis protease activating factor
Atk	Agammaglobulinæmia Tyrosine Kinase
ATP	Adenosine Triphosphate
BAK	BCL2 agonist killer 1
BAX	B-cell lymphoma 2-associated protein X
BCl-2	B-Cell Leukæmia - 2
BDNF	Brain Derived Neurotrophic Factor
cAMP	Cyclic Adenosine Monphosphate
CGRP	Calcitonin Gene Related Peptide
CMAP	Compound Motor Action Potential
CNTF	Ciliary Neurotrophic Factor
CoA	Coenzyme A
CyC	Cytochrome C
DNA	Deoxyribose Nucleic Acid
DRG	Dorsal Root Ganglia
ECM	Extracellular Matrix
EMG	Electromyography / Electromyogram
ERK	Extracellular-signal-regulated kinase
FG	Flouro-gold
FLAIR	Fluid attenuated inversion recovery
FLASH	Fast Low Angle Shot
$FR^{\bullet}$	Free Radical
GAP-43	Growth Associated Protein - 43
GDNF	Glial Derived Growth Factor
GGF	Glial Growth Factor
H_2O_2	Hydrogen Peroxide
IFN	Interferon
IL 10	Interleukin 10
IL 18	Interleukin 18
IL 1β	Interleukin 1B
IL 6	Interleukin 6
IMM	Inner Mitochondrial Membrane
IP	Intraperitoneal
ISEL	*In situ* End Labelling
IT	Intrathecal
JNK	c-jun N-terminal Kinase
LIF	Leukaemia Inhibitory Factor
MAPK	Mitogen Associated Protein Kinase
MDP	Myelin Degradation Products
MMP	Mitochondrial Membrane Permeabilisation

MRI	Magnetic Resonance Imaging
mRNA	Messenger Ribonucleic acid
NAC	*N*-acetylcysteine
NGF	Nerve Growth Factor
NMR	Nuclear Magnetic Resonance
$NO^{\bullet}$	Nitric Oxide
NOS	Nitric Oxide Synthetase
NPY	Neuropeptide Y
NT3	Neurotrophin 3
NTF	Neurotrophic Factor
OMM	Outer Mitochondrial Membrane
ONOO	Peroxynitrate
PAMNF	Panaxonal Marker of Neurofilament
PI3K	Phosphatidylinositol 3-Phosphate
PKC	Protein Kinase C
POD	Postoperative Day
Ras	Rat Sarcoma
RF	Radio frequency
ROS	Reactive Oxygen Species
SC	Schwann Cell
SFI	Sciatic Functional Index
Smac/DIABLO	Second Mitochondrial-Derived Activator of Caspases and the Drosophila Melanogaster Homologue
SNR	Signal to Noise Ratio
STIR	Short Tau Inversion Recovery
TB	True-blue
TdT	terminal deoxyribonucleotidyl transferase
TE	Time to Echo
TNF-α	Tumour Necrosis Factor
TR	Time to Repeat
TRIM	Turbo Inversion Recovery
Trk	Tyrosine Kinase
TUNEL	TdT Nick End Labelling
VIP	Vasoactive Inhibitory peptide
WD	Wallarian Degeneration

CHAPTER 1

Introduction & Literature Review

1.1 INTRODUCTION

Over recent years the novel paradigm of pharmacotherapy to reduce the number of neurons that die as a result of nerve division has been internationally recognised as having the possibility to improve patient outcome after nerve injury (Hart *et al.*, 2008). However, before any human studies could be performed with any scientific rigour an objective method of assessing nerve cell death, regeneration and neuroprotection in live subjects must be established, as current clinical assessment is suboptimal (Jerosch-Herold, 2005).

It has been proposed that magnetic resonance imaging (MRI) could act as a painless, non-invasive, non-irradiating technique (International Commission on Non-Ionizing Radiation Protection 2004) of assessing events within the sensory dorsal root ganglion (DRG) and in degenerating or regenerating nerve fibres, and could lead to a clinically useful, objective means of surveillance of the response to neuroprotective agents, nerve regeneration and target organ reinervation.

Initially this review will discuss nerve injury both as a clinical entity and a neurobiological phenomenon, nerve cell death post-axotomy, the evidence for neuroprotective agents and some of the proposed mechanisms of their actions. Secondly, the role of MRI neurography, and its potential use in the next part of the neuroprotection story will be considered.

1.2 NERVE INJURY, NEURON DEATH AND NEUROPROTECTION

1.2.1 NERVE INJURY

Peripheral nerve trauma is common, with an incidence of 1:1000, or 300,000 cases per year in Europe. At present, despite the techniques of microneural repair being perfected over the last thirty years, such injuries still do not have an encouraging outcome (Lundborg 2000; Kline, 2000). Recovery of sensory function is always impaired (Glickman & Mackinnon, 1990) reflecting reduced cutaneous innervation (Weiberg *et al.,* 2003). Although restoration of gross motor function is more encouraging (Hoang, 2006), fine movement such as the precision grip and manipulative work is impaired, possibly due to lack of sensory feedback and proprioception (Westling & Johansson, 1984; Schenker *et al.*, 2006).

The prolonged, often painful, unpredictable and frustrating path towards only partial sensorimotor restitution has a profound impact on the quality of life of patients (Dagnum 1998), but also a significant socioeconomic impact for society as the estimated healthcare cost to treat and rehabilitate a patient with a median nerve injury is around £47,000 – regardless of the eventual outcome (Rosberg *et al.,* 2005). Further, many people involved in upper limb trauma are young workers in industry or agriculture and 50% of patients who sustain a major upper limb injury never return to work (Jaquet *et al.,* 2001).

The current bleak prognosis for functional sensory-motor recovery is multifactorial, and reflects the fact that axonal injury not only directly damages the involved neurons but initiates a profound pathophysiological cascade involving all parts of the CNS/PNS/target organ axis (Lundborg, 2000). Amongst the implicated issues are the slow rate of

neurite/axonal regeneration; the particularly difficult hurdle for tens of thousands of neurites crossing the site of injury/repair and ongoing re-growth; entry into the correct endoneural tubes to reach appropriate targets (skeletal muscle or skin sensory organs) and the response of these target organs to prolonged denervation, such as muscle atrophy (Gordon *et al.,* 2003). Further, the brain's dynamic and adaptive somatotopic mapping of the motor and sensory areas in the pre-, and post-central gyri as well as sub-cortical areas may hinder functional recovery if the delay before re-innervation is substantial (Lundborg & Richard, 2003).

Finally, and of significant interest to this study, only neurons that survive the initial injury and subsequent repair/regeneration events are able to participate in functional re-innervation (Fu & Gordon, 1997). Important in sensory perception is the number of innervating neurons and the size and overlap of their receptive field – so called innervation density (Kelly *et al.,* 2005). Therefore reduction in the surviving pool of damaged nerve cells is likely to be a major contributing factor to poor recovery. Experimental models of peripheral nerve injury demonstrate death of up to 50% of primary sensory neurons in the dorsal root ganglion (DRG) depending on the experimental model (Arvidsson *et al.,* 1986; Cheema *et al.,* 1994a & b; Degn *et al.,* 1999; Ekstrom, 1995; Groves *et al.,* 1997; Himes & Tessler, 1989; Liss *et al.,* 1994; Liss *et al.,* 1996; Ljungberg *et al.,* 1999; McKay Hart *et al.,* 2002a; Ranson 1909; Rich *et al.,* 1987; Rich *et al.,* 1989; Tandrup *et al.,* 2000; Ygge 1989), and ≈60% of motor neuron cell bodies in the ventral horn of the spinal cord after spinal root injury (Koliastos *et al.,* 1994; Novikov *et al.,* 1997). Similar magnitude of sensory neuronal loss was seen in one of few post-mortem human studies of amputees (Suzuki *et al.,* 1993).

Critically, neuronal cells do not die as a result of traumatic necrosis at the time of injury, but in a controlled fashion by apoptosis over a two-month period (Ma *et al.,* 2001; McKay Hart *et al.,* 2002a). There exists clearly, an opportunity to improve functional outcome of nerve injury if this controlled cell death can be prevented by the neuroprotective agents.

1.2.2 NEUROBIOLOGY OF NERVE INJURY AND REGENERATION

To understand some of the MRI signal changes that occur after nerve injury, it is necessary to review briefly the cellular events that occur after axotomy of peripheral nerves. These processes can be artificially segregated into events at the neuron cell body and proximal nerve stump; events at the distal nerve stump, representing Wallerian Degeneration (WD) and Schwann cell and immune cell activity; and the process of regeneration of surviving neurons.

1.2.2.1 Proximal stump

Axotomy induces a phenotypic change in peripheral neurons, differentiated functions being sacrificed as the cell enters a 'growth mode', and an axon regeneration program is entered (Snider *et al.,* 2002; Skein, 1989). Early signalling events initiating this process include antedromal electrical activity stimulated by the contact of extruding axoplasm with the extracellular milieu (Ambron & Walters, 1996). Retrograde transport of *some* signalling factor occurs by the 'importin' system (Blesch & Tuszynski, 2004), this is subsequently re-enforced by neurotoxic cytokines (e.g. TNF-α) produced by macrophages (Stoll *et al.,* 1989), and LIF from Schwann cells (Curtis *et al.,* 1994; Murphy *et al.,* 1997) as part of the neuroinflammatory reaction. Neurolemmal disruption is repaired in a Ca^{2+} and calpain dependant process of cytoskeletal rearrangement, which is faster in small fibres (Howard *et al.,* 1999). The axon then degenerates proximally until the first node of Ranvier, creating a small area of WD in the proximal stump (Terenghi, 1999).

Axonal transport is both disrupted and modified as a result of injury, with up-regulation of axoplasmic transport motor element expression (kinesin light chain and dynein) (Tonra *et al.*, 1998). Neurotrophic factors produced by Schwann cell in the distal stump diffuse across the injury site and are subsequently retrogradely transported in proximal axons, and NGF, GDNF, NT3, BDNF, LIF and CNTF are distributed differentially to fibres of differing diameters (Terenghi, 1999).

Cell bodies of axotomised neurons undergo changes of chromatolysis, involving somatic and nuclear shrinking, Nissl body displacement, nuclear peripheralisation, central process retraction and accumulation of active mitochondria within the perikaryon. Notably, a small population of cells do not adopt this morphology, but become enlarged and vacuolated (Groves *et al.*, 1997). These cells had been attributed a regenerative role; however they have more recently been demonstrated to die (McKay Hart *et al.*, 2002a).

1.2.2.2 Distal stump after acute injury

The purpose of the events in the distal nerve stump are to remove injured tissue, and axon growth inhibiting myelin (Küry *et al.*, 2001). After nerve division there is bleeding into the transaction site from the *vasa nervosa* and accompanied surrounding tissue injury. The elastic neural tissue retracts and axoplasm pouts from the cut ends. A complex neuroinflammatory reaction ensues, synchronous with the events of WD (Stoll *et al.*, 2002).

The axons in the distal stump detach from their myelin sheath, and degenerate by Ca^{2+} and axonal protease dependant mechanism (George *et al.*, 1995), which is complete by 24-48 hours post injury dependant on axon diameter (Stoll *et al.*, 1989). T-cells and macrophages infiltrate the lesion site at around day 2, spread to the whole distal stump by

day 4, (Stoll *et al.,* 1989a; Stoll & Jander, 1999) and peak at day 5 (Lazar *et al.,* 1999). The axonal debris and myelin sheaths are degenerated and phagocytosed by macrophages and activated Schwann cells (Renolds *et al.,* 1993; Terenghi, 1999). This macrophage led clearance of myelin debris is a prerequisite for neurite ingrowth, because myelin associated glycoprotein and other myelin degradation products (MDPs) factors will inhibit this process. Clearance of all MDPs takes about one month (You *et al.,* 1997).

Schwann cells de-differentiate and proliferate under control of macrophage signalling and MDPs (Terenghi, 1999) and loss of contact with axons (Renolds & Woolf 1993). These cells detach from the endoneural sheath, dowN-regulate protein synthesis, fragment their myelin sheath and divide to form the bands of Büngner; solid columns within basal lamina tubes which act as guidance cues for ingressing neurites (Stoll *et al.,* 1989a; Liu *et al.,* 1995; Terenghi, 1999).

1.2.2.3 Distal stump and chronic denervation

The events of WD are to promote nerve regeneration, but if this is prevented or not possible, more chronic changes occur in the distal stump. Schwann cells loose their responsiveness to Glial Growth Factor 2-6 months after denervation, although they are still able to myelinate axons during this time, cease to express p75 receptor at 3 months, progressively loose expression of the erb-receptor for neuregulin and finally will atrophy and die by apoptosis if denervation is prolonged (Li *et al.,* 1997; Terenghi, 1999; Gordon *et al.,* 2003). Beginning with the neuroinflammatory response fibrin deposition and scarring occur, endoneural tubes fibrosis begins at 28-35 days post injury, narrowing these tubes until they have only 1% of their original diameter by 2 years in man.

Sensory organs atrophy after prolonged denervation, Merkel's discs disappear by 35 days in cats (Liss *et al.,* 1994), Meissners corpuscles after 6 months and Panacinian corpuscles survive for 10 months in the rat (Zelena, 1982). After muscled de-afferentation irreversible loss of muscle mass and destruction of motor end plates occurs by 1m post injury, and is associated with muscle fibre expression of apoptotic genes (Kobayashi *et al.,* 1997; Tews *et al.,* 1997; Lee *et al.,* 2000). More recently however, the reason for this loss of mass has been demonstrated to be partly due to the reduced number of regenerating axons available for reinervation, and depletion of intramuscular satellite cells, which limits the potential for hypertrophy (Gordon *et al.,* 2003).

1.2.2.4 Nerve regeneration and the role of growth factors in axonal outgrowth.

If divided nerve stumps are brought together by nerve repair, grafting or conduit axons will begin a regenerative program 3-14 days after injury (Fu & Gordon, 1997; Terenghi, 1999). Axonal progression through the injury site and into the distal stump is slow, corresponding to the rate of slow axonal transport (Fu & Gordon, 1997), and averages ≈1mm/d, being 0.25mm/d to cross the gap, and progressing at 1-8.5mm/d distally, with the rate being inversely proportional to distance from the soma (Green, 1998). It is estimated that this would represent 800 days (over two years) for a brachial plexus lesion in an adult (Gordon *et al.,* 2003). Axon survival and progression is dependent on contact guidance (Tonge *et al.,* 1996; Tonge *et al.,* 1997) mediated by integrin coupling (Schoenwaelder & Burwidge, 1999) and NTFs (Terenghi, 1999; Lundborg, 2000), both of which are supplied by activated Schwann cells.

NTF signalling from Schwann cells and target organs to ingrowing axons has been extensively studied. Members of the neurotrophin family have a two receptor system (Sutter *et al.,* 1979; Bothwell, 1991; Kaplan & Miller, 2000) which includes a high-affinity

specific tyrosine kinase receptors (Trk receptor) specific for each neurotrophin, and a second neurotrophin receptor ($p75^{NRT}$) a member of the TNF receptor family which binds neurotrophic factors with lower affinity than Trk receptors but which has the same specificity for all members of the neurotrophin family (Kaplan & Miller, 1997). The complexity of NTF-receptor interaction is in part due to affinity of differing neurotrophins for the high affinity tyrosine kinase receptor (Trk) subclasses expressed by populations of neurons.

Control of axonal development and regrowth is complex, being regulated by specific neuronal growth factors and guided by interplay between the microtubule and microfilament systems of the ingressing growth cone and the target extracellular matrix and numerous cell surface molecules (Gordon-Weeks, 2004; Calabrese, 2008). In a recent review of signalling and pharmacological control and regulation of axonal formation Calabrese (2008) records over 25 different agents which enhance neurite formation in a variety of culture systems.

1.2.3 QUANTIFICATION OF NEURONAL CELL LOSS

The fact that sensory and motor nerve cells are lost after neurotomy has been known for almost exactly a century, since the silver staining experiments of the early pioneers of neurobiological research such as Ranson and Cajal (Ranson, 1906 & 1909; McKay Hart *et al.*, 2002a).

More recently however, the phenomenon has been reinvestigated by using a variety of animal models of peripheral nerve injury and neuronal counting techniques including the cat (Risling *et al.*, 1983; Liss *et al.*, 1994), rat (Rich *et al.*, 1989; Himes & Tesler 1989; Ygge 1989; Vestergaard *et al.*, 1997) monkey (Liss *et al.*, 1996). These groups

documented a range of magnitude of this cell death of between 7-50% of the DRG neuronal population. The wide variation in these observations has been partly attributed to differences in experimental models, cell-labelling methodology, time points chosen and, particularly, the quantification method of cell counting (Tandrup, 2004). Most of these studies used an assumption-based model of cell number estimation, such as counting nucleoli in every tenth section after toluidine blue or cresyl violet staining; this methodology that has been shown to be biased, with the mean of all possible estimated tending away from the true value (West, 1993; West, 1999).

.

More accurate neuronal quantification was achieved by theoretical and technological advances in the techniques of assumption free stereology. Based on the principles of Sterio, the Optical Fractionator method was developed by combining a three-dimensional counting probe, the Optical Dissector, with a systemic uniform counting scheme, the Fractionator (West, 1993; West, 1999; Hart & Terenghi, 2004; Tandrup, 2004).

Further quantification of the time scale and extent of sensory neuronal loss was carried out using such optical dissection, immunocytochemical morphological histology, and TUNEL analysis (terminal deoxyribonucleotidyl transferase uptake nick-end labelling) (McKay Hart *et al.,* 2002a). TUNEL positive 'dying' neurons were detected as early as 24 hours post injury, and the rate of death escalated to a peak at 2 weeks, reaching a plateau by 2 months, but with some neuronal loss continuing for up to 6 months. TUNEL positive neurons displayed morphological features of apoptosis such as cytoplasmic granulation, vacuolation, and membrane abnormalities. Healthy L4/5 ganglia pairs were found to contain ≈30,000 neurons. Stereologically detectable and significant loss of neuron numbers was evident at 1 week, and continued until reaching a steady state at 2 months,

when a total of 39.2% of all L4/5 DRG neurons was lost; this was estimated to represent ≈70% of all axotomised cells.

Importantly for future work, these authors used the Cavalieri principle (Gundersen *et al.*, 1988) to calculate the volume of the DRG, by multiplication of the mean section thickness, measured by the microcator on the stereology microscope stage, by the mean cross sectional area of a subset of histological sections, measured by image analysis software. The volume of the DRG, corrected for the age related change in size as the animals grow, was found to vary in proportion to neuronal numbers, and that DRG volume reduction is a statistically robust proxy measurement of neuronal death.

Active neuroprotection was also demonstrated with less TUNEL positive cells and less neuronal loss occurring after nerve repair, with the protective effect being more pronounced by immediate or early repair and compromised as the injury to repair delay was increased. This suggested that for pharmacotherapeutic neuroprotective agents to be effective a window of opportunity existed in the first week after injury.

1.2.4 CELL DEATH AND THE NEUROPROTECTIVE AGENTS

The concept of post-injury neuroprotection and the possibility of supplying exogenous pharmacotherapy systemically or directly to the site of injury has been a recognised goal for several years.

1.2.4.1 Neurotrophin starvation as a mechanism for triggering apoptosis.

The stimulus for cell death has long been presumed to be deprivation of neuronal somata of retrograde transport of target derived NTFs and many experimental trials using neurotrophins to support cell survival and promote regeneration have been tested *in vitro*,

and by a number of delivery systems in animal models (Pitts *et al., 2006*; Terenghi 1999; Yin *et al.,* 1998). However, despite an extensive body of work since the discovery of NGF in the 1940s (Levi-Montalchini, 1998), none of these strategies has led to a clinically acceptable treatment for nerve injury for several reasons, including the complexity of the effects and interactions of different NTFs on fibre subpopulations, unpredictable responses, problematic delivery through the blood-nerve barrier and concerns over potential toxicity and carcinogenicity (Lundborg, 2000; Terenghi, 1999).

Starvation of neurotrophic support is regarded as the most important contributing factor to cell death post axotomy (Fu & Gordon, 1997; Ambron & Walters, 1996). However, the situation may be more complicated (Chan *et al.,* 2003), and possibly reflects the influence of neurotoxic cytokines produced as part of the neuroinflammatory response of WD (Stoll *et al.,* 2002), or abortive entry of terminally differentiated mature cells into the mitotic cycle (El Shamy *et al.,* 1998). DRG neurons die in the S-phase, after having overridden the G1 restriction point of the cell cycle (Friedlander *et al.,* 1996; Borner, 1996). It is interesting to speculate if this may represent a pathophysiological extension of the axotomised nerve cell's phenotypic shift towards regeneration and repair.

When discussing neurotrophin withdrawal, obviously axotomy will disrupt transport of all NT factors to which each specific neuron is sensitive; NGF is the best studied survival promoting factor. Much of the current understanding of NFG receptor interaction and resultant downstream signalling with regard to neuronal survival and apoptosis has come from examining peripheral sympathetic neuron development in the mouse, and the apoptotic attrition of initially overabundant neuronal populations that exist in this ontogenic process (Green & Kaplan, 1995; Kaplan & Miller, 1997, 2000; Kaplan & Stephens, 1994; Miller & Kaplan, 2001a, 2001b, 2003, 2007). As with peripheral sensory

neuronal apoptosis post-axotomy, this cell death is related to nuclear starvation of neurotrophic factors (Fu & Gordon, 1997; Kaplan & Miller, 2000).

NGF mediated activities of TrkA and $p75^{NTR}$ during development of peripheral sympathetic neurons are complex, they seem to act antagonistically to determine the cellular response to neurotrophin concentration in the environment on the in-growing axons. In developing peripheral sympathetic neurons $p75^{NTR}$ has a constitutively active non-ligand dependent pro-apoptotic role (Bredesen & Rabizadeh, 1997; Barker, 2004), which is counteracted by TrkA mediated apoptosis suppression (Majdan & Miller, 1999). This antagonism constructs a system whereby if a neuron does not encounter and sequester a sufficient quantity of an appropriate TrkA activating neurotrophin, in the case of sympathetic fibres NGF, the default p75NTR pro-apoptotic pathway will prevail and destroy the cell through p53 (Mazzoni *et al.,* 1999) mediated pruning of neurons which fail to innervate the correct target organ or neural circuit (Majdan *et al.*, 2001).

Trk signalling in the cell soma, located at a topographically distinct point from the axon is required for cell survival determination decisions and alteration of gene expression. This distant Trk activity requires retrograde transport of vesicle-contained, activated Trk dimers, possibly binding NGF itself (Miller & Kaplan, 2001b), to the cell body.

Post axotomy apoptosis induction is via the 'intrinsic' or 'mitochondrial' pathway (Benn & Woolf, 2004; Polster & Fiskum, 2004), mediated by NTF withdrawal, possibly via the $p75^{NTR}$, expression of which is up-regulated in peripheral neurons post injury, and blockade of which is neuroprotective in vivo (Cheema *et al.*, 2006). Intracellular transduction of such signals forms a dynamic balance of flux through different kinase cassettes; specifically the relative activity of growth factor activated ERK, versus stress

responsive JNK and p38 MAPK may dictate cell fate (Xia *et al.,* 1995; Ham *et al.,* 1995; Ambron & Walters, 1996; Nunez, 1998).

1.2.4.2 Mechanism of Apoptosis

The key stages of commitment and execution of the death program begin at the mitochondrial level (Polster & Fiskum, 2004), with the 'point-of-no-return' and the rate limiting step being collapse of the mitochondrial inner transmembrane potential ($\Delta\Psi m$), which allows mitochondrial membrane permeabilisation (MMP) (Kroemer, 2003). It is noted that mitochondrial accumulate in neuronal perikarya after axotomy (Al Abdula & Martin, 1998). Regulation of the MMP is controlled by members of the B-Cell Lymphoma-2 (BCL-2) family of proteins, which have anti-apoptotic (BCL-2, BCL-Xc, BCL-W) or pro-apoptotic (BAX, BAK, BOK, BCL-Xs) activity and differing subcellular and mitochondrial localisation (Mohamad *et al.*, 2005). Members of this family act as 'sensors' for apoptosis encouraging receptor signalling (Li *et al.*, 1998), growth factor withdrawal (Zha *et al.,* 1996) and cytoskeletal integrity (Puthalakath *et al.,* 1999). The c-Jun activation after NTF withdrawal induces expression and phosphorylation of pro-apoptotic BCL-2 family members (Putcha & Johnston, 2004).

The effector mechanism of MMP is translocation of BAX from the cytosol to the outer mitochondrial membrane (OMM) where, possibly by associating with the voltage-dependent ion channel, it forms breaches or pores in the phospholipid bilayer allowing escape of apoptotic factors in the cytoplasm (Shimizu *et al.,* 2001). The interaction of BAX with the OMM is inhibited by BCL-2 and the other anti-apoptotic family members; the intraneuronal ratio of BCL-2:BAX is predictive of irreversible apoptosis commitment (Gillardon *et al.,* 1996; Middleton *et al.,* 1996). MMP triggers cell death by allowing efflux of molecules that begin the apoptosis execution program (Polster & Fiskum, 2004)

notably cytochrome C (CyC) (Zou *et al.* 1997), which activates the Ca^{2+} dependent Cysteine protease (caspase) cascade at caspase-9 by the interaction of cytosolic CyC and APAF to form the apoptosome complex (Mohamad *et al.* 2005). This construct catalyses cleavage of a proenzyme producing a further regulator protease (caspase-3) which initiated a positive feedback cascade of activation of the downstream effector caspases which cleave essential cellular substrates and further activate proteases such as DNAse-1 thus destroying the cell (Nagata, 2000).

The mechanism of neuronal cell death is therefore dependent on caspase-3 (Kouroki *et al.*, 1998; Cregan *et al.*, 1999) and caspase-9 (Krajewski *et al.*, 1996; Yakovlev *et al.*, 1997) activity, and can be prevented by pan-caspase inhibition (Chan *et al.*, 2003). Such involvement of the caspase cascade allows the neuronal death to be designated as apoptosis in the 'death-style' classification of Assuncao Guimaraes & Linden (2004).

Mitochondria are also implicated in the role of oxidative stress in free radical generation in apoptosis of axotomized neurons. Free radical ($FR^{\bullet}$) mediated DNA damage can be detected within dying neurons (Martin *et al.*, 1999), and may be mediated by increased nitric oxide synthase (NOS) activity (Novikov *et al.*, 1995; He *et al.*, 2000) and increased mitochondrial Nitric oxide ($NO^{\bullet}$) (Brorson *et al.*, 1998; Esteves *et al.*, 1998; Brown & Borutaite, 2001). Supraphysiological $NO^{\bullet}$ accumulation permanently inhibits the electron transport chain at CyC and allows generation of reactive oxygen species (ROS), notably the superoxide ion ($O_2^{-\bullet}$), which reacts with $NO^{\bullet}$ to form peroxynitrate ($ONOO^-$) (Beal, 2000; Keller *et al.*, 1998; Nicholls & Budd, 2000).

Failure of oxidative phosphorylation and ATP depletion eventually caused Ca^{2+} disregulation (Nicholls & Budd, 2000) and can even trigger the MMP (Keller *et al.*, 1998).

Oxidative stress could potentially trigger apoptosis via MMP; however direct evidence of oxidative stress in axotomized peripheral nerves includes the detection of ONOO- and hydroxyl radical mediated DNA damage in apoptotic spinal motor neurons (Martin *et al.*, 1999), increased activity of NOS in neurotomised DRG and the finding of a 30% up-regulation of DRG MN-superoxide dismutase activity (Rosenfeld *et al.*, 1997). This last point may represent a homeostatic response to ROS as this enzyme will deactivate $O2^{-\bullet}$ and $ONOO^-$ by forming the less harmful hydrogen peroxide (H_2O_2).

1.2.4.3 Neuroprotective Agents

The presumed importance of oxidative metabolic disruption and implication of ROS in apoptosis induction led to the proposition of antioxidants as putative neuroprotective agents. Two such molecules, *N*-acetylcysteine (NAC) and acetyl-*L*-carnitine (ALCAR) have been previously studied in the context of murine sciatic nerve neuronal pool apoptosis (McKay Hart *et al.*, 2002b; Wilson *et al.*, 2003; Hart *et al.*, 2004a; Zhang *et al.*, 2005; West *et al.*, 2007a; Wilson *et al.*, 2007; Reid *et al.*, 2009).

1.2.4.3.1 N-*acetylcysteine*

NAC is a sulfhydryl group (thiol) containing, free radical scavenging antioxidant molecule with a long history of clinical use as treatment for hepatocyte toxicity in paracetamol overdose, and as a mucolytic (Prescott *et al.*, 1979; 1989) **(Figure 1.1)**.

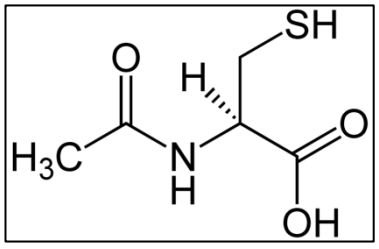

Figure 1.1: Molecular structure of *N*-acetylcysteine. (www.sigma-aldrich.com)

The biological effects of NAC administration to neuronal type cells has been studied *in vitro*, particularly using PC12 phæochromocytoma derived cell lines and sympathetic neuron cultures although to date there is little work studying the response of primary sensory neurons. NAC has direct reductant activity (Kamata *et al.* 1996; Yan *et al.* 1995), interacts with ROS via its sulfhydryl groups (Aruoma *et al.* 1989) and blocks lipid peroxidation by peroxynitrate (Han *et al.*, 1997). NAC blocks the surge on ROS that occurs after occurs after withdrawal of trophic support to sympathetic neurons, inhibiting mitochondrial CyC release (Kirkland & Franklin, 2001); the molecule therefore counteracts several noxious stimuli implicated in the apoptosis induction.

NAC also supplements intracellular levels of glutathione by acting as a cysteine donor (Yan *et al.* 1995; Kamata *et al.* 1996), which is a major neuronal free radical scavenger (Heales *et al.*, 1999), depletion of which causes oxidative stress and neuronal death (Ratan *et al.*, 1994; Wullner *et al.*, 1999). Promotion of glutathione biosynthesis is believed to be the mechanism by which NAC is hepatoprotective against paracetamol (Corcoran & Wong, 1986). However, glutathione up regulation cannot solely explain the neuroprotective effect of NAC, as trophic factor deprived PC12 cells still derive a survival benefit from NAC therapy when glutathione metabolism is inhibited (Yan *et al.*, 1995), and by administration of the L-stereoisomer of NAC which does not influence glutathione levels (Ferrari *et al.*, 1995).

NAC alters cell proliferation and DNA synthesis, blocking cells in the G_1 phase of the cell cycle (Ferrari *et al.*, 1995; Yan *et al.*, 1995; Sekharam *et al.*, 1998). As attempted mitosis of terminally differentiated neurons in response to trophic factor withdrawal has been proposed as explanation for neuronal death, this is an additional mechanism by which NAC may offer neuroprotection post axotomy.

NAC modifies intracellular signalling and transcription. In PC12 cells NAC activates the anti apoptotic ERK-1 kinase pathway (Xia *et al.,* 1995; Yan & Greene, 1998). Further, NAC up regulates p21Ras signalling, a pathway implicated in the trophic effect of several growth factors including NGF (Nobes & Tolkovsky, 1995; Miller & Kaplan, 2001a, 2001b, 2003, 2007). NAC up regulation of Ras is essential for the neuroprotective effect of NAC in growth factor depleted PC12 cells (Yan & Greene, 1998). In the same model, NAC was demonstrated to inhibit induction the pro-apoptotic kinase JNK (Park et al. 1996), therefore NAC would seem to modify both pro-, and anti-apoptotic signalling cassettes to favour survival. Neuroprotection of PC12 cells by NAC is transcription dependent (Yan *et al.,* 1995), as critical Cysteine groups have been identified on some transcription factors, such as NF-kB and AP1 which need to be in a reduced state to allow DNA binding, alteration of transcription via its innate redox activity has been proposed as a further mechanism by which the neuroprotective ability of NAC (Abate *et al.,* 1990; Meyer *et al.,* 1993).

1.2.4.3.2 Acetyl-L-carnitine

ALCAR is a vitamin-like compound synthesized in the liver, kidney and brain from the essential amino acids, lysine and methionine (Calabrese *et al.,* 2006) and is quantitatively and functionally the most significant acylcarnitine ester in the carnitine pool of mammalian tissues, and has several metabolic activities (Rebouche, 2004) **(Figure 1.2)**.

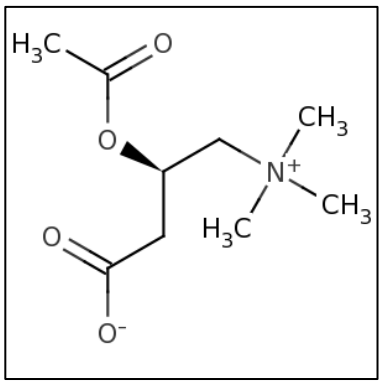

Figure 1.2: Molecular structure of acetyl-*L*-carnitine. (www.sigma-aldrich.com)

It is involved in transporting long-chain free fatty acids across the mitochondrial membrane as part of lipid β-oxidation and facilitating removal of excess short- and medium-chain fatty acids that accumulate during lipid metabolism (Ames 2004). Further, it increases cellular oxygen consumption, stabilizes the inner mitochondrial membrane (Ames 2004). By acting as a reservoir for activated acetyl units, carnitine buffers potentially toxic acyl-CoA metabolites and modulates the ratio of acyl-CoA/CoA ratio (Calabrese *et al.,* 2006; Bremner, 1990). It has been proposed that by acting as a feeding source of free CoA into the tricarboxylic acid cycle can provide "energy properties...in situations of energy crisis" (Jeulin *et al.,* 1996). Like NAC, ALCAR has antioxidant properties (Dhitavat *et al.,* 2002; Hagen *et al.,* 2002).

In vitro ALCAR is neuroprotective, possibly by preventing the mitochondrial uncoupling stage of apoptosis (Virmani *et al.,* 1995) and up regulating NGF receptor activity (Taglialatela *et al.,* 1991). Rat sciatic nerve transaction studies have suggested that ALCAR increases neuronal regeneration (McKay Hart *et al.,* 2002b) and human clinical trials had shown improved target organ re-innervation in HIV neuropathy (Hart *et al.,* 2004b). Further, human dietary supplementation studies have suggested that acetyl-L-carnitine may slow or reverse mild cognitive impairment and progression of dementia in

Alzheimer's disease (Rebouche 2004). ALCAR is neuroprotective for CNS neurons after ischæmic trauma during cardiac arrest and resuscitation by preventing neuronal shift to anærobic metabolism (Zanelli *et al.,* 2005).

In recent years a series of experiments were designed to demonstrate that:

1. ALCAR and NAC act as neuroprotective agents for sensory neurons after rat sciatic nerve division, and have a dose response (Hart *et al.,* 2002b; Wilson *et al.,* 2003; Hart *et al.,* 2004a; West *et al.,* 2007a).
2. NAC is neuroprotective for motor neurons in the ventral horn after rat ventral root injury (Zhang *et al.,* 2005).
3. The effect of NAC neuroprotection is mediated by mitochondrial preservation (Wilson *et al.,* 2003; Hart *et al.,* 2004a).
4. ALCAR promotes sensory neuron regeneration independent of its neuroprotective effect (McKay Hart *et al.,* 2002b; Wilson *et al.,* 2010).
5. Delay in ALCAR treatment for up to 24h post injury does not negatively affect its neuroprotective potential (Wilson *et al.,* 2007).
6. NAC therapy will up-regulate anti-apoptotic genes and down regulate pro-apoptotic genes in cutaneous sensory neuronal populations (Reid *et al.,* 2009).

1.2.4.3.3 ALCAR and NAC are neuroprotective for sensory neurons

In experiments devised to investigate the effect of these neuroprotectants on sensory neurons of the DRG apoptosis was detected by TUNEL staining, while L4/5 ganglia neuronal counts were determined either by optical dissector stereology with the total ganglion neuronal population estimation made by extrapolation of cell density using the Cavalieri principal (McKay Hart *et al.,* 2002b; Wilson *et al.,* 2003; Hart *et al.,* 2004a), or by use of the optical fractionator technique (West *et al.,* 2007a).

DRG morphology in the no-treatment, and sham groups showed many neurons demonstrating features of apoptosis, and this was subjectively improved by low-dose neuroprotectant treatment, and nearly normalised with high dose ALCAR or NAC. In the treatment groups with both ALCAR and NAC there was substantial, statistically significant reduction in the quantity of TUNEL positive cells at two weeks and two months; suggesting that treatment with the neuroprotectants reduced the rate of sensory neuronal apoptosis after nerve injury (McKay Hart *et al.*, 2002b; Hart *et al.*, 2004a).

A protective effect was also seen when assessing total neuronal number, in both studies no-treatment and sham groups lost ≈21% of sensory cells at two weeks and ≈35% at 2 months in the operated side ganglia. Cell death was significantly reduced with ALCAR/NAC treatment, representing rescue of 5,500-6,000 neurons at 2 weeks and over 10,000 cells at 2 months; there was also some evidence for a dose response in both cell morphological assessment and TUNEL positivity at two weeks for both ALCAR and NAC (McKay Hart *et al.*, 2002b; Hart *et al.*, 2004a). Further investigation of the dose response relationship of ALCAR showed that 50mg/kg/day was the optimum dose of this agent, and that the DRG volume is a statistically significant proxy measure of neuroprotection in action (Wilson *et al.*, 2003).

A dose response study for NAC demonstrated a cumulative neuroprotective effect of NAC over a dose range of 1-150mg/kg, with the highest dose providing complete abolition of neuron loss (West et al 2007a). Interestingly this dose is identical to that used in the first steps of treatment with NAC for paracetamol intoxication (British National Formulary, 2010).

1.2.4.3.4 NAC in neuroprotective for motoneurons

Motoneurons in the ventral horn of the spinal cord typically undergo less apoptosis after peripheral nerve injury that their sensory counterparts (Ma *et al.,* 2001; Hu & McLachlan, 2003). However, the amount of cell attrition appears to relate to the distance of the peripheral lesion from the somata (Li *et al.,* 1994; Mattsson *et al.,* 1999), and indeed massive ventral horn motor neuron death is seen after proximal axonal damage at the level of the ventral root, such as occurs in perinatal or high impact brachial plexus injury; as many as 80-90% of motor neurons die after ventral root avulsion (Koliastos *et al.,* 1994; Novikov *et al.,* 1997), and ≈50% after root transection (Zhang *et al.,* 2005). As in sensory neurons, the majority of cell death has been demonstrated to occur over an approximately two-week time course, and similar molecular pathophysiological events have been implicated.

Zhang *et al.,* (2005) assessed the use of NAC as a neuroprotective agent in a murine model of ventral root avulsion and rhizotomy. L5/6 spinal motor neurons were pre-labelled with retrograde tracers, and NAC was administered to treatment groups by either intraperitoneal doses of 750mg/kg/d or 150mg/kg/d, or intrathecally, using an implanted osmotic minipump to deliver 2.4mg/d. Ventral root rhizotomy caused death of 28% of the ventral horn medial gastrocnemius motor neuron population, and a 21% reduction in soma area, while root avulsion killed 53% of such cells with a 31% reduction in soma area in 4 weeks. Intraperitoneal NAC treatment provided dose responsive neuroprotection after rhizotomy, with only 7% neuronal death at 8 weeks in the high dose group; the 17% death for low dose intraperitoneal NAC not reaching statistical significance – intrathecal NAC was of even more benefit, with only 5% of cells succumbing. After root avulsion, low dose intraperitoneal NAC allowed significant 60% neuronal survival, although this was not as effective as the 70% survival found in the intrathecally treated group.

Of potential clinical relevance, one-week delay in institution of intrathecal NAC did not have a significant deleterious effect on neuroprotective ability, however, the total death rate rising from 30-32% to 42% after a 2-week delay (Zhang *et al.,* 2005).

NAC can therefore provide neuroprotection both for sensory neurons after postganglionic axon division, and rescue motor neurons after proximal axotomy.

1.2.4.3.5 ALCAR & NAC provide mitochondrial protection

Evidence for the putative mechanism of ALCAR and NAC's neuroprotective effect being mitochondrial stabilization was also been assessed, using transmission electron microscopy (Hart *et al.,* 2004a, Wilson *et al.,* 2003). Axotomised neurons demonstrated cytoplasmic disruption such as mitochondrial swelling, loss of architecture, crystal disruption, vacuolation or rupture. Further, there was disruption of the endoplasmic reticulum, and nuclear changes of apoptosis such as chromatin condensation, nuclear irregularity or fragmentation. In cells that had received low dose ALCAR, only some cristal disruption was noted, and with high dose ALCAR or NAC cell ultrastructure was generally normal, with only occasional mitochondrial swelling **(Figure 1.3)**. The striking preservation of mitochondrial morphology lends weight to the proposition that the neuroprotective effect of these agents is mediated by alleviation of oxidative stress by ameliorating other detrimental bioenergic processes.

1.2.4.3.6 ALCAR increases sensory neuron regeneration

Past experiments in vivo and cell culture systems had suggested that ALCAR had the ability to enhance neurite outgrowth and regeneration after nerve injury (Fernandez *et al.*,

1989; Taglialatela *et al.,* 1991; Manfridi *et al.,* 1992), which had been attributed to up-regulation of the neuron's responsiveness to NGF.

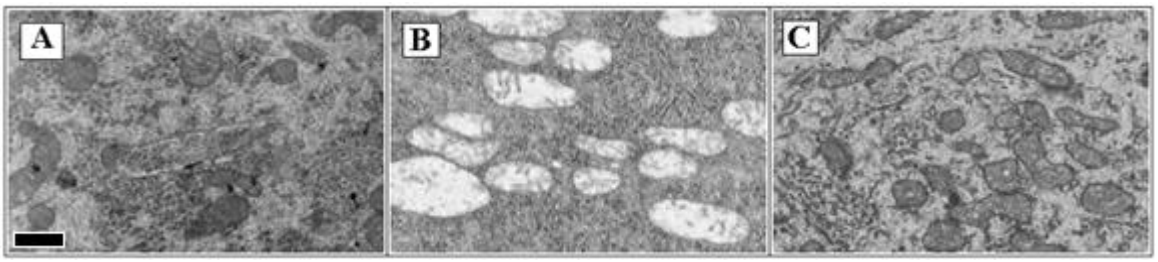

Figure 1.3: Effect of NAC on mitochondrial morphology. tEM of L5 DRG neuronal somata with no injury (A), two weeks after axotomy (B) and two weeks post axotomy with NAC treatment (C) - The mitochondrial disruption seen in B is prevented in C by NAC treatment (scale bar = 500nm) (Modified from Hart *et al.*, 2004a with permission).

However, increased neurite activity may simply represent augmented regeneration potential of the larger sensory neuron pool as a result of neuroprotection.

To investigate the potential regeneration promoting effects of ALCAR in isolation, McKay Hart *et al.*, (2002b) performed standard murine sciatic nerve division, and after a two-month delay, by which time neuronal loss is essentially complete, repaired these lesions with reversed sciatic nerve isograft. ALCAR was administered intraperitoneally at 50mg/kg/d beginning on the day of nerve grafting. At six weeks post repair, regenerating fibres crossed the full extent of the harvested nerve/graft construct, but there significantly greater axonal regeneration in the ALCAR treated group than in controls. These data suggest that ALCAR treatment, independent of its neuroprotective effect can augment the capacity of sensory neuronal fibres to regenerate through a nerve graft.

In a separate experiment ALCAR associated regeneration was assessed by visualisation of myelinated fibres distal to the sciatic repair site, by immunohistochemistry against protein gene product 9.5 in hind paw footpad skin as a marker of very small nerve (including non-

myelinated fibre) dermal reinervation, and by wet muscle weights of the gastrocnemius as an index of muscle re-innervation (Wilson *et al.*, 2010). The results showed that the mean number of myelinated fibres and myelin thickness distal to the nerve coaptation were improved by ALCAR administration compared to sham treated groups. ALCAR also increased ingrowth of small nerves into the footpad dermis by 210% compared to sham treatment and led to less wet muscle mass loss. These findings suggest that ALCAR will act to globally promote and foster peripheral nerve regeneration of heterogeneous sensory populations' as well motor fibres.

1.2.4.3.7 Small delays in commencement of ALCAR therapy do not adversely affect neuroprotective effect.

Observations of clinical logistics demonstrate that after an acute injury there is often a lag period of days or hours before a patient with a peripheral nerve injury arrives at a specialist reconstructive centre. The effect of delayed administration of ALCAR was investigated after sciatic nerve transection (Wilson *et al.*, 2007). Delays between 6 and 24 hours in treatment commencement had no effect on the neuroprotective effect of ALCAR with no neuron loss in these groups compared to DRG from the contralateral control side. Even a prolonged delay of a full week after injury led to less neuronal apoptosis than in animals with no treatment although these differences did not reach statistical significance.

1.2.4.3.8 NAC Treatment prevents apoptosis in susceptible neuronal population by affecting the balance of apoptotic markers.

It has been reported that not all neuronal sensory subpopulations in the rat DRG undergo the same rate of apoptosis after sciatic nerve injury; with the vast majority of cell death occurring in the cutaneous afferent neurons whereas muscle propreoceptive sensory neurons are spared (Welin *et al.*, 2008). To further investigate this phenomenon, levels of

apoptotic related gene activity within these two cell subpopulations was analysed by staining neurons with a retrograde tracer, isolating individual labelled cells from frozen section samples by using laser microdissection and subjecting aggregates of each cell type to quantitative real time PCR (polymerase chain reaction) amplification to study mRNA levels of specific genes (Reid *et al.,* 2009). mRNA from the anti-apoptotic BCL-2 protein and the pro-apoptotic BAX and apoptotic effector caspase 3 were quantified both with and without NAC treatment in nerve transection groups. Axotomy leads to up-regulation of BAX and caspase 3 in apoptosis prone cutaneous sensory neurons, and down regulation in the more robust muscle afferent population. NAC treatment led to further down-regulation of pro-apoptotic markers in muscle afferents and also caused significant down-regulation of BAX and caspase 3 in cutaneous fibres. The pro-apoptotic marker BCL-2 did not alter expression levels in either cell subpopulation after axotomy alone, but was significantly up-regulated in both groups by NAC treatment. Leading to a high BCL-2:BAX ratio in subpopulations not destined to die.

These finding add more evidence suggesting that the neuroprotective effect of NAC is not purely mitochondrial protection by scavenging of reactive oxygen species but involves a more complex system including alteration of signalling and translation events. NAC rescue of PC12 cells in culture involves activation of the Ras-ERK signalling pathway (Yan & Green, 1998), and such NAC mediated Ras-ERK signalling has more recently been demonstrated to up regulate BCL-2 in a cell culture model of Alzheimer's disease (Hsiao *et al.,* 2008).

1.3. MRI IMAGING OF THE PERIPHERAL NEUROMUSCULAR SYSTEM

1.3.1 THE NEED FOR MRI IN ASSESSMENT OF NERVE INJURY

A significant hurdle in commencing a clinical study of neuroprotection in a human population is the inability to use histological methods of neuronal counting in live subjects. Surveillance of neuronal loss and rescue in humans must therefore rely on clinical assessment of nerve function, neurophysiological assessment or some non-invasive imaging technique. Several systems for *in vivo* assessment of nerve function have been proposed, both for murine models and in human subjects.

There are many cited strategies to draw inferences of neuromuscular function in rodents, these have a wide spectrum of invasiveness, and all have some drawbacks. Electrophysiology and Nerve Conduction Testing can measure the velocity of propagation, peak amplitude and area of a compound action potential, but can give inappropriate interpretation of return of function (Varejão *et al.,* 2001; Kanaga *et al.,* 1996). Electromyography (Wessig *et al.,* 2004; Bendszus *et al.,* 2004; Grant *et al.,* 1999) and other methodologies such as foot withdrawal response to electrical stimulation (De Konig *et al.,* 1986), muscle wet weight, single muscle contractile force measurement (Varejão *et al.,* 2001) and animal gait track analysis (Shenaq *et al.,* 1989) do not give full and reliable information on the level of regeneration.

Assessment of nerve recovery in people is no simpler, and in surgical practice often only clinical tests of motor function and sensory distribution are used. EMG is the current 'gold standard' for motor assessment, but it is investigator dependent and painful, unsuitable for testing of children and anticoagulated/coagulopathic patients, and presents

difficulty if serial examination is needed. Further, anatomical considerations can limit utility of EMG, such as proximal lesions (root avulsion) or limb mutilation (Koltzenburg & Bendszus, 2004). EMG however does have utility in monitoring various aspects of the response to injury, but can only detect regeneration at the stage of fibres reinnervating targets (Grant *et al.,* 1999).

Testing of sensory function is complicated by the range of sensory modalities subserved by the skin, and the different fibre types involved. The basic discrimination of light touch, pressure, vibration, heat, cold and fast pain and possibly itch (Ganong, 1997) is complicated by central processing of these elements to derive compound sensations or 'synthetic senses' such as vibratory sensibility, stereognosis, and functional tactile gnosis (the ability to recognise and identify textures and shapes) (Lundborg & Richard, 2003). Some higher sensory modalities are still being discovered, such as the c tactile afferent system of hair baring skin that projects to temporal insula, thought to be involved in the emotional and hormonal response to skin-to-skin caress (Olausson *et al.,* 2002).

In a recent systematic review of a battery of testing modalities for sensory functions, only monofilaments and shape-texture identification met the criteria for a standardized test (Jerosch-Herold, 2005). The last of these testing methods has been refined into a commercially available set of objects and testing protocol named the Shape-Texture Identification test (STI™) (Rosen & Lundborg, 1998). Probably the most used sensory clinical test is 'two point discrimination' (2PD) (Grant *et al.,* 1999), but Lundborg & Rosen (2004) have commented that over reliance on this technique has lead to "enormous implausible variability" in reported sensory recovery after injury.

In man, as well as in animal models therefore a modality was lacking that could distinguish between individual elements of the nerve injury/repair sequence, including death of the sensory neuron pool, axon regeneration and organ re-innervation. It is in this role that MRI demonstrates great possibilities (Grant *et al.*, 2002).

1.3.2 MRI NEUROGRAPHY

The potential of Nuclear Magnetic Resonance (NMR) to create a biological imaging technique was realised and pioneered by Damadian in 1971. He realised that the nuclear magnetic relaxation times of normal and neoplastic tissue differed (Damaidian, 1971), leading to patenting of a 'cancer scanner' in 1974 (United States Patent and Trademark Office 1974); to the first human MR image in 1977, and marketing of the first commercial MRI scanner in 1980 **(Figures 1.4 & 1.5).**

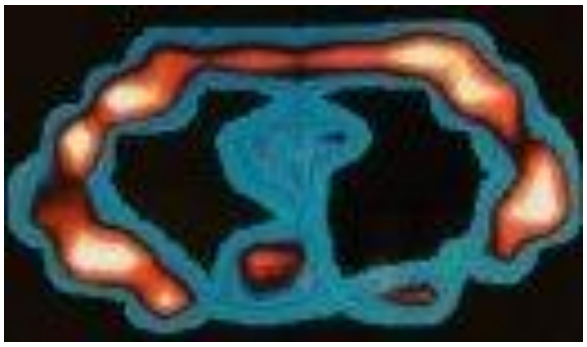

Figures 1.4 & 1.5: 'Indomitable' the World's first MRI scanner, and the first human MR image - an axial section through thorax showing the chest wall and centrally the heart.
(From http://fonar.com)

By applying principles of back projection, gradient and frequency encoding, the Fourier transform and echo-planar imaging, MRI techniques have been evolved to the current standard by contributors such as Ernst, Lauterbur and Mansefield (The Nobel Assembly

2003). Controversially (Culver, 2003), these three latter scientists have been awarded Nobel prizes for their work concerning MRI, but Damadian has so far not received this honour.

Detailed discussion of the physics and hardware technicalities involved in generation of an MR image are beyond the scope of this review, however, some basic principles are required. The basis of MR imaging is recording the radiofrequency (RF) energy emissions released as the magnetic moment of unpaired protons relax from precession at the Larmor frequency towards their natural alignment within a strong, generated magnetic field after cessation of a RF pulse (Westbrook, 2002). By use of a 2D Fourier transform function, the data from the sums of phase and frequency encoding per voxel can be transformed into an image (Elster, 1994).

Of relevance to neural imaging studies are the concepts of T_1 recovery, T_2 decay and pulse sequencing. T_1 recovery is the regaining of longitudinal magnetization after cessation of a RF pulse and is caused by 'spin lattice energy transfer' from nuclei to their surroundings, T_2 decay is caused by the exchange of energy from one nucleus to another causing loss of spin phase coherence. Crucially, the T_1 and T_2 properties of hydrogen nuclei in fat and water differ, and therefore by changing parameters of the RF pulses, gradient applications and intervening time periods ('Pulse sequence') specifically the 'time to repeat' (TR) and 'time to echo' (TE) images can be produced with different fat to water contrast, so called T_1-, or T_2-weighted images (T_1w & T_2w) (Schild, 1990; Westbrook, 2002). Neurological MR imaging studies have used a variety of pulse sequences including the conventional 'spin echo' or 'gradient echo' sequences and more complex fast or turbo sequences, these frequently have elaborate, often commercially patented, acronyms; but at the most basic

level are designed to achieve specific contrast or reduce imaging time (Shild, 1990; Elster, 1994).

Of potential interest to our group, MRI can be used to visualise:

1. Nerve response to injury and regeneration.
2. Small neural structures at an almost microscopic level of detail, and accurately assess their volume.
3. DRG in humans and rats.

1.3.2.1 MRI of Nerve after Injury

Possibly the first MR neurogram, of rabbit forelimb nerves, was generated using fast spin-echo sequence with fat suppression (Howe *et al.*, 1992), this was made possible by anisotropic properties of nerves whereby water diffuses longitudinally along nerves more readily than in other directions (Grant *et al.*, 2002).

Similar technology allowed publication of the first human MR neurogram of an isograft repaired human tibial nerve, by the same group (Filler *et al.*, 1993). Even as early as this, obvious signal intensity differences between myelinated nerve and regenerating graft were documented.

After this landmark, several groups began to MR image nerves in pathological conditions, commonly in compression syndromes. The Carpal tunnel syndrome was assessed using T_1w, T_2w, proton density and short τ-inversion recovery (STIR) scanning (Britz *et al.*, 1995). This group found T_2 signal increase in the median nerve in the carpal tunnel of all symptomatic patients, and quantitatively greater STIR signal hyperintensity in the nerves of those patients with worse clinical disease. These findings correlated to EMG results,

and both signal and configuration changes improved to some extent after clinically successful carpal tunnel release.

More proximally, the same group demonstrated similar results at the elbow, assessing ulnar nerve entrapment and compression in the cubital tunnel (Britz *et al.,* 1996). Again, MRI was both sensitive and specific when compared to intraoperative findings, and interestingly somewhat more sensitive than 'gold standard' EMG (97% vs. 77% correct diagnosis of compression). Around the same time, the first evidence was published that neural T_2 signal enhancement will normalise after nerve repair, but remains hyperintense for a prolonged period after irreversible damage (Daley *et al.*, 1997).

In response to these successful human case reports, several groups began to use animal models of nerve injury, and very high field research magnet scanners with novel phased array coils to systematically study MRI of nerve, key objectives were to establish the time points of signal change after injury and during regeneration, and to establish what physiological parameters gave rise to these NMR differences.

Initial workers correlated MR changes to histology, finding T_2 change at the lesion site and distally, and eventual normalisation; these differences seeming to mirror the onset and completion of WD and nerve œdema (Does & Snyder, 1996; Cudlip *et al.,* 2002). Further, T_2 spectroscopy can provide information about fluid compartmentalisation, when 'myelin', 'intracellular water' and 'extracellular water' were examined, degenerating nerves showed decreased amplitude of the 'myelin' component and increased T_2 signal of the 'intra-' and 'extracellular' peaks, suggested to reflect breakdown of distal stump axons and intraneural œdema (Stanisz *et al.,* 2001)

Aagaard *et al.,* (2003) compared transient nerve injury (crush), with irreversible (cut and capping) of the rat sciatic nerve to serial MRI and functional recovery by gait track analysis. Multi-time point histology was also used, immunostained for neurofilament on cross-sectional area of nerve 5mm distal to the cut or crush. By the first scan at post-operative day 7, nerve injured by either method was strongly T_2 hyperintense. However, in crushed nerves, this normalized between post-operative day 21-28, this being around the same time that gait track analysis regained normality, and histologically increasing numbers of regenerating, myelinated axons were found distal to the injury, with scanty myelin degradation products (MDPs). In contrast, in the cut nerve group, T_2 and STIR hyperintensity was qualitatively greater, and persisted until post-operative day 60 **(Figure 1.6)**. No neurofilament positive regenerating axons were found in the distal nerve stump, but there was significant quantity of MDPs until POD 60. It was therefore demonstrated that nerve regeneration correlates with T_2w signal normalisation, but that this will occur at ≈60 days even in degenerating axons. At no point were any changes in T_1w signal noted.

Figure 1.6: Axial STIR sequence MRI of rat hind quarters, showing normal sciatic nerve in the thigh ('L' arrow) and T_2 hyperintensity in the distal stump of the axotomised right nerve ('R' arrow) 28 days post-injury, scale bar = 1cm (Modified from Aagaard *et al.*, 2003).

In a similar study Bendszus *et al.,* (2004) added more frequent time points of MR imaging, beginning at one day post-operatively, and different imaging parameters (T_1w, T_2w, double spin echo, TRIM sequences and gadolinium contrast enhanced fat suppressed T_1w images) and compared MR results with EMG recording as well as immunohistology. Notably, this study was performed with a 1.5 Tesla scanner, which is comparable to machines used in human clinical practice (Elster 1994). To assess the relative contribution fluid distribution within the nerve to T_2w signal response histological sections were digitised, and assessed using 2D surface area analysis.

MRI signal changes were first detected between the time of loss of voluntary movement activity and the finding of spontaneous pathological activity, i.e. in the time after functional loss of impulse propagation and the first detectable proof of denervation. T_2 signal elevation correlated with the massive histological axonal degeneration and breakdown of cell integrity during WD. Initially however, the extracellular compartment of the proximal stump cross sections was not enlarged, suggesting that the T_2 change is not likely to be attributable to water proton shift, in the early stages. However, by one-week post-lesion, endoneural œdema was marked, and this was likely to be responsible for the subacute plateau of T_2 signal enhancement. Re-detection of voluntary activity correlated with normalisation of MRI signals, and histological return of normal fibre density and extracellular space volume (Bendszus *et al.,* 2004).

The same group pioneered use of a MR contrast agent Gadofluorine-M which, by gaining access to degenerating nerves through breaches in the blood-nerve barrier that occur during WD, persistently highlighted degenerating fibres. Further, because enhancement is reversible on successful regeneration, moving zones of proximodistal nerve growth were made visible (Bendzus *et al.,* 2005).

MRI has therefore been shown to be a sensitive tool to detect axonal lesions and motor regeneration, as distinct from neuropraxic grade injury, which has only local T_2 signal hyperintensity at the site of compression (Britz *et al.*, 1995), and that this axonal trauma can be visualised as early as 24h post-lesion which is before detectable EMG denervation activity (Bendszus *et al.*, 2004).

There have been several proposed reasons for the observed T_2w signal change, these include increase water content, or transient increased permeability of the blood-nerve barrier during neuronal injury (Seitz et *al.*, 1989). However, as discussed by Aagaard *et al.*, (2003), as water proton content increase should be accompanied by increase in the T_1w signal, which does not occur. Ingress in inflammatory cells, such as macrophages, into the degenerating nerve stump can be detected by MRI (Bendszus & Stoll, 2003), and might be expected to change the T_2w signal, however, histological finding of similar numbers of such inflammatory cells in axotomised and neurotomised nerves at post-operative day 60, after MR signals have normalised stand against this proposal (Aagaard *et al.*, 2003).

Aagaard *et al.*, 2003 propose that a likely explanation for the observed signal differences is myelin turnover, the changes in intensity being correlated with the presence, and subsequent clearance of MDPs. In axonotmesis injury, the MDPs have a shorter half-life in the distal nerve stump as they are re-cycled for ensheathing of regenerating nerves (Muller *et al.*, 1986), and therefore MDPs are cleared at an earlier time point. Further evidence for this 'myelination' proposal of signal change comes from the enhancement on both de- and re-generating neurons with gadoflouraine-M, which binds to fibrillary structures and vesicular formations of myelin debris. This enhancement was noted until complete regeneration was seen (Bendszus *et al.*, 2005).

A More recent study of signal changes post axotomy was reported by Bher *et al.,* (2009), using a 4.7T experimental scanner and analysing T_2-weighted fast spin echo sequences. This group demonstrated T_2 hyperintensity in the distal stump of sciatic nerves which had been either tansected and repaired or permanently divided. In coapted nerves T_2 hyperintensity was obvious by 6 days post injury, reached a plateau phase between days 14-21 before returning to normal between days 35-42 and reaching normality by 63 days post-operatively. In the permanent division group signal change occurred faster, to a greater extent and for an increased duration, but mirroring the findings of (Aagaard *et al.*, 2003) that even when nerve regeneration does not occur dist stump signal changes will eventually normalise. Comparison with histological fibre counting and analysis of presence and amount of myelin present in the distal stump after both injury models is interesting; in repaired nerves, histological detection of fibre regeneration crossing the coaptation site and into the distal stump at 14 day correlates well with beginning of normalisation of T_2 signal, as did final resolution of signal changes as day 42 correspond to progressing fibre accumulation, size increase and myelin thickness. As in the study by Aagaard *et al.,* (2003) however, no convincing explanation for the eventual return to normality in the non-regeneration group were suggested.

MRI neurography therefore has the potential to visualise degenerative changes in neurons before there is unambiguous EMG changes of axonotmesis, image re-generation before neurites reach sentinel muscles (Koltzenburg & Bendszus, 2004) and potentially help diagnosis between different grades of nerve injury.

1.3.2.2 Microscopic and Volumetric Analysis with MRI

Two of the properties of MRI which have progressed rapidly in recent years are increasing image resolution, allowing near microscopic levels of detail to be achieved, and combining

MR scans with image analysis software to calculate surface area of elements in planar pictures and reconstruct these to calculate the volume of three dimensional neural structures.

1.3.2.2.1 Microscopic Resolution

The eventual picture resolution of an MR image is a function of the scanned volume element (voxel), which is the 3D element of body tissue rendered as one digital pixel on the resulting reconstructed cross sectional scan (Westbrook 2002). The intrinsically low signal-to-noise ratio (SNR) of MRI becomes increasingly problematic when fine resolution images are produced, due to the small amounts of water in each voxel, but resolution can be increased by using stronger main magnetic field strength, thinner section slices, longer acquisition times and custom designed hardware such as imaging coils (Jacobs & Cherry, 2001; Natt *et al.,* 2002; Farooki *et al.,* 2002). Spatial resolutions as low as 10μm have been achieved by several groups at field strengths ranging from 4.7-14T; imaging of such small areas has been described as micro-MRI (μMRI) (Jacobs & Cherry 2001; Ullmann *et al.,* 2010).

Post mortem studies allow longer imaging time, and therefore higher resolution, but do not take advantage of the intrinsic non-invasive nature of MRI. Examples of such very high resolution imaging are the μMRI atlas of mouse development of Jacobs *et al.,* (1999) **(Figure 1.7)**, and the resolution of post mortem human median nerve to a resolution fine enough to visualise fascicular architecture and the intraneural connective tissue layers (Bilgen *et al.,* 2005) **(Figure 1.8)**.

Figure 1.7: Post-acquisition reconstruction of 3D spin-echo MRI of the 10.5 dpc mouse embryo. There is no scale in the original paper; however the average crown-rump lenth at this stage is 3.3-3.9mm (Theiler, 1989) (figure from Jacobs *et al.*, 1999).

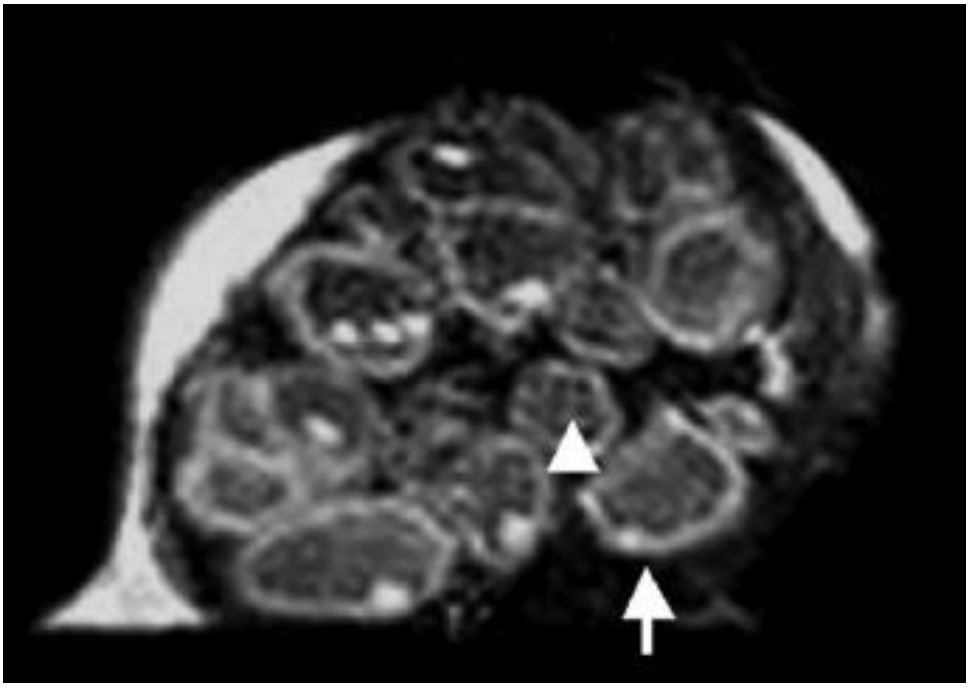

Figure 1.8: T_2 weighted dual-echo spin-echo sequence of human median nerve demonstrating perineunium (up arrow) and fascicular architecture within the endoneurium (arrow head). There is no scale in the original paper (Figure from Bilgen *et al.*, 2005).

In vivo μMRI has associated difficulties of potential movement of the subject and necessarily shorter scanning time as anæsthesia can only practically be maintained for a limited period. Natt *et al.,* (2002) cite a large spectrum of voxel sizes used for imaging mouse brain *in vivo* ranging from 78x156x343μm at 7T to 98x156x1500μm at 11.7T.

This group, using a 2.3T field with T_1w 3D FLASH sequences were able to achieve section thickness of 156-938μm, and managed to image structures as small as the hippocampus and medial Habenular Nucleus, which are normally only visualised using microscopic histology. The acquisition time in these experiments was 1-1.5 hours, which included set up, animal arrangement in a stereotactic frame, scout image generation and definitive scanning. Interestingly, in the same paper, intra-ocular injection of 'smart contrast' agent (Mg^{2+} as an analogue of Ca^{2+}) was used to delineate fibre tract projection pathways. Hyperintense signal was located to the retina, optic tract, lateral geniculate nucleus and superior colliculus, demonstrating the potential therefore of μMRI to be used for neurophysiological axonal tracing in living animals.

In vivo μMRI imaging has also been applied to humans (Farooki *et al.,* 2002). Healthy volunteers had the median nerve in the carpal tunnel imaged in a narrow bore 8T clinical 'limb' scanner. In comparison to 'standard' 1.5T clinical scans nerve anatomy was demonstrated in much higher resolution (slice thickness 2mm) allowing epineural and fascicle identification, although there was not the same signal-to-noise ratio and clarity as the *ex vivo* studies of Bilgen *et al.,* (2005).

1.3.2.2.2 Volume Estimation

Investigators undertaking volumetric studies often use variations on 3D volumetric sequences, these techniques stimulate all of the tissue within a 'region of interest' with an RF pulse, and acquire data from the full volume of this tissue, these data are 'sectioned' into 2D slices by a phase encoding stage of the image reconstruction. 3D sequences are believed to provide more accurate basis for volume estimation as each image slice is more homogeneous and isotropic than those acquired by standard sequential slice acquisition (Sprawls 1988; Johnston *et al.,* 1999).

Several groups have demonstrated volumetric analysis of neural structures using sequential MRI slices, either using simple measurement or more sophisticated computer assisted calculation, both in human studies and animal models (Gadeberg *et al.,* 1999; McDaniel *et al.,* 2001; Wolf *et al.,* 2002; Marziali *et al.,* 2004; Nagel *et al.,* 2004).

The earliest of these studies aimed at assessing disease load in human multiple sclerosis patients by measuring the total brain plaque volume (Gadeberg *et al.,* 1999). In an experimental method analogous to stereological assessment of tissue volume with an optical dissector, the group used a transparency printed with counting grids applied to hard copy MRI films to assess lesion surface area, and extracted a depth measurement from the number of 3mm slices over which lesions extended. Interestingly, but somewhat discouragingly, by applying the same scanning parameters to a contrast filled 'phantom' this group estimated the error measurement in their surface area assessments to be between 15-200% (dependent on object size). This was attributed to an element of overprojection due to the thickness of slices, and partial volume effect, which causes inaccuracy at detecting edges of elements due to each voxel being attributed a grey scale pixel value based on the average signal value of all the tissues contained within it (Tofts *et al.,* 2005).

These authors suggested that development of hardware advances allowing thinner slices would reduce this error, and suggest a mathematical formula to reduce overprojection bias (Gadeberg *et al.,* 1999).

Probably the first use of volumetric neurological *in vivo* μMRI was reported by McDaniel *et al.,* (2001), who used a mouse model of ischæmic forebrain neurodegeneration scanned using a custom made surface coil, with head restraint, in a 7.1T 15cm bore scanner. Parameters included 3D Spin-echo (T_1) and 3D diffusion-weighted spin-echo pulse sequences and total scan time was 1.36-2.4h. Volumetric analysis of the forebrain and the ventricles was performed by assessing the surface area of each structure in each slice with image analysis software, and multiplying total cross sectional area by slice thickness. This group did document a forebrain volume reduction during 30 days after an ischæmic insult, which paralleled the histological detection. However it is noted that the calculation of structure volume used in this paper for both MRI and histological analyses does not have the statistical robustness as the Cavalieri principle, with its insistence on assessing a systemic random sample of sections and beginning the field of interest outside of the sample.

At almost the same time as Natt *et al.,* (2002) demonstrated that μMRI could image structures such as the hippocampus at microscopic detail, an American group published a μMRI protocol to calculate the volumes of rat hippocampus, cingulate cortex and granular cortex (Wolf *et al.,* 2002). This group used a 7T scanner and moderate spin-echo sequences to get *in vivo* in plane resolution of 125μm. The method of volume assessment was derived by tracing structure outline on axial images using an image analysis package and then using a software function to calculate the 3D volume, however the mathematical model used by this system was not discussed in the paper. Although volume values for

many structures are given, this paper does not compare these MRI measurements to those of alternative paradigms.

In one of few human volumetric MRI studies Marziali *et al.*, (2004) used 3D gradient echo sequences to produce normative data on pre-pubescent human pituitary gland size, and managed to reduce measurement error to 0.2-0.4% when the system was assessed with a 'phantom'.

One of the potential sources of error in these volumetric μMRI assessments is the manual tracing of image element surface area, as this is user dependent. In the study of Nagel *et al.*, (2004) advances in image analysis processing allowed an automation of this step. The per-slice surface area of cerebral œdema and infarct produced after middle cerebral artery occlusion and reperfusion was calculated by manually selecting one 'seed point voxel', which is defiantly within the œdematous area, the software then includes in the count all pixels in direct connection with the 'seed point' that have a pre-determined grey scale value. This technique is of potential value if the area of imaging interest has a reasonably large signal difference from the surrounding tissue.

Interestingly, in all of the *in vivo* volumetric studies cited, there is little mention of the logistical difficulties of scanning such animals, except by Wolf *et al.*, (2002) who states that deep anæsthesia was needed, and that paralysis and mechanical ventilation could be used to reduce motion artefact.

1.3.2.2.3 MRI of DRG

For many years MR has been used in human spinal and radicular imaging, and for diagnosis of orthopædic and neurological disease. There has been particular interest in the DRG as inflammation and œdema of these structures is implicated in the generation of the neurological pain that accompanies intervertebral disc herniation (Mulleman *et al.,* 2006). Early anatomical MRI studies verified that the spinal roots, DRG and nerves could be identified running within the skeletal structures (Kostelic *et al.,* 1991; Sasaki 1995; Hasegawa *et al.,* 1996) but there have been few morphological or volumetric analyses.

Castillo & Mukherji (1996) demonstrated subjective enlargement of DRG and nerves in four case studies of patients with differing neuropathies. Aota *et al.,* (2001) assessed DRG swelling in the setting of disc prolapse, by assessing ganglia œdema by width measurement, and impingement by showing indentation. This study demonstrated that MRI can assess at least semi-quantitatively morphological change in human DRG.

There has been much work published concerning MR imaging of the brachial plexus, especially its anatomy in relation to infraclavicular nerve blocks (Raphael *et al.,* 2005; Sardesai *et al.,* 2006), and including demonstrable neural atrophy and fibrosis after radiotherapy (Iyer *et al.,* 1996).

Until 2007, no studies using true volumetric MRI analysis of human or animal DRG volumes could be found until West *et al.,* (2007b) used 3D volumetric assessment of DRG applied to an established rat model of sciatic nerve transection. Histological DRG volume reduction had been shown to be a statistically valid proxy measure of post-axotomy neuronal death (Hart *et al.,* 2002a; Wilson *et al.,* 2002), and this study demonstrated that μMRI is a suitable non-histological tool for following this reduction in volume over time.

In the study, rats were scanned *ex vivo* four weeks after unilateral axotomy, and their DRG were then harvested and processed for histology, allowing neuronal cell counts and ganglion volume estimation assessed by the optical fractionator and the Cavalieri equation (Hart & Terenghi, 2004). For the volumetric analysis of the MRI images were digitised and quantified by image analysis software. The cross sectional of the DRG was traced manually in each slice, and surface area calculated by the software.

MRI demonstrated a significant reduction in DRG volume of the axotomised side compared to non-axotomised side and ganglia in non-operated control rats. Further, there was a strong and significant correlation between MRI and stereological assessment of volume loss ($p<0.001$). There was similarly a relationship between MR DRG volume and histological cell count (West et al 2007b).

In summary, the use of MRI was demonstrated to provide a reliable index of DRG volume loss, and a proxy measure of neuronal apoptosis after nerve injury.

1.4. AIMS OF THIS PROJECT

The currently poor sensory functional recovery after upper nerve injury is largely attributable to apoptosis of a large population of DRG sensory neurons, which are therefore lost to the regenerative effort after nerve repair, thus lowering eventual innervation density. This death of sensory neurons that occurs after peripheral axotomy has been characterised by analysis of some of the apoptotic elements responsible for cell death and two clinically useful neuroprotective agents have been found to minimise this neuron loss and promote

nerve regeneration. 3D μMRI can be used as a viable proxy measurement of DRG volume reduction which reflects this neuronal cell loss in an *ex vivo* murine model.

The global aims of this project are to further investigate:

- The duration of NAC therapy needed to achieve maximal neuroprotection.
- The use of volumetric MRI analysis as an index of DRG volume change in response to nerve injury and pharmacological intervention.
- The application of MRI to assess signal changes in rat sciatic nerve after transection and during regeneration, including after neuroprotectant therapy.
- The ability of a high frequency ultrasound system to image rat sciatic nerve in health and after injury.
- The effects of ALCAR and NAC on survival and behaviour of isolated primary sensory neurons *in vitro*.

CHAPTER 2

N-acetylcysteine Treatment Duration Study

2.1 BACKGROUND & EXPERIMENTAL DESIGN

Primary sensory neuronal cells, located in the dorsal root ganglion (DRG) undergo cell death in a time dependent manner after sciatic nerve transection (Groves *et al.,* 1997; Vestergaard *et al.,* 1997; McKay Hart *et al.,* 2002a); this results in the cell death of around 40% of DRG neurons by two months post injury (McKay Hart *et al.,* 2002a). Previous work has established the ability of the neuroprotective agents NAC and ALCAR to prevent such neuronal apoptosis, and has determined optimal dosing regimens for each substance (McKay Hart *et al.,* 2002b; Wilson *et al.,* 2003; Hart *et al.,* 2004a; West 2007a). In these studies neuroprotectant was administered every day and treatment continued until the end of the experimental time point. The effect of shorter durations of treatment, such as whether neuronal cell death would resume after withdrawal of neuroprotectant support, is unknown. If the potential benefits of neuroprotectant therapy are to be translated to the clinical arena the proposed duration of treatment must be considered.

The investigation reported here was designed to investigate the effect of NAC treatment duration on neuronal survival after axotomy. Four groups (n=4) of adult male Sprague Dawley rats underwent standardised sciatic nerve transection and capping operations. The animals in these groups were then treated with NAC at 150mg/kg/d for 7 days, 14 days, 30 days and 60 days respectively, with all groups surviving for the full 60 days **(Figure 2.1)**. L4 and L5 DRG were histologically processed for stereological neuron counting.

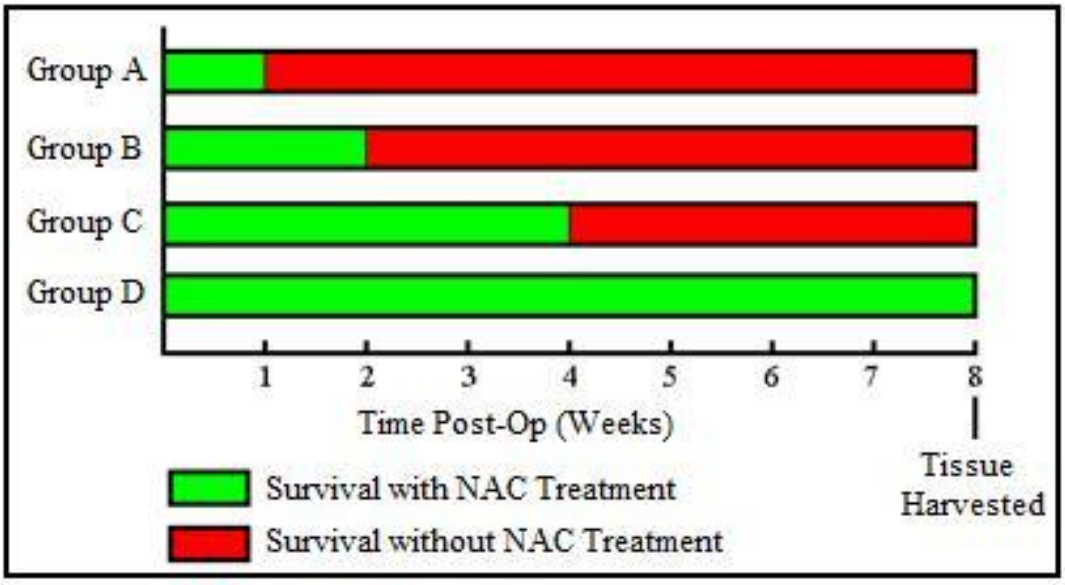

Figure 2.1: Diagrammatic representation of the experimental design of the NAC treatment duration study

2.2 MATERIALS & METHODS

2.2.1 PRACTICAL PROCEDURES

2.2.1.1 Animals

All animals used during the investigations were young adult male outbred albino Sprague Dawley rats (Harlan Sprague Dawley Inc.), mean starting weight 243.65g (SD 26.43g). The animals were housed in the Biological Services Facility of the University of Manchester, where daily veterinary advice was available. All work was performed under the auspices of the Animals (Scientific Procedures) Act 1986 (ASPA 1986), after completion of an in house training programme approved by the Universities Accreditation Scheme.

2.2.1.2 Anæsthesia, Monitoring and Analgesia

All surgical procedures were performed under Isoflourane® inhalational anæsthesia (5% Isoflourane delivered in 100% oxygen at 2l/min). Full anæsthesia was characterised by loss of the righting reflex, pain withdrawal but with stable spontaneous respiration. On

the operating table this anæsthetic plane was maintained via a nose mask with 1.5-2.5% Isoflourane delivered in 100% oxygen at 0.5L/min, and confirmed by frequent assessment of the corneal reflex and withdraw response to hind paw web space pressure and direct visualisation of respiratory motion. Following surgery the animals were recovered by turning off the anæsthetic vaporiser but maintaining the flow of 100% oxygen until some spontaneous movement was observed. Once conscious, the animals were transferred to a warming cabinet (35°C) with provision of softened food and water. Once fully recovered the animals were again removed into larger communal cages (2-4 animals per cage) and returned to their normal housing environment. After invasive procedures, postoperative analgesia was provided with a single subdermal injection of the opioid buprenorphine (Temgesic^{TM}) at 0.03mg/kg during recovery from anæsthesia.

2.2.1.3 Sciatic Nerve Transection and Capping (SNTC)

After induction of anæsthesia the animal was positioned on its side and the fur over the hind limb shaved. The area was disinfected using 0.5% clear chlorhexidine gluconate and a 2cm wound was made 1cm caudal to the hip joint following the line of the femur. The skin was retracted and blunt dissection used to make a muscle splitting incision in the *biceps femoris* and *gluteus superficialis* muscles exposing the sciatic nerve running in the plane deep to these and superficial to the *adductor* and *semimembranosus* muscles.

Under operating microscope magnification (x3.8) a 1cm long segment of nerve was freed from its connective tissue envelope using blunt dissection and atraumatic epineural nerve handling. The nerve was double ligated with a 6/0 polyamide 66 (Ethilon^{TM}) suture at a level corresponding to the upper border of the *rectus femoris* muscle. The nerve was then transacted with a single cut of straight bladed microsurgical scissors between these sutures. The cut ends of the nerve were sutured into the pre-made sterile silicone caps using 9/0

polyamide 66 (Ethilon^{TM}) to act as a physical barrier to regeneration. To further prevent any regeneration or distal to proximal stump signalling, the capped ends were turned away from each other and buried in separate intramuscular pockets with 5/0 polyglactin 910 (Vicryl^{TM}) sutures.

The muscle layers were closed with a single continuous 4/0 polyglactin 910 (Vicryl^{TM}) suture. The skin was apposed using the same material, firstly with a continuous subcuticular stitch with buried knots, followed by simple interrupted superficial stitches.

2.2.1.4 *N*-acetylcysteine Treatment

Animals which had undergone sciatic nerve transection and capping were treated with NAC at 150µg/kg/day given by intraperitoneal injection into the lower abdominal quadrant on the side contralateral to the operation. NAC used was Parvolex® (UCB Pharma) which was supplied as 10ml glass vials of 200mg/ml, containing the additives, sodium hydroxide disodium edetate and water for injection. The solution was stored at 4°C and was made up daily for injection with sterile normal saline (NaCl 154mmol/l) to a volume of 0.5ml. The animals were weighed every third day during the duration of treatment and the doses adjusted appropriately. No complications at the injection site occurred during the experiments.

2.2.1.5 Animal Euthanasia

In order to humanely kill the animals before tissue harvesting, the animals were placed individually into an air filled induction box, which is then filled with 100% carbon dioxide (CO_2) at a rate of 2L/min for 5 minutes. Subjected to this slowly rising concentration of gas, the animal gently lost consciousness; death was confirmed by cervical dislocation.

2.2.1.6 Dorsal Root Ganglia Harvest

Following MR scanning (*cf.* Chapter 3), a midline dorsal skin incision was made from the mid-thoracic region to the base of the pelvis, and the skin removed bilaterally down to the muscular fascia over the animal's rump and hind limbs. The pelvis and lumbar vertebræ were exposed by removal of the paravertebral and posterior abdominal wall muscles. The sciatic nerve or its divided branches were exposed by dividing the overlying muscles similarly to the surgical procedure. On the operated side, the nerve stump was inspected to ensure that the caps had remained *in situ* and that regeneration had not occurred. The proximal stump was then followed cephalad to the sciatic notch of the already exposed pelvis. The sacroiliac joints were disarticulated and the posterior part of the sacrum and the vertebral transverse processes were removed with bone nibblers to allow exposure of the intrapelvic course of the sciatic nerve and its constituent spinal nerves up to the exit of these nerves from the intervertebral foramina.

Using micro-rongeurs the rest of the neural arch of the lumbar vertebræ was removed exposing the spinal cord, roots and the DRG. The L4 and L5 DRG were verified by counting caudally from the L1 vertebra and were removed by cutting with micro-scissors, leaving a length of the roots proximally and spinal nerve distally to allow correct orientation during later stages of tissue processing. The freed DRG were then placed in labelled vials containing 4% paraformaldehyde. In all experiments L4 and L5 from both the axotomised and contralateral, non-operated sides were collected, the latter acting as internal controls.

2.2.2 HISTOLOGICAL TECHNIQUES

2.2.2.1 Fixation, Cryoprotection, Blocking and Storage

Harvested DRG were fixed in 4% paraformaldehyde for 72h at 4°C, followed by washing in PBS solution and immersion in a cryoprotection solution of 15% sucrose with 0.1% sodium azide in PBS. Three changes of this solution were made over 48h, again at 4°C. After cryoprotectant equilibration the spinal nerve and rootlets of the DRG were trimmed and the tissue immersed in OCT (Bright®) embedding medium, using 10x10x12mm aluminium foil 'boats' made using a Perspex template. The filled boats, containing the appropriately aligned DRG, were snap frozen over liquid nitrogen and then stored at -40°C until sectioning.

2.2.2.2 Cryostat Microtomotomy

Frozen sectioning was performed on a Leica™ CM30505 Cryostat, with the chamber and chuck temperatures set to -24°C. DRG were cut transversely at 50μm and thaw mounted on to glass slides coated with Vectabond™ reagent (Vector Laboratories Inc) to increase tissue adhesion. All sections from the DRG were collected, with twenty sections being positioned serially onto each slide, aligned using a pre-marked template applied to the back of the slide. The DRG were randomly aligned with respect to their axial plane within the OCT block, therefore providing variability in the exact orientation of the sectioning which is a prerequisite of Cavalieri volume estimation (Gundersen and Jensen, 1987). Enough of the proximal nerve roots and distal spinal nerve were included in the sectioning to ensure that the whole of the DRG neuron containing tissue was sectioned. Sections were placed in racks and dried at 50°C overnight before staining.

2.2.2.3 Fluorescent staining

DRG tissues were stained with a combination of bisbenzimide H33342 (Hoechst; λEx. 343nm, λEm. 483nm) and propidium iodide (PI; λEx. 536nm, λEm. 617) **(Appendix 4)**. Bisbenzimide is an intercalating fluorescent nuclear stain, binding DNA between the adenine/thymine base pairs (Ciancio *et al.,* 1998); propidium iodide binds stoichiometrically to both DNA and RNA, and stains cytoplasm if the tissues have been permeabilised (Riccardi & Nicoletti, 1996). Staining was carried out in a Perspex slide incubator with all solutions applied directly to the slide in an attempt to reduce section loss. Axotomised and control DRG from each animal were always stained simultaneously. After staining, the slides were mounted using fluorescence protecting Vectashield™ medium (refractive index 1.44). Coverslips were sealed using DPX, and the slides stored in light exclusion boxes at 4°C prior to quantification.

2.2.4 STEREOLOGICAL NEURON ESTIMATION

2.2.4.1 Neuron population estimation – The Optical Fractionator

Estimates of the neuronal population in the sciatic pool vary with counting technique used, but are in the region of 14000-20000 neurons in L5 and around 30000 in L4/L5 (Bergman & Ulfhake, 1998; Tandrup, 1993; Groves, 1997; McKay Hart *et al.,* 2002a). This large population favours stereological estimation rather than serial reconstruction. The statistically unbiased optical fractionator technique combines neuron counting using an optical dissector with the fractionator method of systemic random sampling (West *et al.,* 1993; Dorph-Petersen *et al.,* 2001).

The equipment used for stereology comprised of an Olympus BX61 epiflourescence microscope fitted with motorized stage allowing controlled movement in the X-Y planes, and which monitors the excursion of the objective lens in the z-axis during focussing. An

Olympus WU fluorescent filter (excitation 330–385 nm, dichroic mirror 400 nm, emission >420 nm) allows simultaneous visualisation of both the PI and H33342 staining, with a live video output to a computer installed with Stereo Investigator™ 6 software (SI) (MicroBrightField, Inc).

A systemic random selection of neuron containing sections is sampled; under x10 magnification, and with the filter set to visualise PI staining, those DRG sections containing neuronal cell bodies were identified. A random number generator was used to allocate one of the first four of these as the start section; this and each subsequent 4th section were quantified until the full neuron containing region had been sampled, ensuring a representative sample of >10 sections for each DRG. The neuron containing area of each section was outlined and the SI program overlaid a randomly orientated virtual sampling grid onto this selected area, ensuring that quantification sites were also chosen according to the rules of systematic random sampling **(Figure 2.2)**.

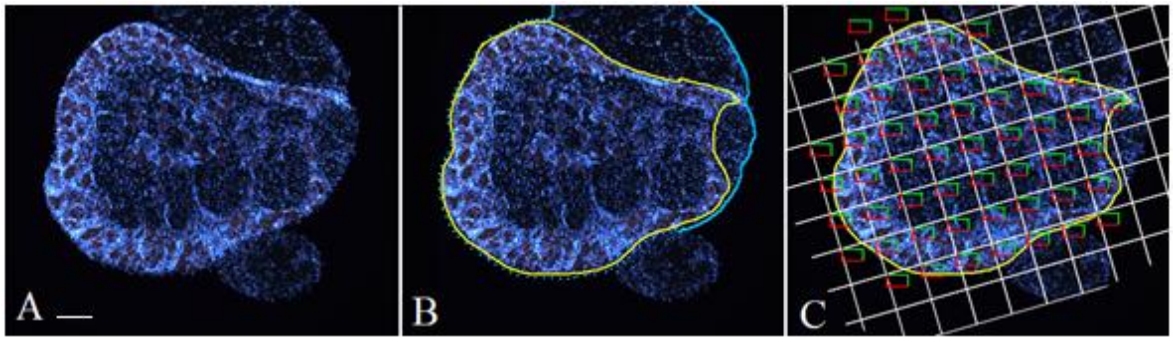

Figure 2.2: Summary of the sampling undertaken by Stereo Investigator® software. A - A single section of DRG stained with propidium iodide (showing neuronal cytoplasm red) and Hoechst 33342 (nuclei are pale blue) viewed at x10 magnification under the WU-fluorescent filter. B – Tracing boundaries; demonstrating the difference between the neuron containing area (yellow outline) and the whole DRG perimeter (blue) (*cf*. Chapter 3). C – The application of the randomly orientated sampling grid (white) applied with relation to the neuron containing region (yellow outline), and its relationship of this to the counting frames/dissectors (red and green boxes) used for optical dissection. Note that if any part of the traced area enters a sampling grid site a dissector will be applied, even if that dissector does not cover part of the section. Scale bar = 50µm.

Switching to a narrow plane of focus using a parafocalised x60 oil immersion objective lens and the H33342 filter the optical dissection was commenced. With the microscope stage under control of SI each site on the sampling grid was visited. A three-dimensional virtual counting frame (dissector) was then constructed by SI within the thickness of the tissue section; each dissector has three mutually perpendicular inclusion and exclusion faces **(Figure 2.3)**.

Focusing through the section, neurons were counted if their nuclei came into focus within the counting frame providing that no part of the nucleus crossed one of the exclusion faces. Application of these counting rules assures population estimates are not affected by cell size, shape, distribution or density (Gunderson *et al.*, 1998a, 1998b; Hart & Terenghi, 2004) **(Figure 2.4)**. To compensate for neurons plucked from the leading edge of the tissue during sectioning a 'guard zone' is included between the top of the section and the start of the dissector (Dorph-Petersen *et al.*, 2001).

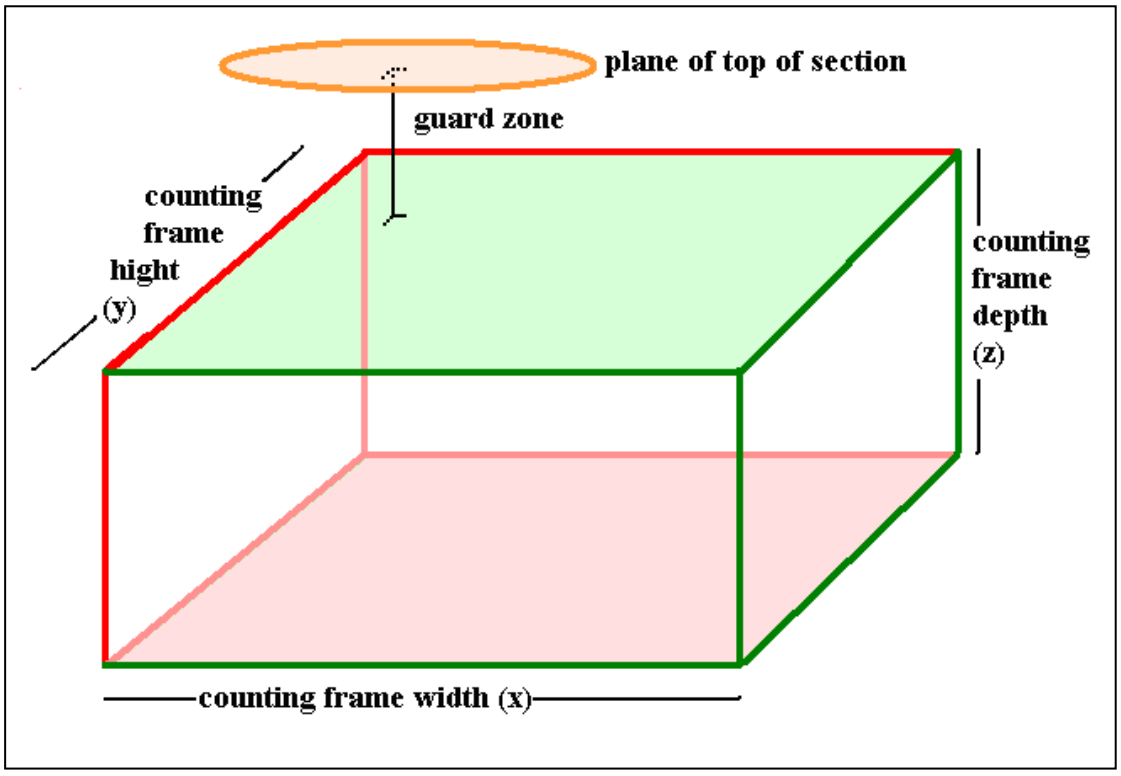

Figure 2.3: Caption over.

Figure 2.3 (Previous page): Diagram of Optical dissector - The superior facing, viewer facing and right facing surfaces are 'inclusion' planes; neurons crossing these, but not their opposite counterparts are counted.
.

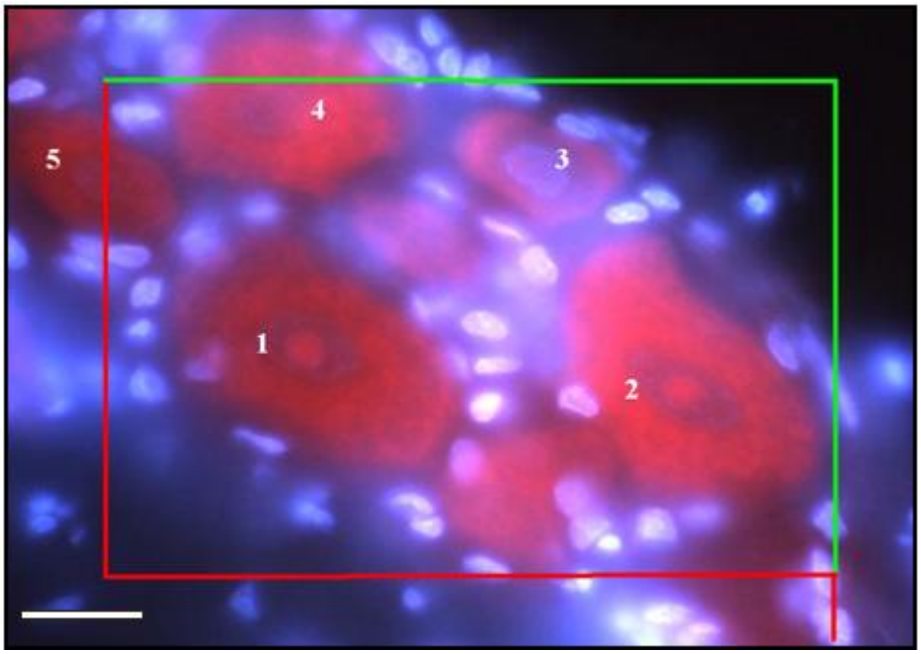

Figure 2.4: Optical Dissection, x60 magnification view of same tissue as figure 2.2. Neuron nuclei '1' and '2' are in focus within the bound of the dissector and are thus counted. Neuron '3' was in focus at a plane superficial to the ceiling of the dissector and is thus excluded. Neurons '4' and '5' have yet to come into focus, if they do so within the depth of the dissector '4' will be counted, however '5' would cross an exclusion plane and therefore not be counted. Scale bar 20µm.

Estimated neuron populations can be calculated because the ratio of DRG actually sampled to the whole neuron containing volume is known i.e. the fraction of the total number of sections, the fraction of the sectional area and the fraction of the dissector depth to the measured section thickness **(Table 2.1)**. Multiplication of the reciprocal of these fractions gives a neuron estimate for the whole DRG:

$N = Q.(t_{nw}/d).(1/asf).(1/ssf)$

Where:

N = Population neuron estimate

Q = Measured neuron count

t_{nw} = Number weighed section thickness

d = Depth of dissector

asf = Area sampling fraction

ssf = Section sampling fraction

Number weighed section thickness is used in this calculation rather that mean section thickness in order to minimise the biasing effect of any homogeneous non-uniform tissue shrinkage (Dorph-Petersen *et al.*, 2001). The measured section thickness at each counting site received a number weighting proportional to the quantity of neurons counted in that dissector; the mean of these weighted thicknesses is used.

Table 2.1: Parameters for Stereological Neuron Estimation	
Section Periodicity	4
Sampling Grid (x)	250 µm
Sampling Grid (y)	250 µm
Sampling Grid Area (xy)	62500 μm^2
Counting Frame Depth (z)	12 µm
Counting Frame Width (x)	110 µm
Counting Frame Height (y)	110 µm
Counting Frame Area (xy)	12100 μm^2
Counting Frame Volume (xyz)	145200 μm^3
Upper guard zone (z)	6 µm
Section Thickness (cut)	50 µm
Section Sampling Fraction 0.25	0.25
Number Weighted Mean Section Thickness	Measured
Area Sampling fraction (Grid to Frame)	0.194

2.2.5 DATA ANALYSIS AND STATISTICS

All analyses were performed blind to the axotomised side of the animal. Significance of differences between axotomised vs. control sides were analysed using student's t-test while one-way ANOVA with Bonferonni post-hoc testing was used for intergroup analysis. All statistical comparisons were carried out using GraphPad Prism®(v 4.03) software.

2.3 RESULTS

There were no significant differences between the non-axotomised control side neuron counts between groups. No significant neuronal loss was demonstrated in animals treated every day from injury until death (t –test of axotomised vs. control $p = 0.2$). All groups with partial therapy had lower neuron counts in the axotomised ganglia than the control side quantitatively related to the period of NAC administration, with a reducing degree of significance when compared using intra-group t-testing (7d control vs. axotomised $p < 0.005$; 14d control vs. Axotomised $p < 0.05$; 30d control vs. axotomised $p < 0.05$) **(Table 2.2, Figure 2.5)**.

As well as absolute neuron counts, data relating to neuron loss were analysed; with neuron loss being calculated as 'control neuron count - axotomised neuron count', with the difference being expressed as a percentage of the control count, inter-group comparisons were made by one-way ANOVA with Bonferonni post-hoc comparisons.

Table 2.2: NAC Treatment Duration Study - L4+L5 Neuron Counts				
Treatment Duration	Control Ganglia (L4+L5) mean (SD)	Axotomised Ganglia (L4+L5) mean (SD)	Mean Neuron Loss	Mean Percentage Neuron Loss
7 Days	30940 (1095)	24999 (441)	5941**	19.16%**
14 Days	30202 (170)	27410 (512)	2792*	9.24%*
30 Days	31578 (1017)	29790 (930)	1787*	5.64%*
60 Days	32279 (380)	32038 (388)	-56	-0.17%
Where ** = p<0.005 and * = p<0.05 on intra-group t-testing				

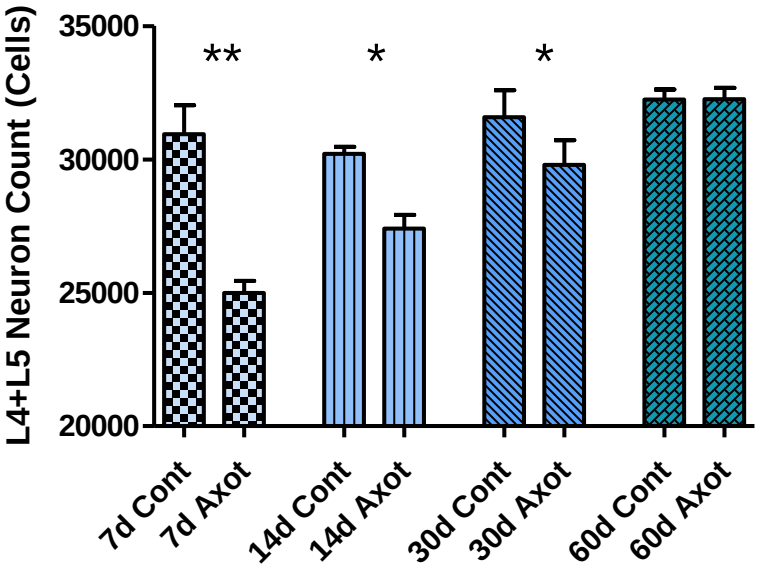

Figure 2.5: Effect of NAC duration of treatment on L4+L5. Plotted as combined neuron counts with SD. Asterisks relate to intra-group t-testing: ** = p < 0.005; * = p < 0.05

There was no significant neuronal loss in the 60d treatment group compared against no loss (-0.17%, SD 0.74%, ANOVA vs. 0 p > 0.05). In the partially treated groups there was highly significant neuron loss with only 7 days treatment compared to the experimental control of full treatment (19.16%, SD 1.47%, ANOVA vs. 60d p > 0.005) and 14 days (9.24%, SD 2.10%, ANOVA vs. 60d p<0.005) and less strongly significant loss for 30 days (5.64%, SD 2.00%, ANOVA vs. 60d p>0.05) **(Table 2.2 and Figure 2.6)**.

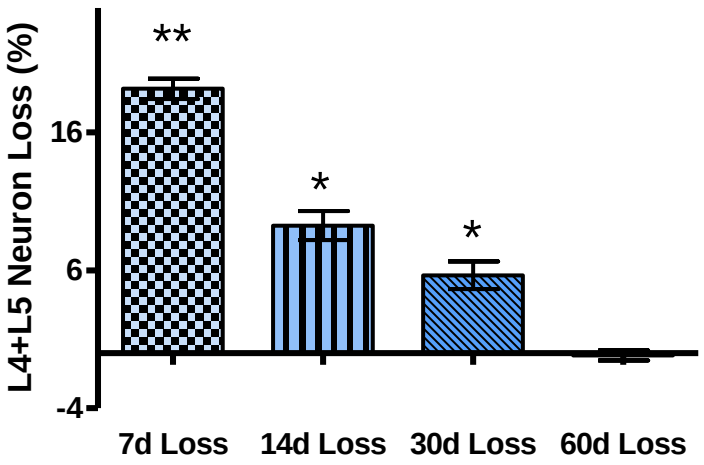

Figure 2.6: Effect of neuron loss with treatment duration with NAC. Aterisks represent significance in one-way ANOVA vs. 60d treatment (** = $p < 0.005$, * = $p < 0.05$)

2.4 DISCUSSION

2.4.1 METHODOLOGY AND EXPERIMENTAL DESIGN

2.4.1.1 Animal Model

The animal model of mid-thigh sciatic nerve transection and capping is a well recognised technique, is relatively simple to perform and has been consistently confirmed to prevent any spontaneous nerve regeneration (Hart *et al.* 2002; Wilson *et al.* 2003; Hart *et al.* 2004a; Wilson *et al.* 2007; West *et al.*, 2007). The use of the upper border of the quadratus femoris muscle as an anatomical landmark for the site of nerve division serves to standardise the injury, since the proximity of a transection to the DRG affects neuron loss (Ygge 1989).

No problems were encountered during recovery from Isoflourane anæsthesia, and observation of normal animal behaviour and lack of signs of discomfort postoperatively

suggests that buprenorphine analgesia is effective. The method of wound closure was modified from that of previously published work by the addition of a subcuticular suture underlying the usual superficial interrupted stitches after three animals suffered wound dehiscence on the first postoperative day. Wound opening did not recur after this modification.

Animals tend to chew the nails and toes of denervated feet after sciatic transection (McVean, 1975; Weber, 1993), with this 'autotomy' behaviour primarily affecting the lateral aspect of the foot and third to fifth digits. There is sparing of the medial foot and toes, reflecting their innervation by the saphenous branch of the femoral nerve which is not injured during sciatic transection (Devor *et al.*, 1979). Veterinary consultation was sought for all animals which had autotomised to any extent, and early withdrawal from the study and sacrifice advised for any rat in which this was deemed to adversely affect animal welfare. Autotomy rates and animal loss were significant enough to lead to at least one repeat of the experiment, eventually reaching group numbers of n=4, however, rates of autotomy encountered were within the range of previously published studies (Blumenkopf & Lipman, 1990; Lewin-Kowalik *et al.*, 2002; Clavijo-Alvarez *et al.*, 2007).

2.4.1.2 Experimental design

Critical appraisal of this experiment raises some methodological questions which must be discussed. The first of these is animal number within groups, previous experiments by our research group have published data based on analysis of 6 animals per group (McKay Hart *et al.*, 2002a, Hart *et al.*, 2002; Hart *et al.*, 2004a) or n = 5 per group (Wilson *et al.*, 2003; West *et al.*, 2006a; Wilson *et al.*, 2007) and this is the first experiment in which n = 4 has been submitted. The use of n = 4 was not through choice, but reflected surviving animals who had not undergone significant autotomy. While using higher numbers of subjects

adds increased validity to statistical findings, in the present study as stands, significant differences between groups were found; it has to be accepted that the effect of two similar counts with a group may have exaggerated significance as group number reduces.

The second issue is the fact that this study does not include absolute (no operation) control, sham operation control and no-treatment groups. This again pertly reflects autotomy attrition from groups as only animals surviving for the full sixty days have been included – decisions regarding experimental planning were made in consultation with the Home Office Inspector. In defence of the presented methodology, all previous work using similar techniques has shown no significant neuronal cell loss for absolute control groups or sham operated groups, and there is no reason to assume that this study should be any different (Hart *et al.,* 2002a; Hart *et al.,* 2002b; Wilson *et al.,* 2003; Hart *et al.,* 2004a; West 2007a). Further, the findings of West *et al.,* 2007b suggest that using non-operated side internal controls gives a more sensitive index of neuronal loss that comparison with another group of absolute control animals. Exclusion of a 'no treatment' group represents logistical restraints due to animal autotomy and guidance by the Home Office Inspectorate and cognisant of the principle of 'reduction' in laboratory animal work. All previous experiments by our research group that have included two month survival point for control-operated animals have reported predictable loss of around 35% (McKay Hart *et al.,* 2002a, McKay Hart *et al.,* 2002b; Hart *et al.,* 2004). Lacking repeat data specific to this experiment, tentative comparison with these findings will be made.

2.4.1.3 Stereology

Optical dissection combined with systemic random sampling is a robust, theoretically sound technique. It avoids the statistical bias of assumption based estimation techniques (Hedreen, 1998; West, 1999) and, by the inclusion of adequate guard zones at the top and

bottom of the section, does not suffer from underestimation inherent in a physical dissector due to lost neurons (West 1993). Use of the dissector for DRG neuron populations has been verified against empirical measurements (Pover & Coggeshall, 1991).

The use of fractionator sampling when estimating neuronal populations is theoretically more valid than using a density based calculation as was used in earlier work (McKay Hart *et al.*, 2002a; McKay Hart *et al.*, 2002b; Wilson *et al.*, 2003; Hart *et al.*, 2004a) because the final neuron count is independent of the size of the sampled region. The fractionator technique therefore does not rely on the accuracy of the contour tracing of the neuron containing area – hence excluding one observer dependent measurement variable. For all assessed ganglia, greater than 100-200 neurons were counted, which is a prerequisite for accurate population estimate (West 1999), and the proportion of the size of the counting frame to the counting grid was well over 4% (Harding *et al.*, 1994).

The L4+L5 neuron populations in non-axotomised ganglia measured in the NAC treatment duration studies were equivalent to those described previously by members of our group (Hart *et al.*, 2002; Wilson *et al.*, 2003; Hart *et al.*, 2004a; Wilson *et al.*, 2007; West *et al.*, 2007b) and by others using optical (Bergman & Ulfhake, 1998; Tandrup, 1995) and physical (Groves *et al.*, 1997) dissectors. Standard deviations of neuron populations for L4+L5 in the NAC treatment duration study were generally within the range of those in previous optical dissector experiments, (400-10000 neurons) with a few unexplained exceptionally low values, possibly reflecting two or three animals having similar counts in an experiment with lower animal number per group (*cf.* 2.4.1.2), standard deviations would be likely to increase with biological variation if more animals were analysed.

*2.4.3 N-*ACETYL CYSTINE TREATMENT DURATION

The potential to promote primary sensory neuronal survival after peripheral nerve injury using the novel paradigm of pharmacotherapy with NAC or ALCAR has been well established and the optimal doses of each agent determined with dose response analyses (Hart *et al.,* 2002b; Wilson *et al.,* 2003; Hart *et al.,* 2004a; West *et al.,* 2007b).

All previous experiments have demonstrated that with optimal dose therapy (NAC or ALCAR) given continuously from the day of axotomy until death of the animal, *complete neuroprotection* is achievable, the results of the 60d treatment group in the present NAC treatment duration study again verify this possibility. Of prime importance to clinical translation of NAC/ALCAR treatment, is to investigate the logistics of such therapy; it was demonstrated that for sensory neurons, a delay in beginning ALCAR therapy for up to 24h post injury, such as is likely to occur in clinical practice, did not adversely affect neuronal survival at two week post injury (Wilson *et al.,* 2007). However, a delay of seven days, while still providing some benefit over no treatment, allowed ≈20% cell death to occur. These finding demonstrate the clinical necessity of starting treatment as soon as possible post injury to maximise benefit. It is noted that this delay in treatment experiment used ALCAR, and that a similar study has not been performed evaluating sensory neurons with NAC treatment. The only data pertaining to NAC and treatment delay comes from a study of spinal cord motor neuron neuroprotection with high dose intrathecal NAC after spinal motor root avulsion; one week delay in treatment did not significantly alter neuron loss versus full treatment, but effects were deleterious with a two weeks delay (Zhang *et al.,* 2005).

The NAC treatment duration study was designed to investigate how long treatment should continue. The time points selected for analysis were chosen cognisant of the work of

McKay Hart *et al.,* (2002a); which demonstrated that after axotomy with no treatment, 7 days was first point at which neuronal loss became significant, 14 days corresponded to the time of peak apoptosis rate, and that the majority of cell death had occurred by two months post axotomy. Thirty days was also chosen as an intermediate period, where the rate of apoptosis was beginning to level, but some death still occurring.

With no treatment at two months post axotomy there was a 35% neuronal loss (McKay Hart *et al.,* 2002a & b). In all groups in the treatment duration study there was substantially less neuronal death (7 day treatment ≈19%; 14 day treatment ≈9%; 30 day treatment ≈6%; 60 day treatment ≈0%) suggesting that even relatively short duration of treatment has a significant neuroprotective effect. This was the first study in which a period of time elapsed between cessation of treatment and DRG harvest, and it can be concluded that rather than apoptosis being simply delayed by NAC therapy, the neuroprotective effect is long-lasting; a large proportion of cells which wound have died with no treatment have actually survived.

The molecular mechanisms of the pro-survival effect of NAC remain incompletely understood, but it probably reflects synergistic effects of NAC to modify multiple cellular systems (*cf.* 1.2.4.3). NAC has innate reducing activity (Aruoma *et al.,* 1989; Kamata *et al.,* 1996; Yan *et al.,* 1995) and supplements intracellular glutathione levels (Yan *et al.,* 1995), both of which may affect neuronal redox status, possibly resisting oxidative stress, which is implicated in the ætiology and execution of the apoptotic programme within denervated neurons (Martin *et al.,* 1998; Novikov *et al.,* 2005). Further, NAC has anti-proliferative activity (Sekharam *et al.,* 1998) and causes modification of intracellular signalling and transcription events such as activation of p21Ras, a signalling pathway

essential for neuroprotection of PC12 cells after trophic factor withdrawal (Kamata *et al.*, 1996).

McKay Hart *et al.,* (2002a) found little difference between neuronal losses at two months versus six months with no treatment; therefore it is likely that not all axotomised cells will undergo apoptosis even without any neuroprotective treatment. It seems likely that NAC therapy could function by two broad mechanistic paradigms, although these need not be mutually exclusive. NAC could reduce the toxic effects of axotomy directly, for example by free radical scavenging or activation of the downstream effectors of the neurotrophin signalling cascades; this would lower the magnitude of the noxious stimulus delivered to the entire neuronal population as a result of neurotrophin withdrawal, and therefore it would increase the number of individual cells receiving a 'dose' of toxicity below that cell's 'lethal' threshold. Alternatively, NAC could affect specific subpopulations of neurons, raising their tolerance to pro-apoptotic stimuli, such as BCL-2 to BAX ratios at a transcriptional level (Reid *et al.,* 2009), or blocking abortive entry of some populations into the cell cycle (Ferarri *et al.,* 1995). Specific neuronal subpopulations have been demonstrated to react differently to axotomy, with cutaneous fibres sustaining a higher rate of death than muscle propreoceptive fibres with this being mirrored by up-regulation of pro-apoptotic molecule transcription as detected by real time (RT)-PCR in cutaneous fibres (Welin *et al.,* 2008; Reid *et al.,* 2009). Treatment of axotomised animals with NAC in this model reduced transcription of pro-apoptotic Caspase 3 and modifies BCL-2 to BAX mRNA expression ratio such that anti-apoptotic BCL-2 predominates (Reid *et al.,* 2009). The reasons and mechanisms behind such subpopulation behaviours remain unknown.

Translation from a murine model to clinical therapy in the human population may not be direct, and to date no studies of neuroprotectant administration after nerve injury in man

have been performed. Before translation, significant decisions to be investigated such as a choice of proxy measure of neuronal population change (*cf.* Chapter 3), dosing regimen (West *et al.,* 2007a), dosing method given NACs significant first-pass metabolism is likely to reduce the effectiveness of oral administration (Cotgreave *et al.,* 1987; Cotgreave, 1997) and duration of therapy.

In the human clinical scenario of a mixed nerve injury, treatment with NAC rather than ALCAR seems to have intuitive merit as NAC can also protect motor neurons (Zhang *et al.,* 2005), although this benefit needed higher doses than to prevent death of cutaneous sensory populations. The optimum dose of NAC for sensory cell protection post-sciatic neurotomy in rats has been demonstrated to be around 150mg/kg/d (West *et al.,* 2007a). However doses delivered clinically may need to be adjusted in proportion to the mechanism of nerve injury i.e. crush, transection or avulsion, which have been demonstrated to affect degree of neuronal apoptosis (Groves *et al.,* 1997; Degn *et al.,* 1999; McKay Hart *et al.,* 2002a; Zhang *et al.,* 2005). Also the additional need to protect motor neurons has to be taken into consideration, as for their survival intraperitoneal doses up to 750mg/kg/d is needed (Zhang *et al.,* 2005). Furthermore, the site of injury along the nerve's proximo-distal axis has to be evaluated, as more proximal injuries such as brachial plexus pathology resulting in a greater degree of neuronal death (Ygge, 1989).

Intraperitoneal injection such as used in this model by-passes first pass hepatic metabolism and is thus proposed as equivalent to intravenous (IV) therapy in man. NAC has a long history of IV use in paracetamol (acetaminophen) overdose with a good record of safety other than minor hypersensitivity reactions in 0.2-3% of patients (Prescott *et al.,* 1979; Mant *et al.,* 1984; Mahadevan *et al.,* 2006). The plasma half-life of NAC in humans is in the region of 5.6h in human adults (Olsson *et al.,* 1988; Prescott *et al.,* 1989) meaning that

by the end of a 24h period only about 1/16th of a once daily dose would be present in plasma. The current dosing regimen for paracetamol intoxication is continuous infusion (150mg/kg over 15m followed by 50mg/kg over 4h and finally 100mg/kg over 16h), giving a total of 20 ¼ hours of treatment (British National Formulary 2009). Given that a patient with a mixed nerve injury is likely to be an inpatient for several days is would seem to make practical sense to treat patients either with multiple IV doses per day or a continuous NAC infusion such as used above for paracetamol toxicity for the duration of their pre-, and post-operative inpatient stay. Treatment may be more difficult to continue once a patient is otherwise fit for discharge; the oral bioavailability of total NAC is only around 9% (Olsson *et al.*, 1988) suggesting that very high doses of oral NAC might be needed to provide adequate intracellular concentrations. In the NAC dose response study a small but significant neuroprotective effect was found with treatment at 10mg/kg/d (West *et al.*, 2007a), it could be that oral dosing, while less potent than IV administration may still confer some benefit in the post-op patient population. An alternative strategy might include continuous subcutaneous infusion of NAC; bronchodilator administration by such means on an ambulatory, out-patient basis is well established to treat the subset of severe asthmatics unresponsive to traditional therapy (Cluzel *et al.*, 1990). Animal studies to investigate subcutaneous administration of NAC are lacking, but would be easy to perform in future.

Extrapolation of the results of the treatment duration study presented here to clinical application of NAC therapy would suggest that a large proportion of sensory neuronal cells at risk from apoptosis after nerve injury could be saved with one month's NAC therapy, but the maximal effect is likely only to be achieved by maintaining treatment until regenerating axons come again in contact with an endogenous source of neurotrophic support. Nevertheless, in the light of the prolonged regeneration time required after

proximal neurotomy, and given the often suboptimal patient compliance with long-term medication (Chapman, 2004), especially in the younger patient population (Staples & Bravender, 2002) to whom nerve injury most commonly occurs (Jaquet *et al.*, 2001), it is reassuring to believe that a relatively short duration of NAC therapy may support substantial primary sensory neuronal survival.

CHAPTER 3

Assessment of Magnetic Resonance Imaging to Assess the *N*-acetylcysteine Treatment Duration Study

3.1 BACKGROUND & EXPERIMENTAL DESIGN

Before translation of the potential benefits of NAC neuroprotective therapy to the human clinical arena (*cf.* 2.4.3) there is the need to develop a reliable, non-invasive measure or proxy-measure of dorsal root ganglion neuronal populations because current clinical tests of nerve regeneration such as two-point-discrimination, are subjective, variable and unreliable (Lundborg & Rosen, 2004; Jerosch-Herold, 2005). Magnetic Resonance volumetric analysis of neuronal structures has a clear precedence in human neurobiology (*cf.* 1.3.2.2) and based on this idea, the previous work by our group suggests that *ex vivo* L4 ganglion MRI volumetric analysis could provide a non-invasive and non-irradiating index of DRG volume and therefore proxy measure of neuron loss (West *et al.*, 2007b). In this chapter, the ability of the MRI scanning protocol (West *et al.*, 2007b) to correlate the survival of DRG neuronal populations with the effect of the NAC treatment duration study (*cf.* Chapter 2) will be assessed.

The MRI protocol used in this study images both right and left L4 DRG and as such allows for using the non-axotomised ganglia as an internal control. A series of assumptions must be made if L4 only MRI DRG volumetry is to be used as a sole outcome measure of an experiment; first that assessment of L4 only versus L4 plus L5 totals for neuron counts is valid, second that DRG volumetry does function as a proxy measure of neuronal cell death and third, that MRI imaged DRG volume provides a valid index of both histological DRG volume and neuron counts. Each of these assumptions will be tested using the results of the NAC treatment duration study.

The experimental NAC treatment was identical to that shown in chapter 2 (*cf.* 2.1; 2.4.1.2) with four groups of four animals undergoing standardised sciatic nerve transection and capping, and being treated with 150mg/kg/d intraperitoneal NAC for 7 days, 14 days, 30

days or 60 days with all animals surviving for the full 60 days before MRI scanning and histological quantification of L4 and L5 DRG volume and stereological neuron counts.

3.2 MATERIALS AND METHODS

3.2.1 SURGERY, NAC TREATMENT AND MORPHOMETRY

Surgery, animal welfare, preparation of the histological slides and stereological neuron counting of axially sectioned L4 and L5 from control and axotomised DRG were carried out as described in chapter 2 (*cf.* 2.2.1.1 - 2.2.4.1), with slide labelling being coded so as to blind the researcher to the animal and side of origin.

3.2.2 MAGNETIC RESONANCE IMAGING OF THE L4 DORSAL ROOT GANGLION

MRI scanning of each animal was performed on the day of animal euthanasia at 60 days post sciatic nerve transection. The operating schedule was designed so that only 2-3 animals reached the 60d time point on any given day, allowing scanning immediately after the animal was killed and minimising delay of DRG harvest and fixation post-mortem. Imaging was carried out on a 7T actively shielded 15cm horizontal bore MRI scanner (Magnex UK Ltd, Abingdon) driven by SMIS console software (Magnetic Resonance Research Systems, Guildford UK) housed in the Department of Imaging Science in the University of Manchester **(Figure 3.1)**. A 2cm custom built transmit/receive surface radio-frequency coil was used for all DRG imaging **(Figure 3.2)**.

Figure 3.1: The University Of Manchester's 7T small animal MRI scanner.

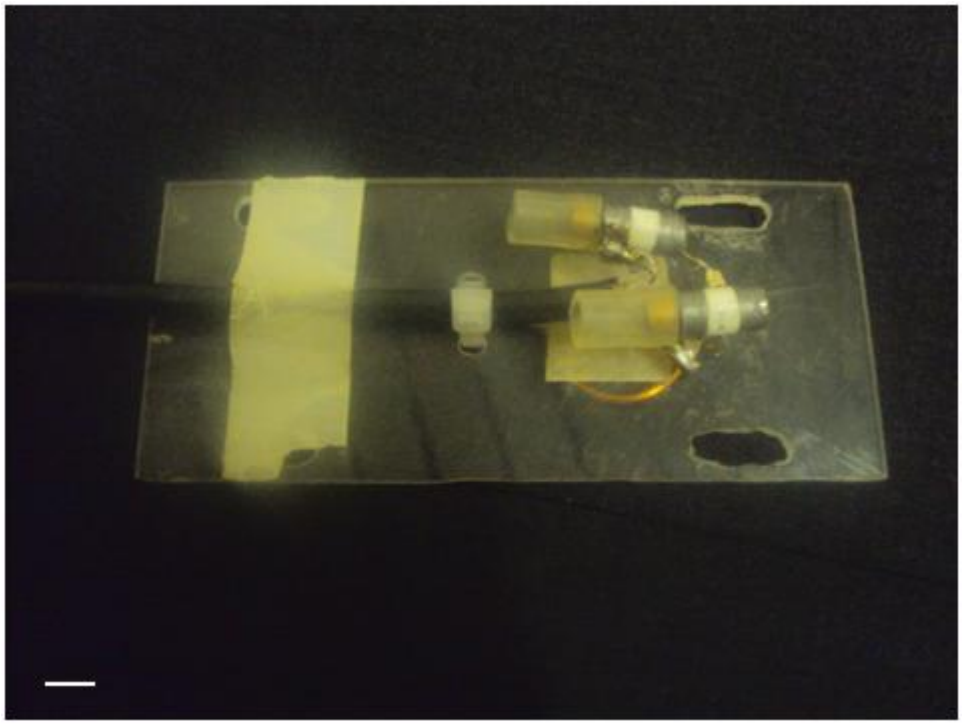

Figure 3.2: The 2cm surface coil. This is secured to the animal's back, with the copper wire loop centred over the L4 area. Scale bar 1cm.

3.2.2.1 Animal positioning

After the animal had been killed, it was positioned within a plastic 'probe' in order to hold it steady within the magnet bore **(Figure 3.2b)**. The surface coil was centred over the area of the L4 DRG (1cm cranial to a line transecting the tips if the iliac crests (West *et al.*, 2007a)) and held tightly in place with masking tape, ensuring that the coil was level in all planes. The rat/probe/coil assembly was pushed into the magnet bore, ensuring that the centre of the coil was positioned as close to the isocentre of the magnetic field as possible

3.2.2.2 Signal optimization

Prior to imaging three signal optimization stages were performed to achieve the best signal-to-noise ratio.

1 - Once in the scanner bore an oscilloscope was used to 'tune' the surface coil, i.e. adjusting the 'tune' capacitor of the coil in order to match its resonance frequency to that of the hydrogen nuclei that are to be imaged.

2 - Using the Fourier Transform function of the SMIS console the magnet was actively 'shimmed' by making Progressive small changes in the current flowing through the 'shim coils' of the main magnet are made in order to maximize the homogeneity of the field over the area of interest (Elster 1994), in order to obtain the optimal signal from the animal.

3 - After the pilot imaging stage (*vide infra*), but prior to starting the final 3D sequence, a single coronal slice sequence was run with the phase-encode gradient set to zero. This allowed modification of the radio-frequency attenuator off-set and flip angle to maximise signal without causing image clipping.

3.2.2.3 Pilot scans and 3D imaging

In order to verify that the area of interest of the animal is at the isocentre of the field (thus producing most signal) and to target the final image block correctly in all three anatomical planes, a series of pilot images are generated on each animal (for sequence parameters see **Appendix 7)**. The on-screen display of the SMIS console will display images from the last sequence scanned, SMIS allows positioning of the orientation of slices of the next sequence to be run over the existing image of the last scan, allowing accurate positioning of the final 3D sequence to be fixed with respect to the three orthogonal anatomical planes. The full set-up, optimisation and scanning time for each animal was between 2-3 hours.

3.2.2.3.1 Scout Image: A very rapid scan (time ≈2 sec) in all three planes, on which the isocentre of the main field was marked. This verified that the animal was positioned correctly within the bore, and that the surface coil was positioned over the target area and level **(Figure 3.3)**.

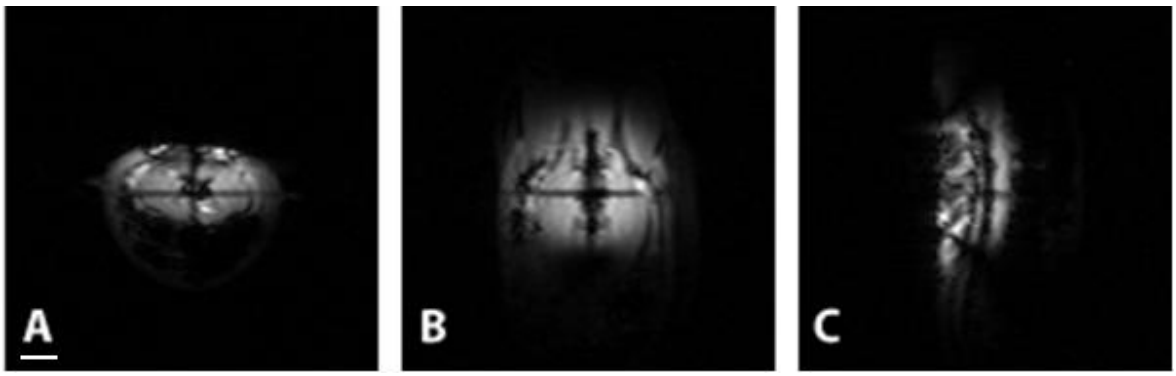

Figure 3.3: Scout Images. The three very low resolution images: A. axial, B. coronal C. sagittal. The dark cross seen at the centre of each image represents the planes of the scanner's isocentre of magnetic field; these images are used to verify correct placement of the animal and surface coil within the main scanner, with care being taken to match the region of the L4 DRG to the isocentre marks in each axis. Scale bar = 1cm.

3.2.2.3.2 Low Resolution Sagittal Image: An eight slice scan positioned over the axial scout image. This allows identification of the long axis of the spinal cord and DRGs (blue arrow in **Figure 3.4**), and placement of the central image of the next scanning sequence to be positioned as close to the long axis of the cord as possible.

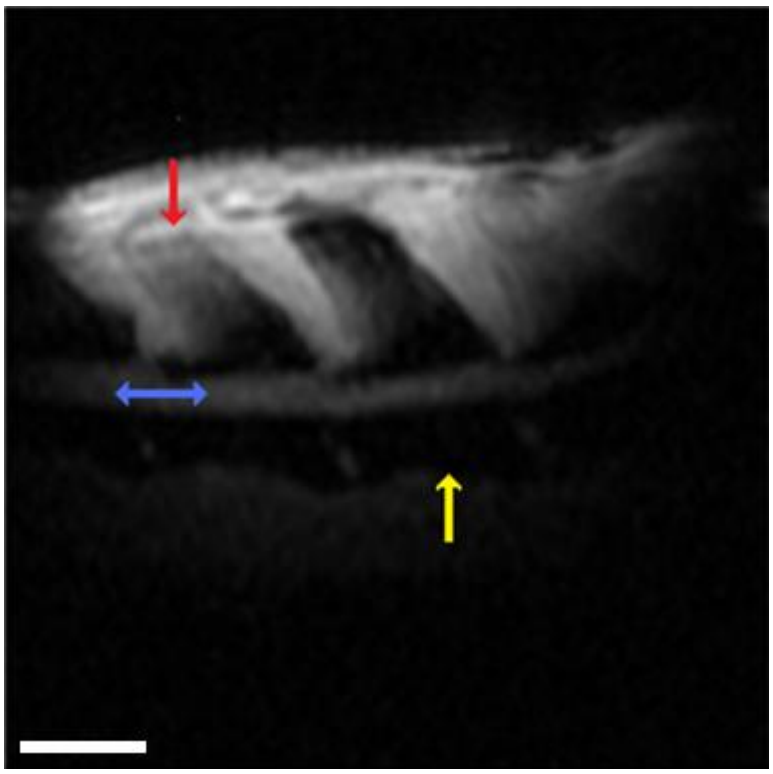

Figure 3.4: Low resolution sagittal image demonstrating the spinal cord (blue arrow), the bony vertebral body of L4 (yellow arrow) and spinous process of L5 (red arrow), the animal's dorsal skin is to the top of the picture and head to the right. Scale bar 0.5cm.

3.2.2.3.3 Coronal Image: Initially, an eight slice low resolution scan positioned over the lumbar area of the sagittal images **(Figure 3.5)**. This included pelvic wings, and the spinal cord and DRGs in longitudinal section. Using the tips of the iliac crests as landmarks, the L5 DRG and counting rostrally, L4 DRG are identified. If the anatomy was not clearly demonstrated in this initial sequence a longer high resolution coronal sequence was used, giving more slices and better definition.

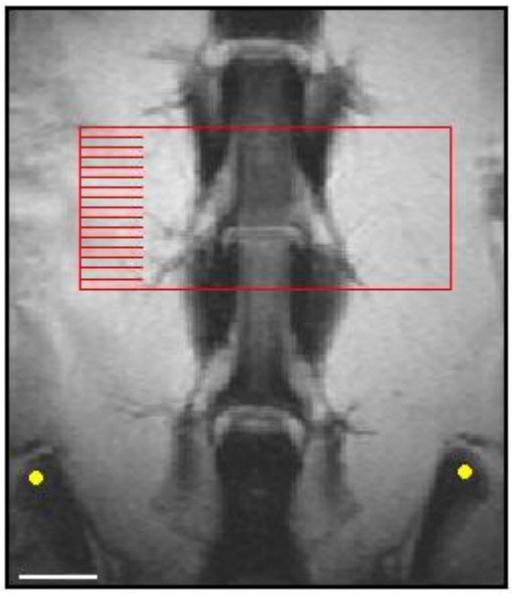

Figure 3.5: High resolution coronal MRI image, the animal's head is toward the top of page. The L4 and L5 DRG swellings are easily identified leaving the central spinal cord. The relationship of the L5 ganglia to the tips of the iliac crests (yellow spot) is noted. The red box represents placement of the imaging block over L4 DRG and the slice orientation of the subsequent axial 3D sequence. Scale bar 0.5cm.

3.2.2.3.4 Axial 3D Image: The final scan used a transverse 3D gradient echo volume acquisition imaging slab with a 30x30x8mm field-of-view, positioned over the image of the coronal scan to include the full extent of the L4 DRG bilaterally. Scan time was 43 minutes, generating 32 axial images, with an 117x117μm^2 resolution and 0.25mm slice thickness, cutting the DRG across their short axis for an 8mm segment **(Figure 3.6)**. To maximise signal for each animal the 3D pulse flip angle and radio-attenuator off-set (RAOS) was selected for each animal. A single slice 2D gradient echo sequence with the same TE and TR as the 3D sequence was positioned parallel to the plane of the surface coil (*i.e.* coronal), and crossing the DRG was run with the phase encode set to zero; multiple flip angle and RAOS values were entered until the resultant signal was maximised without causing image clipping. Such choosing of the pulse angle gives the resultant images T1 as well as proton density weighting.

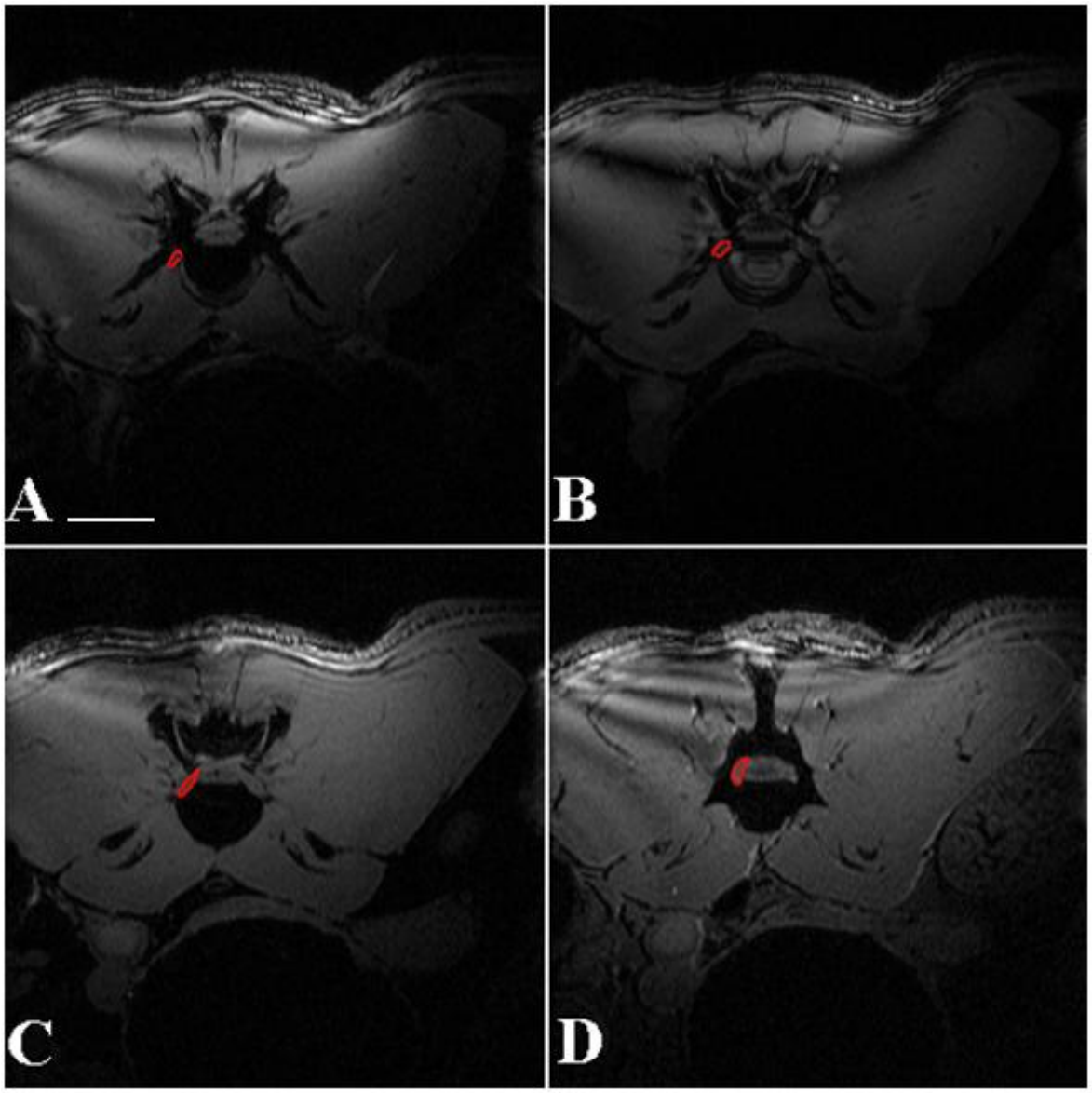

Figure 3.6: 3D axial MRI images of spinal cord and DRG (marked in red on the animal's right). Representative sample of slices from the 32 image stack, proceeding cranially A-D, the DRG emerges from the intervertebral foramen traverses rostro-medially to merge with the spinal cord. Scale bar 0.5cm.

3.2.2.4 Magnetic Resonance DRG Image Analysis and Volume Calculation

Using the SMIS software each slice was converted to **.tif** format and exported to the analysing computer using a digital storage medium. The data were quantified using Image-Pro Plus® v5.1 (Media Cybernetics) program. The full run of 32 images was opened, from these 21 sequential slices, starting with the last slice in which the L4 intervertebral disc was visible and proceeding in a cranial sequence, were selected. Thus a constant 5.25mm DRG segment, beginning from a fixed anatomical landmark was quantified for each animal.

On each slice, working at x2 magnification, the contour of the DRG was traced bilaterally; the calibrated software deriving a measurement of cross sectional pixel area for the section of DRG in each slice. The proximal end of the DRG lies in close approximation with the spinal cord and cauda equina, in this region, often became difficult to distinguish DRG from the neighbouring neural tissue. In these cases, the perimeter of the cord was traced in the most proximal image in which it could be clearly defined and this outline applied to subsequent slices. Conversion of pixel areas as measured on Image Pro Plus to actual sectional area in square millimetres is straight forward, as the MRI parameters are set to produce an image of 256x256 pixels representing a field of view of imaging of 30x30 mm; the area represented by each pixel is therefore is equal to ($30^2/256^2$) or $0.013733mm^2$, multiplication of the measured pixel area by this constant gives the area of each measured section in mm^2.

The volume of the DRG segment was calculated according to the principle of the 16^{th} century Italian mathematician Bonaventura Francesco Cavalieri (Gundersen & Jensen 1987; Gosh 1998). Cavalieri states that the volume of any object is equal to its mean cross-sectional area multiplied by its height; more practically, if even an irregularly shaped

object is sectioned into a series of equidistant slices with constant separation between such sections, the object's volume will equate to the sum of each cross-sectional area multiplied by the section separation. Gundersen and Jensen (1987) note that certain rules must be applied to this basic premise if the measurement is to remain unbiased; while any orientation of the planes of section relative to the object is permissible, the plane orientation and separation must remain constant. Further, the positioning of the sectioning construct over the object must be randomised, i.e. the position of the first plane to hit the target object is not allowed to be predetermined. The accuracy of the Cavalieri volume measurement as represented by the coefficient of error (CE) improves as the distance between sections decreases and the number of sections analysed increases, at least ten sections are recommended to achieve CE of less than 5% (Gadeberg *et al.,* 1999).

Application of the Cavalieri principle to the MRI image analysis allows calculation of DRG volume by multiplication of the sum of the cross-sectional area from the 21 analysed images by the known section thickness thus:

$$\mathbf{V\text{-}MRI = \Sigma a\text{-}MRI \,.\, t\text{-}MRI}$$

Where

V-MRI = MRI calculated volume of the DRG segment

Σa-MRI = Sum of the MRI measured cross sectional area from the 21 slices

t-MRI = MRI slice thickness (0.25mm - as set in the MRI sequence parameters)

3.2.3 HISTOLOGICAL DRG VOLUME MEASUREMENT

Histological volume measurements were performed on the same axially sectioned, fluorescently stained DRG tissue sections as used for stereological neuron counting in the NAC treatment duration study and utilising the same microscope and imaging suite (*cf.* 2.2.4.1). Beginning with a randomly preselected member of the first four histological

sections to contain neurons as viewed from the proximal end of the DRG at x10 magnification using the propidium iodide filter each 4th subsequent section was analysed until a total of 14 sections had been quantified (analysis of 14 sections included the entire neuron containing area in all ganglia) **(Figure 3.7)**.

Analysis of the DRG histological volume was again made cognisant of Cavalieri's principle with the cross sectional area and mean actual post-processing section thickness for each DRG being measured. For each section using the Olympus BX61 microscope with the x10 lens and propidium iodide filter the perimeter of the entire DRG complex including the neuron containing area and the associated axon tracts was traced, but by convention excluding adherent connective tissue and the axons of the often adherent grey rami communicantes, giving a measurement of cross sectional area for each analysed tissue section (*cf.* Figure 2.2b). In the frequent event that the full extent of the DRG section did not fit within one monitor screen view at x10 magnification, the SI software, in control of the motorised x-y microscope stage was able to slightly move the field of view, while maintaining superimposition of elements of the perimeter tracing already performed. The mean post processing section thickness was also directly measured in a manner analogous to sampling for stereological neuron counts. Over each traced full DRG perimeter a randomly orientated sampling grid was constructed (*cf.* Figure 2.2c), under x60 magnification, using the combined H33342 and PI filter and with the stage under control of SI each systematically randomized sampling site was visited **(Table 3.1)**.

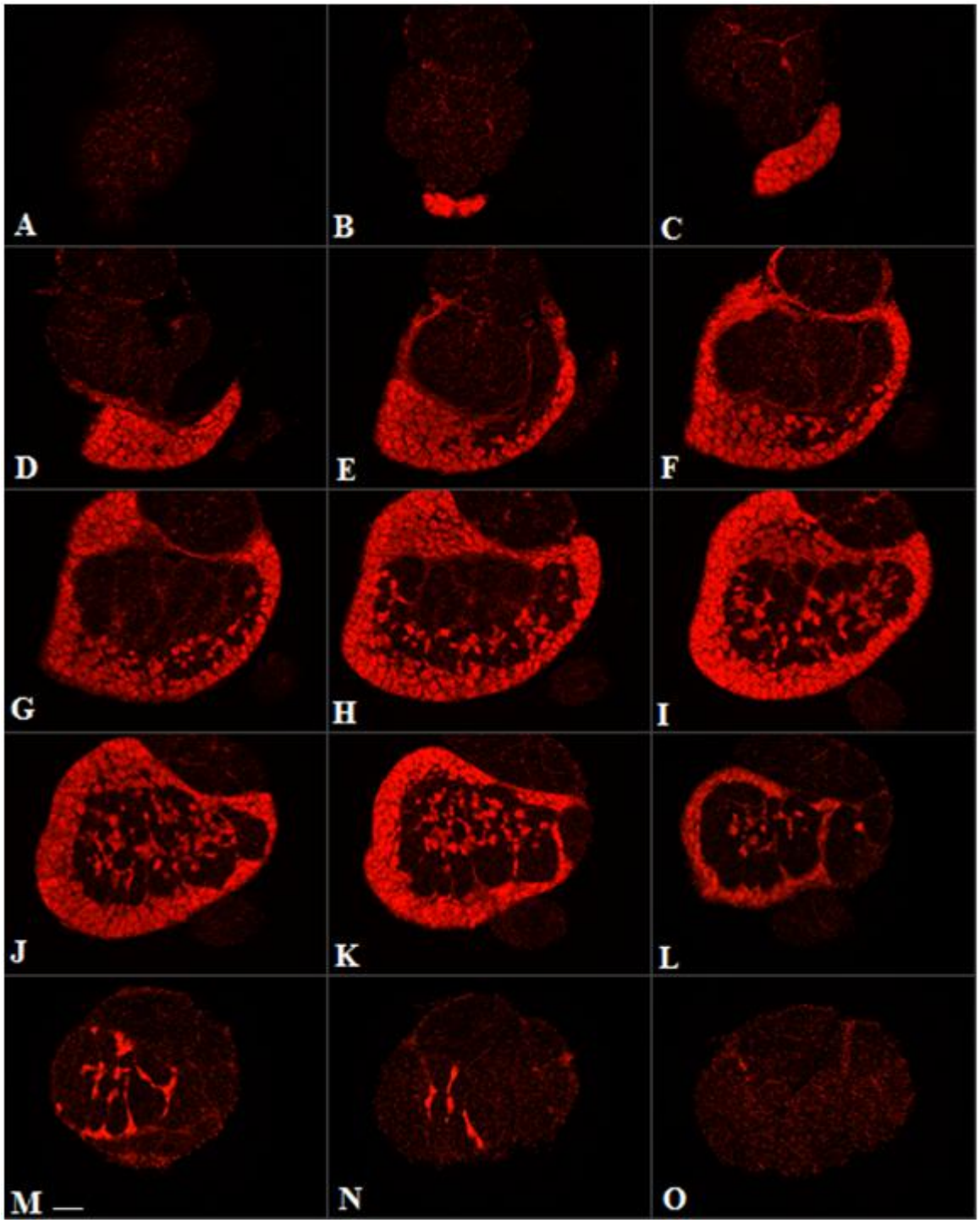

Figure 3.7: DRG histological sections. Representative images from an axially sectioned DRG; every 4th serial section is seen at x10 magnification using the PI filter. Heading proximo-distally from A-O the joining of the spinal roots can be seen in A and B, passing through the neuron containing region of the DRG proper (B – N) with the neurons (Bright red staining) tapering out toward the axon only spinal nerve (Dull punctate staining) (O). Section B is the first section in which neuronal cell bodies can be identified and a selection of this and thirteen subsequent sections is demonstrated to cover the full neuron containing region (B-O). Scale bar (M) = 50μm

At each site the section thickness was measured by recording the position of the z-depth of the microscope focus axis as the point at which cell nuclei first come into focus, be they neurons or glia, and the depth at which the last nuclei just leave the plane of focus. This directly measured the section thickness at each site, from which mean thickness per section and per ganglia was easily derived.

The Histologically measured DRG volume is therefore calculated as per Cavalieri's principle, thus:

$$\mathbf{V_{hist} = (\Sigma a\text{-}hist \,.t\text{-}hist)/ssf}$$

Where

V_{hist} = Histologically calculated volume of the DRG.

Σa-hist = Sum of the measured cross sectional area from the 14 sample sections.

t_{-hist} = Mean of the measured section thickness from all sampled sites in all sample sections.

ssf = Serial section fraction (0.25, as every 4th section was quantified)

Table 3.1: Parameters for Histological DRG Volume Measurement	
Section Periodicity	4
Sampling Grid (x)	250 μm
Sampling Grid (y)	250 μm
Sampling Grid Area (xy)	62500 μm^2
Section Thickness (cut)	50 μm
Section Sampling Fraction 0.25	0.25
Mean Section Thickness	Measured

3.2.4 DATA ANALYSIS AND STATISTICS

Student's t-testing was used for compassion of paired data, such as assessing differences between axotomised and non-*a*xotomised sides. One way ANOVA was used for comparison between groups with Bonferonni post-hoc testing. Correlation between

different measurement modalities were assessed using Spearman's Rank Coefficients. All statistical comparisons were carried out using GraphPad Prism® (v 4.03) software.

3.3 RESULTS

To validate the experimental design of this MRI study it was necessary to verify several hypotheses; firstly that analysis of L4 only neurons will yield similar results compared to L4&L5 counts. Second, that DRG volume and volume reduction is an appropriate proxy measure of neuron counts and loss. To test accuracy of the MRI imaging protocol, it is required to correlate the MRI measured volume to both histological volume and neurons counts. Finally, the validity and utility of MRI imaging will be confirmed by comparison of the overall neuron counts in the NAC treatment duration study against MRI only measurement.

3.3.1 TESTING L4 ONLY NEURON COUNTS AGAINST L4 & L5

3.3.1.1 Correlation of L4 Neuron counts and percentage neuron loss to L4&L5

Absolute neuron counts for L4 only versus L4&L5 combined counts assessed by animal and by contralateral side correlate well **(Figure 3.8)**, with Spearman's $r = 0.81$ and $P < 0.005$, which is unsurprising as the L4 count forms part of the combines L4&L5 total.

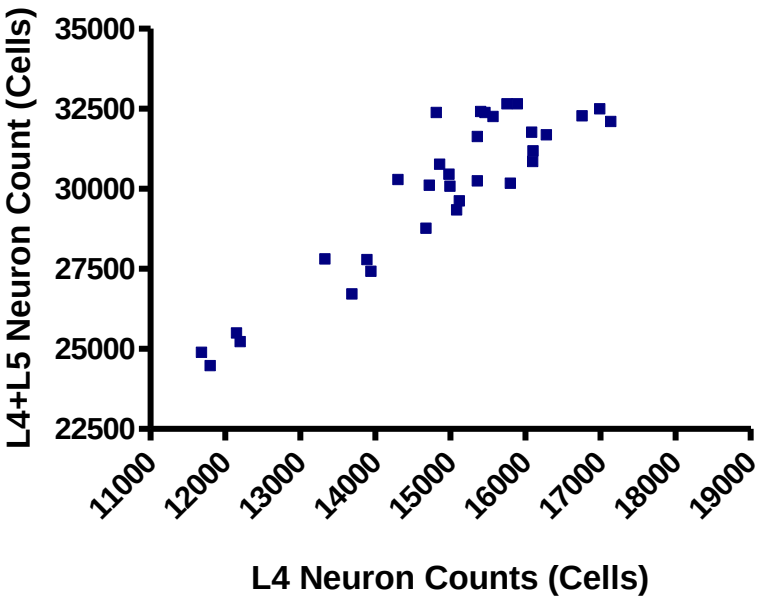

Figure 3.8: Scatter plot demonstrating correlation of absolute neuron counts between L4 and L4&L5 Spearsman's Correlation coefficient =0.81, p < 0.0005

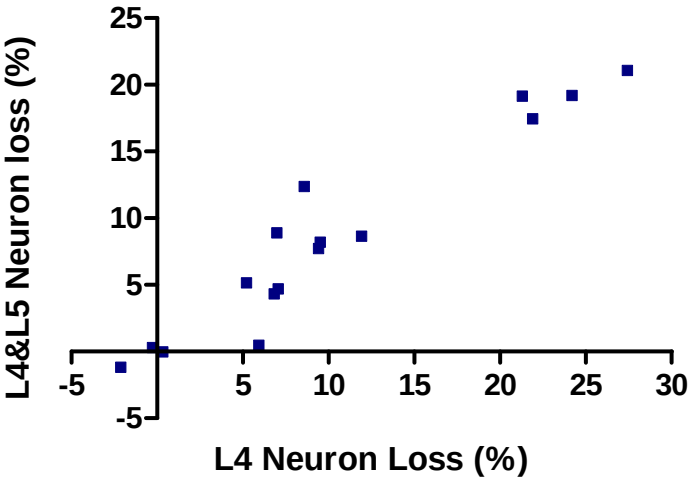

Figure 3.9: Scatter plot demonstrating correlation of *percentage neuron loss* in axotomised ganglia against the control ganglia per side as measured by L4 only or L4&L5. Correlation is highly significent (Spearsman's correlation coefficient = 0.92, p < 0.0005)

Comparison of neuron *loss* between L4 and L4&L5 rather than absolute volume show an equally strong correlation (Spearman's r = 0.92, p < 0.005) **(Figure 3.9)**.

3.3.1.2 Assessment of the NAC treatment duration study using only L4 neuron counts

Using the data of the NAC treatment duration study (*cf.* Chapter 2) absolute neuron counts for L4 only closely mirror the results for L4+L5 (*cf.* 2.3) **(Table 3.2; Figure 3.10)**. There were no significant differences between the non-*a*xotomised control ganglia between groups. The 60 day treatment group had no significant difference between axotomised and control ganglia (t-test $p = 0.7$), verifying the neuroprotectant effect of continuous NAC therapy. Using L4 only neuronal counts, there were differences between groups with different treatment duration with a similar pattern as seen for combined L4&L5 counts; 7d control vs. axotomised $p < 0.005$; 14d control vs. Axotomised $p < 0.005$; 30d control vs. axotomised $p < 0.05$.

Table 3.2: NAC Treatment Duration Study - L4 Neuron Counts

Rx Duration	Control Ganglia (L4) mean (SD)	Axotomised Ganglia (L4) mean (SD)	Mean Neuron Loss	Mean Percentage Neuron Loss
7 Days	15715 (761)	11966 (220)	3749**	23.70%**
14 Days	15020 (227)	13719 (240)	1301**	8.67%**
30 Days	16329 (761)	16104 (853)	1280*	7.80%*
60 Days	15724 (235)	16050 (585)	120	1.01%

Where ** = $p<0.005$ and * = $p<0.05$ in intra-group t-testing

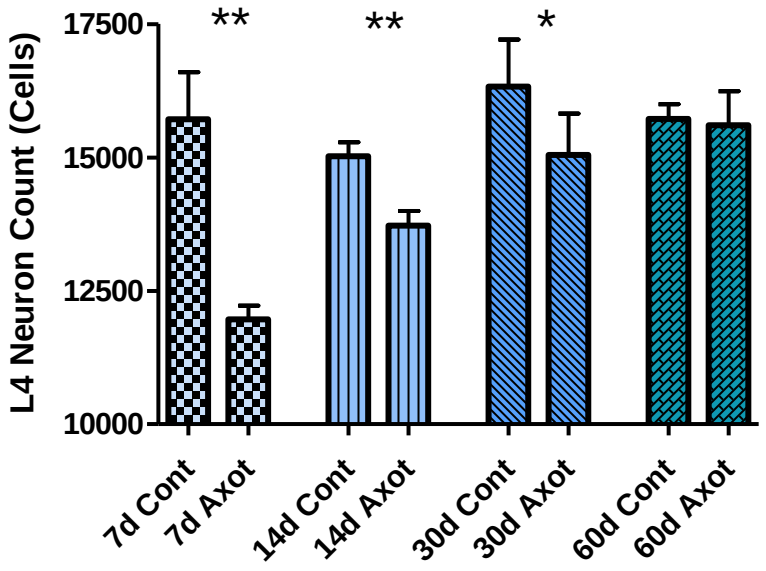

Figure 3.10: Effect of NAC duration of treatment on L4 ganglia only neuron counts. Plotted as neuron counts with SD. Asterisks relate to intra-group t-testing: ** = $p < 0.005$; * = $p < 0.05$

Analysis of L4 neuron loss as a percentage of the non-axotomised ganglia again displayed a similar pattern to L4+L5 losses, highly significant loss after 7 days (23.70%, SD 2.77%, ANOVA vs. 60d $p>0.005$) and less significant loss after 14 days (8.67%, SD 1.17%, ANOVA vs. 60d $p>0.05$) and 30 days treatment (7.80%, SD 2.9%, ANOVA vs. 60d $p>0.01$) **(Table 3.2; Figure 3.11)**. The only noteworthy difference between L4 and L4&L5 analysis was that L4 only counts showed higher mean percentage loss for the 7 day treatment group than does L4&L5 (24% vs. 19%), this difference just reaching significance when analysed by a non-pared t-test ($p = 0.043$).

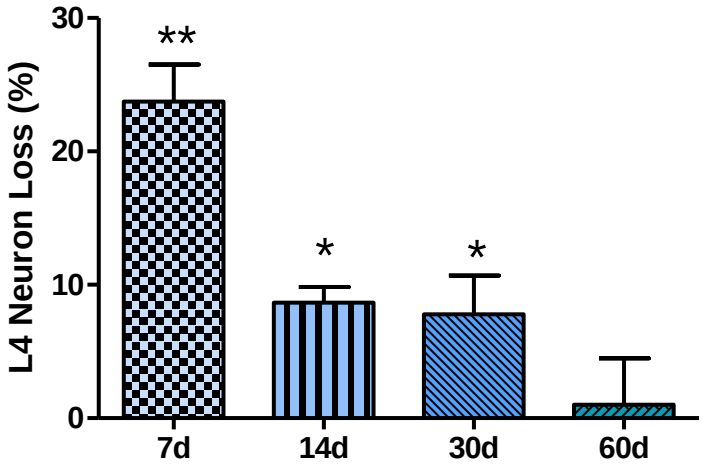

Figure 3.11: Effect NAC treatment duration on neuron loss, measured by L4 neuron count only. Plotted as percentage nearon loss with SD. Astriks represent significance in one-way ANOVA vs. 60d treatment (** = $p < 0.005$, * = $p < 0.05$)

3.3.2 TESTING L4 HISTOLOGICAL VOLUME AGAINST L4 NEURON COUNTS

3.3.2.1 Correlation of L4 histological volume to L4 neuron counts

Absolute histological DRG volume correlates strongly to neuron counts (Spearman's correlation coefficient 0.68, $p < 0.0005$) **(Figure 3.12)**. Further, there is an even more significant relationship between modalities when their percentage loss after axotomy and differing duration of NAC treatment are compared (i.e. percent neuronal loss vs. percent DRG volume loss) (Spearman's correlation coefficient 0.94, $p < 0.0005$) **(Figure 3.13)**.

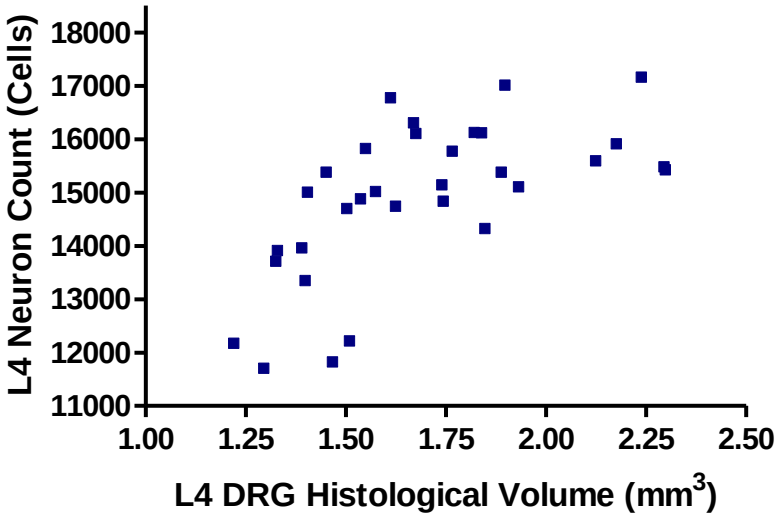

Figure 3.12: Scatter plot demonstrating correlation between histological L4 DRG volume and L4 nouron counts. Spearsman's correlation coefficient = 0.68, $p < 0.0005$

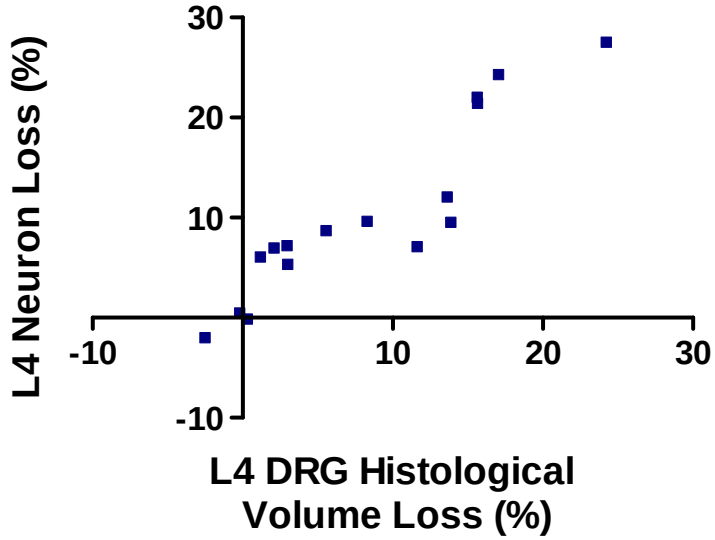

Figure 3.13: Scatter plot demonstrating correlation of *percentage loss* in axotomised L4 ganglia against the control L4 ganglia per side as measured by neuron count or histological volume. Correlation is highly significent (Spearsman's correlation coefficient = 0.94, $p < 0.005$)

3.3.2.2 Assessment of the NAC treatment duration study using L4 histological volume.

Quantitative L4 histological volumetric data in the different treatment groups were similar to the results seen for both L4&L5 neuron counts. There were no significant differences between the internal contralateral control ganglia **(Table 3.3; Figure 3.14)**. The 60 days treatment group showed no significant differences between control and axotomised sides (t-test p = 0.69). Partial duration NAC therapy post axotomy showed reduction in histological volume of the axotomised ganglia with a pattern that was duration dependent; being highly significant at 7d (p = 0.002) significant at 14d (p = 0.02) but not reaching significance at 30d treatment (p = 0.17).

Analysis of L4 DRG histological volume loss showed significant reduction with only 7 days NAC treatment (18.18%, SD 4.11%, ANOVA vs. 60d $p < 0.005$) or 14 days (9.89%, SD 3.66%, ANOVA vs. 60d $p < 0.05$), but not reaching significance at 30 days (5.47%, SD 5.48%, ANOVA vs. 60d $p > 0.05$) **(Figure 3.15)**.

Table 3.3: NAC Treatment Duration Study - L4 Histological DRG Volume

Treatment Duration	Control ganglia L4 histological volume mean (mm^3) (SD)	Axotomised ganglia L4 histological volume mean (mm^3) (SD)	L4 mean histological volume loss (mm^3) (SD)	Mean histological volume loss (%)
7 Days	1.67 (1.27)	1.37 (1.37)	3.04 (6.49)	18.18%**
14 Days	1.51 (1.03)	1.36 (3.88)	1.52 (6.54)	9.89%*
30 Days	1.89 (2.81)	1.78 (1.89)	1.12 (1.29)	5.47%
60 Days	1.96 (2.93)	1.97 (3.12)	-6.86 (3.18)	-0.25%

Where ** = $p>0.005$ and * = 0.05

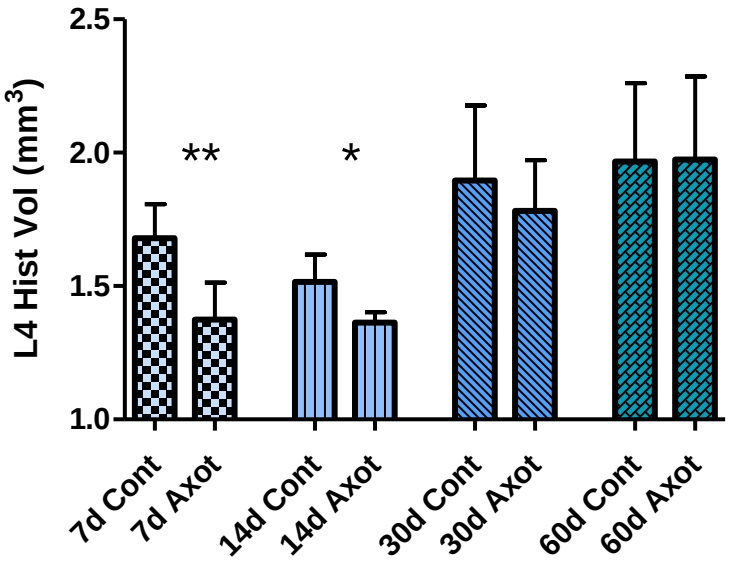

Figure 3.14: Effect of NAC duration of treatment on L4 ganglia only histological volumes. Plotted as volume with SD. Asterisks relate to intra-group t-testing: ** = $p < 0.005$; * = $p < 0.05$

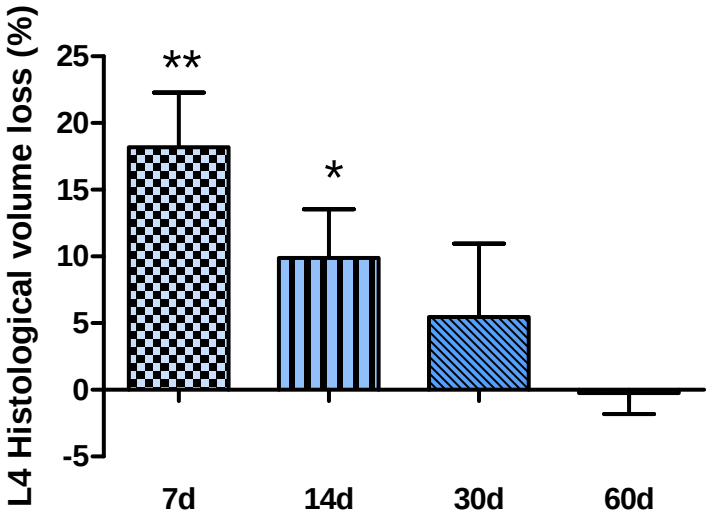

Figure 3.15: Effect of NAC treatment duration on L4 histological volume. Plotted as percentage histological volume loss with SD. Asterisks represent significance in one-way ANOVA vs. 60d treatment (** = $p < 0.005$; * = $p < 0.05$)

3.3.3 TESTING MAGNETIC RESONANCE IMAGING

3.3.3.1 Correlation of MRI L4 Volume against Histological L4 Volume

L4 volume measured by MRI correlated reasonably to histological L4 volume (Spearman's correlation coefficient 0.54, $p < 0.005$) **(Figure 3.16)**, with a much stronger correlation observed for assessment of percentage volume loss (Spearman's correlation coefficient 0.86, $p < 0.005$) again confirming the superiority of assessing percentage of intra-group loss against absolute measures **(Figure 3.17)**. As in this instance both MRI and histological measurement are assessing the same subject (L4 DRG volume), The MRI protocol measures a 5.25mm long section of tissue (21 slices of 0.25mm thickness) while the histological methodology assesses volume over a pre-shrinkage length of 2.8mm of DRG (14 sections of 50µm with a section sampling fraction of 0.25) and therefore MRI measurement of L4 volume returns a higher absolute volume measurement per ganglion, however correlation between these differing measures is significant.

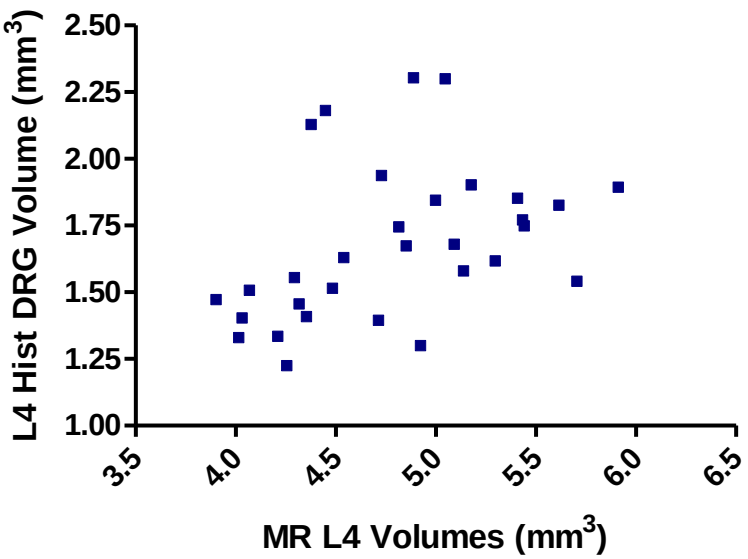

Figure 3.16: Scatter plot demonstrating correlation between MR L4 volume and Histological L4 volume. Spearsman's correlation coefficient = 0.54, p = 0.0022

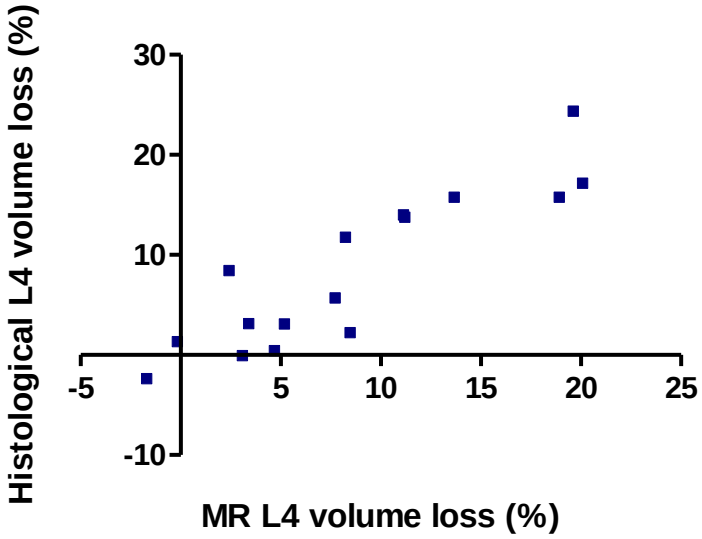

Figure 3.17: scatter plot demonstrating correlation between MR assessed L4 volume loss and histological L4 volume loss. Spearman's Correlation Coefficient = 0.86, $p < 0.005$)

3.3.3.2 Correlation of MRI L4 Volume against L4 Neuron Counts

The purpose of using MRI assessment of L4 volume is to assess if it is a valid proxy measure of DRG neuron population and neuron loss following sciatic nerve injury, and preceding analyses were of relevance in testing the methodological 'soundness' of MRI quantification. MRI L4 volume results correlated well to L4 neuron counts (Spearman's correlation coefficient = 0.48, $p < 0.05$) **(Figure 3.18)**, although there was a better relationship observed on comparison of MRI volume and histological volume as these data are obtained from analysis of the same tissue structure. A yet stronger correlation was observed between percentage neuron loss and percentage MRI measured L4 volume loss (Spearman's correlation coefficient = 0.83, $p < 0.005$) **(Figure 3.19)**.

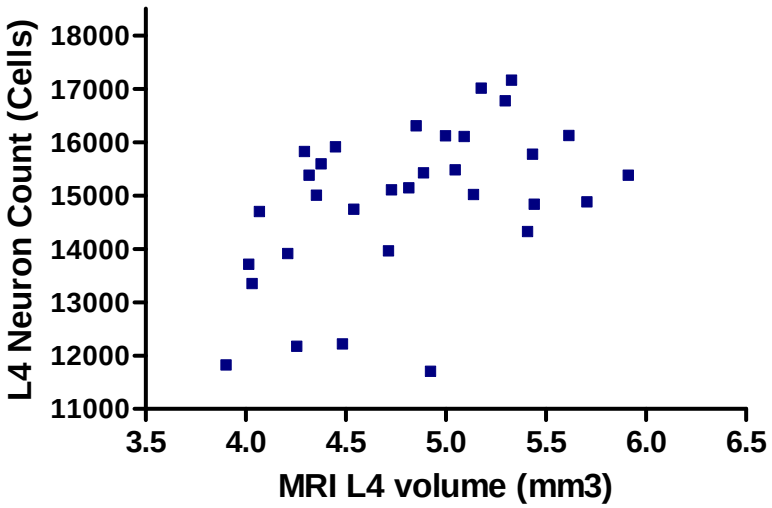

Figure 3.18: Scatter plot demonstrating correlation of MRI L4 volume to L4 neuron count.
(Spearman's correlation coefficient = 0.48, $p < 0.05$)

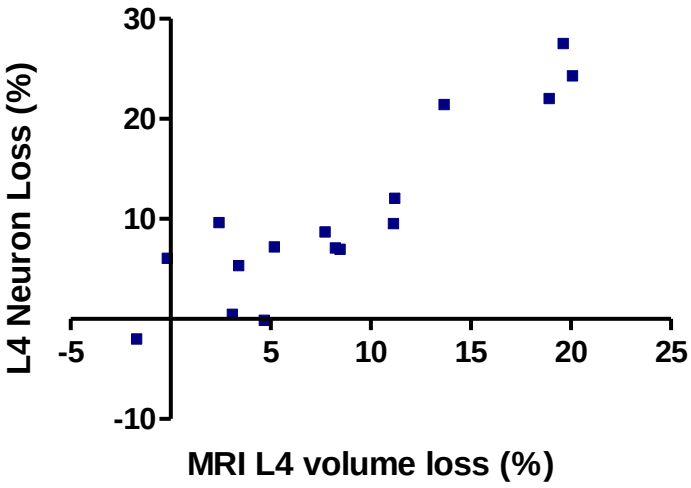

Figure 3.19: Scatter plot demonstrating correlation between MRI L4 volume loss and L4 neuron loss.
(Spearman's correlation coefficient = 0.83, $p < 0.005$)

3.3.3.3 Assessment of the NAC treatment duration study using L4 MRI volume

The results of the NAC treatment duration study were analysed using MRI L4 volume measurement **(Table 3.4)**.

Table 3.4: NAC Treatment Duration Study – MRI Measured L4 Volume

Treatment Duration	Control Ganglia (L4) mean volume mm^3 (SD)	Axotomised Ganglia (L4) mean volume mm^3 (SD)	Mean Volume Loss (mm3) (SD)	Mean Percentage Volume Loss (SD)
7 Days	5.36 (0.40)	4.39 (0.42)	0.97 (0.15)**	18.11%**
14 Days	4.59 (0.38)	4.25 (0.33)	0.34 (0.17)	7.42%*
30 Days	5.18 (0.66)	4.80 (0.28)	0.38 (0.21)	7.10%*
60 Days	4.99 (0.44)	4.91 (0.41)	0.08 (0.14)	1.52%

Where ** = $p < 0.005$; * = $p < 0.05$.

The MRI data showed the same trend of changes as observed with neuron counts (L4 or L4&L5) and with L4 histological volume analyses **(Figure 3.20)**. There is no significant difference between control ganglia of different groups, and two month NAC treatment also prevented MR volume reduction (t-test of contralateral control vs. axotomised side $p = 0.34$). MRI detected highly significant difference in DRG volume when animals were treated with NAC for only 7 days post axotomy (t-test of control vs. axotomised $p < 0.005$), and less significant reductions in the other treatment groups (14d axotomised vs. control $p < 0.05$; 30d axotomised vs. control $p < 0.05$).

Comparison of MRI volume loss between groups again showed the same general trend as both the neuron counts and histological DRG volume quantification **(Figure 3.21)**, with no significant loss detected for 60 days treatment. A highly significant volume reduction was detected in the 7 day treatment group (18.1% +/- 4.1% vs. 1.5% +/- 2.9%, 7d vs. 60d $p>0.001$), but there was no significant volume loss detected in groups treated for 14 days (7.4% +/- 3.6% vs. 60d $p>0.05$) or 30s day (7.1% +/- 3.5% vs. 60d $p>0.05$). In both cases there was detection of volume reduction in the axotomised side, but the large standard

deviations in these measurements prevented these from reaching significance when compared to the 60 day group.

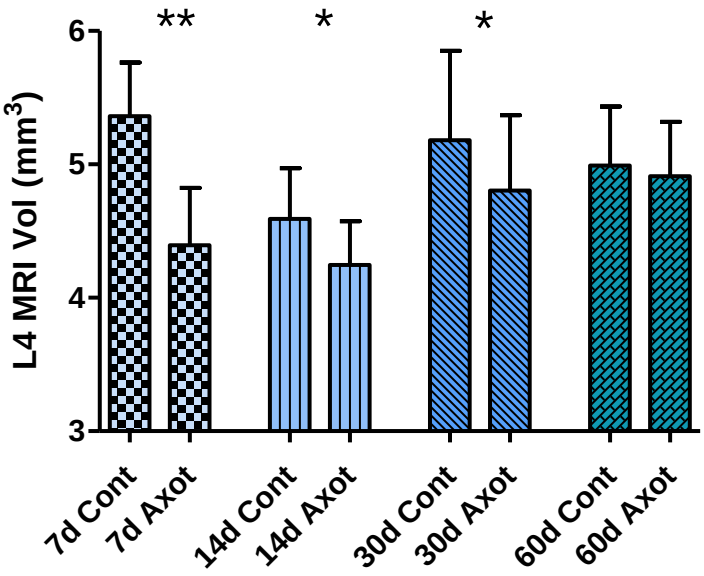

Figure 3.20: Effect of NAC duration of treatment on MRI measured L4 volume. Plotted as mean volume with SD. Asterisks relate to intra-group t-testing: ** = p< 0.005, * = p< 0.05.

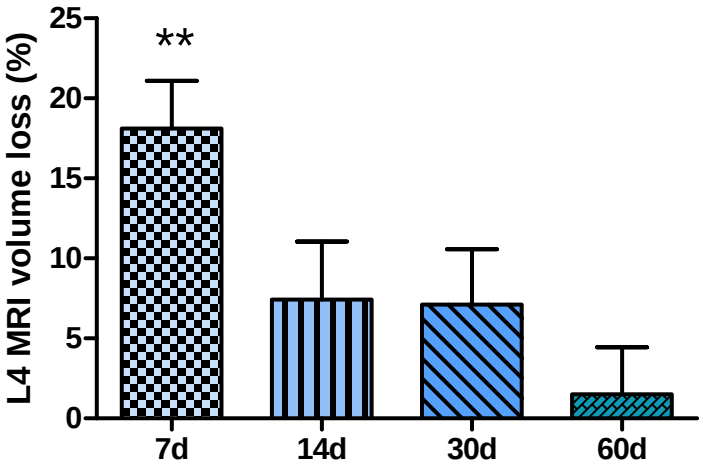

Figure 3.21: Effect of NAC treatment duration on MRI measured L4 DRG volume. Plotted as percentage volume loss with SD. Asterisks represent significance in one-way ANOVA vs. 60d treatment (** = < 0.005)

3.4 DISCUSSION

3.4.1 METHODOLOGY

3.4.1.1 Histological volume quantification

The histological protocol to measure DRG volume was designed to comply with the Cavalieri method of volume estimation (Gundersen & Jensen, 1987). The Analysis of a set number of sections (n=14) pre-determined to include all sections containing neuronal cell bodies allows a better comparison between ganglia of different sizes and the similarly constant length of tissue measured by the MRI protocol than would assessing the volume of only neuron containing sections such as performed in earlier stereological experiments of our research group (McKay Hart *et al.,* 2002a McKay Hart *et al.,* 2002b; Wilson *et al.*, 2003; Hart *et al.,* 2004a; Wilson *et al.*, 2007). Gundersen & Jensen (1987) suggest that the co-efficient of error (CE) in the Cavalieri estimate will reduce to acceptable value by analysing greater than ten sections – the fourteen sections included in volume measurement reduced CE to an acceptable mean 0.02188 (0.01 – 0.03). The second assumption of the Cavalieri method is the first section to cross the region of interest must not be pre-determined; this rule was met by beginning the measurement from a randomly chosen section from the first four to contain neurons. The final pre-requisite is that the orientation of sectioning is random and that the plane of sectioning does not change; lining up the DRG in the OTC blocking medium before freezing for sectioning is only judged 'by eye' and so the exact plane of sectioning for each DRG is subject to variation. Once sectioning had started however, the whole of the ganglia was processed, with no re-positioning of the OTC block or the microtome chuck ensuring that all sections shared the same orientation.

All histological tissue shrinks during processing and variability in such size reduction could introduce an element of bias into the volume analysis (Dorph-Petersen *et al.,* 2001). To minimise such the effects, all sectioning and staining followed strict protocols to ensure

that all groups of ganglia were exposed to the same environmental conditions during processing. Frozen sectioning and staining by water-soluble fluorescent media do not containing any dehydration steps, hence effect of shrinkage should be minimised (Bergman *et al.*, 1999; Hart & Terenghi, 2004). Further, measurement of post-processing tissue thickness, assessed from a systematic random sample of sites across each ganglion, was used for volume calculation, and in this way the shrinkage which occurs, especially during the 'air-drying' step of sectioning is accounted for in the methodology.

3.4.1.2 MRI volumetry

The protocol used to locate and image the L4 DRG bilaterally was the same as that used in one previous study (West *et al.*, 2007b) and is also designed cognisant of Cavalieri's principle. Briefly, consistent placement of the animal within the magnet bore and the three-axis pilot scans allow relatively easy localisation of the L4 DRG bilaterally and the DRG are imaged in the axial plane, along their long axis, ensuring that the maximal possible number of sections is acquired, reducing the coefficient of error (Gundersen *et al.*, 1988). Quantification of a fixed number of images, based on an anatomical landmark ensures that a consistent length (5.25mm) of spinal nerve/DRG/roots complex is measured.

Choice of a 3D sequence was influenced by the high resolution offered, and the generation of rectangular slices of more precise thickness than those acquirable with standard 2D-scanning (Johnston *et al.*, 1999). Slice thickness was reduced as much as possible (0.25mm) in order to minimise the effects of overprojection while still delivering high signal images (Gadeberg *et al.*, 1999). Image analysis of the MRI scans is carried out to the ultimate precision of a digital pixel (0.0.14mm^2) and using the Image Pro Plus software suite. Although there is the possibility to introduce some variability by manual contour tracing and difficulty in identifying cut-off points between anatomical structures, these

measurement errors are likely to be constant when all analysis is performed consistently by the same observer. Further when using the Cavalieri principle to measure volume, even reasonably large inaccuracy in contour tracing does not adversely affect the eventual coefficient of error if a large enough number of section is analysed (Gundersen *et al.*, 1988).

3.4.2 VALIDITY OF L4 NEURON COUNT AS A MEASURE OF L4&L5 COUNT

The vast majority (98%) of sciatic nerve component neurons are present in L4 and L5 with a small contribution from L6 (Swett *et al.,* 1991). However, equal distribution between L4 and L5 cannot simply be assumed, especially as segmental distribution in the thoracic neuronal pool does not seem to be homogeneous (Ygge *et al.*, 1981). These findings and studies reporting different neuronal populations between sides when only one metameric level of the lumbar ganglia had been analysed (Schmalbruch, 1987a & b; Groves *et al.*, 2003) have led to the vast majority of DRG neuron population studies citing results for combined levels. Previous studies demonstrated reduced coefficient of variation (9%) when analysing L4&L5 over L4 or L5 alone (14%), (Hart & Terenghi, 2004) and studies in which NAC or ALCAR has been administered report findings using combined L4&L5 counts (Hart *et al.*, 2002b; Wilson *et al.*, 2003; Hart *et al.*, 2004a; Wilson *et al.*, 2007).

The MRI equipment can only image one ganglion pair as the surface coil is too small to span multiple levels. The assumption that L4 only analysis, as used in the MRI protocol would mirror combined counts therefore needed to be confirmed. Using the neuron counts as generated in the NAC treatment duration study (*cf.* Chapter 2), a close correlation was demonstrated between L4 and L4&L5 absolute neuron populations as well as percentage neuron loss although L4 only analysis did tend to overestimate L4&L5 neuron loss. If the NAC treatment duration study is repeated using only L4 neuron counts the

trend of results is unaffected. In the NAC treatment duration study there was little difference between control ganglia neuron counts for L5 or L4 (L5 mean 15441, SD 446; L4 mean 15697, SD 535), and this variation was within the range cited by our and other groups (Hart & Terenghi, 2004). In the axotomised treated groups, there was a trend for L4 only count groups to show a greater loss of neurons than L4+L5; this phenomenon being more evident for the higher value losses in the 7 day treatment group. Overall, the present results of neuronal counts of L4 rather than L4&L5 combined ganglia neuron counts showed a good correlation and yield similar information with regard to the effect of NAC treatment duration as shown in Chapter 2.

3.4.3 VALIDITY OF L4 VOLUME AS A MEASURE OF L4 NEURON COUNT

Previous work by our group has demonstrated a reduction in the volume of the neuron containing region of the DRG accompanies neuron loss post axotomy, and that these reductions follow the same time course (McKay Hart *et al.*, 2002a). Further, volume as well as neuron counts are maintained by ALCAR treatment (Wilson *et al.*, 2003). The MRI pilot study (West *et al.*, 2007b) also studied L4 neuron count to histological volume relationship, finding a strong correlation similar to that presented here.

Repeating the treatment duration study with L4 histological volume only shows a similar pattern to the L4&L5 combined neuron count data both for L4 volume alone and degree of volume loss further evidencing the validity of single ganglion volume assessment as a proxy measure of neuronal loss. The only potentially significant difference between the NAC duration study as assessed by L4&L5 combined neuron count compared to histological L4 quantification is loss of 'significance' of the 30 day treatment group in the volumetric study. However, in the 30 day treatment L4 volume group both t-testing against the non-axotomised group and ANOVA of volume loss against the 60 day

treatment group only just failed to reach accepted levels of significance; it is possible that these results may become more distinct if the experiment was repeated with larger group numbers.

3.4.4 VALIDITY OF MRI L4 VOLUME AS A MEASUREMENT OF NEURONAL LOSS.

The reasonably strong correlation of MRI L4 volume to both histological L4 volume and L4 neuron count shown in this study support the premise that MRI will be useful research tool; indeed both the MRI-to-volume and MRI-to-neuron count correlations in the NAC treatment duration study were stronger than those discussed previously (West *et al.*, 2007b), possibly reflecting the larger number of subjects included in this experiment. In the data presented here, the correlation between volume measurements is stronger than that between MRI volume to neuron populations ($\rho = 0.54$ and 0.48 respectively), intuitively this would be the logical situation, as two measures of the same innate structure, albeit by different methods would seem to be more likely to be related than MRI volume to neuron count.

Analysing the NAC treatment duration study using MRI L4 volume as the only outcome measure highlights some important similarities to assessment of combined L4&L5 neuron counts but also some significant and potentially important caveats. The general pattern of volume reduction in axotomised ganglia being maintained, intra-group t-testing reached significance for all partially treated groups in spite of the lager standard deviation and coefficient of variance values for MRI assessment versus L4&L5 neuron counting. Significant MRI volume loss was only detected for 7 days of NAC treatment on inter-group ANOVA, although some degree of loss was documented for 14 and 30 days as well. As discussed with regard to histological volume measurement, not detecting a significant

reduction for an experimental group with a given assessment methodology is not the same as a significant difference not being present. Over-reliance on only MRI assessment and statistical significance rather than trends could lead to the potentially misleading statement that 'all treatment groups with longer than 7 days treatment show no *significant* volume loss compared to full treatment for 60 days'. Whilst this statement is *true* according to the data presented here, it can easily be seen that such an interpretation could lead to a spurious overestimation of the ability of NAC to influence biological events, and care must be taken when interpreting findings.

3.4.5 COMPARISON WITH OTHER NEUROLOGICAL VOLUMERTRIC MRI STUDIES

Since the first publication of this protocol by West *et al.,* 2007b no other groups have adopted DRG MRI volumetry, and so direct comparison with other work is not possible. As discussed earlier however (*cf.* 1.3.2.2) the techniques of very high resolution micro-MRI have been demonstrated to visualise small neuronal structures (Natt *et al.,* 2002; Osechinskiy & Kruggel, 2009) and independently to allow volume assessment of CNS structures in a variety of animal models and human pathological conditions (Gadeberg *et al.,* 1999; Marziali *et al.,* 2004; Moats *et al.,* 2003; Mikko *et al.,* 2000; Nagel *et al.,* 2004; Wolf *et al.,* 2002; Gudziol *et al.,* 2009). Within the capabilities of animal research micro-MRI equipment is the possibility to produce histological resolution such as the 10μm slice thickness imaging atlas of zebrafish brain reported by Ullmann *et al.,* (2010), which at the time of publication was the highest resolution achieved in the vertebrate nervous system. Diffusion weighted sequences have been reported to be able to measure individual axon diameter in the rat corpus callossum (Barazany *et al.,* 2009).

Few studies which investigate neural MRI volumetry utilise histological volume and/or stereological neuronal population control; however those which have done so have verified the accuracy and validity of imaging. Comparison of histological stereology to MRI volume quantification has been applied to other pathological models, such as specific brain regions in neurodegenerative disease after neuro-vascular insults (Bobinski *et al.,* 2000; McDaniel 2001; Nemanic *et al.,* 2002; Zarow *et al.,* 2005). Bobinski *et al.,* (2000) compared post-mortem MRI scanning brains of Alzheimer's disease (AD) patients to histological volumetric and stereological neuronal counting quantification of areas of the hippocampus, subiculum and parahippocampal gyrus; demonstrating very strong correlation between volume measurements, with MRI tending to underestimate histological volume by ≈5%. The authors report finding strong correlation between neuronal counts and MRI volume, however as absolute result values are not stated the relationship between these modalities cannot be commented upon. In a similar experiment Zarow *et al.,* (2005) compared post-mortem hippocampal neuron counting and volume measured using an optical dissector, to the last clinical MRI and neurocognitive assessments carried out on patients with AD or vascular dementia. This group found close correlation between neuron count, histological volume and MRI volume, as well as between MRI volume and clinical findings. While the published data does not allow calculation of the agreement between MRI and histological values in terms of a 'loss' value, it gives strong reinforcement to the concept that MRI assessed volume can be used as an index of a complex clinical phenomenon in humans, such as cognitive function, or as we propose peripheral nervous system regeneration. Similar correlation between in vivo MRI hippocampal volume and clinical performance tests in AD patients was reported by Csernansky *et al.,* (2004)

Turning to animal models, McDaniel *et al.,* (2001) investigated the effect of forebrain ischæmia in transgenic mice known to be hyper-susceptible to such an insult. Measuring volume of the dorsal hippocampus by planimetric histology and micro-MRI in a 7T research scanner a histological volume reduction of ≈15% was demonstrated 30 days after 10 minutes of uni-hemispheric ischæmia which compared with a lesser, but still significant 7% reduction on MRI. Nemanic *et al.,* (2002) studied the effect of intracerebral injection of neurotoxic agents, assessing the effect by MRI volumetric analysis of damaged hippocampal tissue using two different pulse sequences (T_1 weighted and Fluid attenuated inversion recovery (FLAIR) sequences). This group demonstrated almost 1:1 volume reduction ratio between FLAIR and histology, and a slight underestimation of volume loss for T1 weighted imaging. Prabhu *et al.*, (2000) compared histological and MRI assessment of growth of tumours in a mouse glioma model, again finding strong correlation of volume between modalities, with a slight MRI underestimation.

In the majority of studies comparing MRI to histological volume of anatomical structures including the results presented here and the pilot study of DRG quantification (West *et al.*, 2007b), MRI seems to consistently underestimate volume loss as assessed by histology, even when the effects of tissue shrinkage are compensated for (Bobinski *et al.,* 2000). This phenomenon seems to extend to other highly sensitive imaging modalities, as both micro-MRI and micro-computed tomography (CT) underestimate the volume of tumours in a rat model of glioma (Engelhorn *et al.,* 2009). There are some exceptions to this pattern, such as the study reported by Herz *et al.,* (2006) assessing MRI and histological volume of ischæmic areas produced after cerebral vessel occlusion in rats; in this study, although there was close correlation between modalities MRI significantly returned larger volume assessments. The explanation for this however is likely to be attributable to the MRI sequence choice in this experiment, as the images were heavily T2 weighted, and likely

therefore to analyse areas of neuronal loss, but also surrounding cerebral œdema, which would not be quantified by subsequent histology. In the DRG imaging protocol, such peri-lesional swelling wound not be relevant, as the 3D sequence used has relatively neutral weighting, and at two months post axotomy the post injury swelling of the DRG has been shown to be resolved (McKay Hart *et al.*, 2002a)

3.4.6 CONCLUSION

MRI has a well documented pedigree for volumetric assessment in the nervous system, being verified against both histological and clinical control.

The series of assumptions necessary to use L4 MRI volume as a proxy index of combined L4&L5 neuron populations appear to be valid, and MRI has again been demonstrated to return significant and scientifically useful results, being demonstrated to act as a sensitive proxy measure of neuron populations. When compared against combined L4&L5 neuron counts (acting in this experiment as the 'gold standard' of neuronal population assessment) MRI L4 DRG volumetric assessment provides a remarkably similar pattern of findings, however, a caveat must be acknowledged, cognisance of which will be needed for effective future experimental planning. MRI volume measurements have greater innate variability than neuron counting and therefore less 'resolving power' than stereology and should lead future experimental design to involve group endpoints that are likely to result in fairly large neuron/volume differences. The results of our group mirror the findings of many others that MRI assessment of volume will tend to underestimate comparable histological analysis, whilst not detracting from the innate utility of the technique; this also should be born in mind in future experimental planning. The MRI protocol is maybe less suited to experiments dealing with sequential small changes in volume such as a dose response

experiment or the NAC treatment duration study as used here as compared to a more binary treatment versus control experimental paradigm.

The principle of MRI as a proxy measure of DRG neuron population and apoptosis after axotomy has again been shown to be valid, and worth pursuing, both as a research tool and to be taken forward into the human clinical arena. The eventual ideal of a NAC interventional trial in human patients with peripheral nerve injury with volumetric MRI of the DRG as one of the a primary assessments of outcome along with clinical tests of nerve recovery hopefully moves one step closer with the favourable results of MR in this report. It is possible that some of the methodological difficulties of micro-volumetric scanning in animals may be less problematic in human scanning where the DRG will have a volume that is orders of magnitude greater than the tiny rat DRG which may facilitate imaging and volumetric analysis. As yet unpublished pilot data from our research group using a 4T clinical research MRI scanner and the assistance of professional radiologists have managed to image volunteer DRG in cross section with what appears to be a good signal to noise ratio, although these studies are in a very early stage, they seem to demonstrate that human patient volumetric MRI of the DRG will be feasible bring the long anticipated goal of a clinical trial of NAC a step closer to fruition.

CHAPTER 4

Further Imaging Studies of the Peripheral Nervous System

4.1 BACKGROUND AND EXPERIMENTAL DESIGN

No attempt had been made previously (West *et al.*, 2007b), or during the NAC treatment duration study to image live animals due to the potential loss of image resolution associated with in vivo scanning. However, the potential of such *in vivo* MRI imaging would be of benefit to future studies, as it would allow the monitoring of physiological events in the same animal over a period of time by using serial imaging. For this reason, a pilot study was carried out, scanning a live, anæsthetised rat in order to examine the feasibility and associated effects on image quality of this type of investigation.

Both Magnetic Resonance Imaging (MRI) and Ultrasound (US) scanning are in frequent use in clinical Plastic and Reconstructive Surgery to diagnose lesions of the peripheral and central nervous system and for pre-operative planning, with applications ranging from imaging peripheral nerve injury to the brachial plexus or arm/forearm nerves (Cokluk et *al.*, 2004; Cokluk & Aydin, 2007) upper limb major nerve tumours (Stelow *et al.*, 2004; Gruber *et al.*, 2007). Over a decade MRI has been demonstrated to be able to identify effects of axonal injury on the distal stump of a peripheral nerve in human patients (Filler *et al.*, 1993; Britz *et al.*, 1995; Britz *et al.*, 1996; Daley *et al.*, 1997). Subsequent animal studies by a number of groups (*cf.* 1.3.2.1) have further investigated this phenomenon demonstrating that changes in T_2 and other more sophisticated sequence parameter signals can be seen at the site of nerve injury and normalise with nerve regeneration (Aagaard *et al.*, 2003; Bendszus *et al.*, 2004; Behr *et al.*, 2009). To define an imaging protocol to mirror these studies would obviously represent an opportunity to assess by MRI the effects of the neuroprotective agents; particularly as ALCAR has been demonstrated to enhance peripheral nerve regeneration in histological studies (Hart *et al.*, 2002c; Wilson *et al.*, 2009).

Ultrasound of peripheral nerves is a commonly used clinical test (Khachi *et al.,* 2007) but is usually limited by resolving power of clinical ultrasound equipment to imaging studies of the main upper limb nerves in the arm and forearm); there are no reports of US imaging of human digital nerves. High frequency ultrasound (HFUS) technology is now becoming available to research science (Andonian *et al.,* 2009; Sullivan *et al.,* 2009; Marion *et al.*, 2010). The much higher wavelength of sonar energy emitted by an HFUS probe allows visualisation of structures at very high resolution, at the trade off of reduced tissue penetration. A Vevo 660® high frequency ultrasound system (VisualSonics, Toronto, Ontario, Canada) was kindly made available to this researcher for a brief time in order to carry out pilot studies imaging neural tissue by the Imaging Research and Development Team from AstraZeneca (Alderly Park, Cheshire, UK).

Three experimental investigations therefore form the substance of this chapter:

1. Volumetric L4 DRG MRI scanning *in vivo*.
2. Attempts to visualise the rat sciatic nerve using the University of Manchester's 7T small animal MRI scanner.
3. Use of high frequency ultrasound to visualise the rat sciatic nerve and nerve regeneration.
4. Use of high frequency ultrasound to visualise volunteer human digital nerve in the index finger.

4.2 MATERIALS, METHODS & EXPERIMENTAL DESIGN

4.2.1 EXPERIMENT ONE: *In Vivo* Volumetric L4 DRG MRI Scanning

A young adult male outbred albino Sprague Dawley rat (Harlan Sprague Dawley Inc.), weight 252g was anæsthetised by inhalational oxygen driven Isoflourane as described for operating in the NAC treatment duration study (*cf.* 2.2.1.2). Induction was carried out in a preparation room adjacent to the MR laboratory, and after reaching an appropriate plane of anæsthesia, the animal was transferred to the scanning probe and the surface coil applied as described in 3.2.2.1. As ongoing anæsthetic is administered via a non-metallic tube, this can be maintained in position over the animal's snout and placed within the bore of the scanner. Repeat clinical examination to monitor anæsthesia is not possible when the subject is within the magnet bore, and so respiratory rate, monitored by a piezoelectric pressure pad (Graseby Medical) was used as the sole index of animal welfare within the scanner. The L4 DRG volumetric scanning protocol and subsequent image analysis steps were followed exactly as described in Chapter 3 (*cf.* 3.2.2.2 – 3.2.2.4). After scanning, the animal was removed from the scanner, assessed for signs of life before being killed by cervical dislocation. The dead animal was re-imaged following the same protocols and image analysis as used during anæsthetised scanning.

4.2.2 EXPERIMENT TWO: Attempted MRI of the Rat sciatic Nerve

To image the sciatic nerve the same 2cm surface coil utilised in the DRG volumetric protocol was used for some scans, while others used a 8cm internal diameter custom made volume coil **(Figure 4.1)** into which the whole animal in its plastic 'probe' holder were inserted. This alternative coil gave less 'magnified' views of the whole animal rather than a ≈2cm diameter sphere of highly detailed image. A number of different MRI sequences were used to image animals in this experiment, including those which had been designed

for the DRG imaging protocol and others selected from the sequence library of the SMIS software console **(Appendix 7)**.

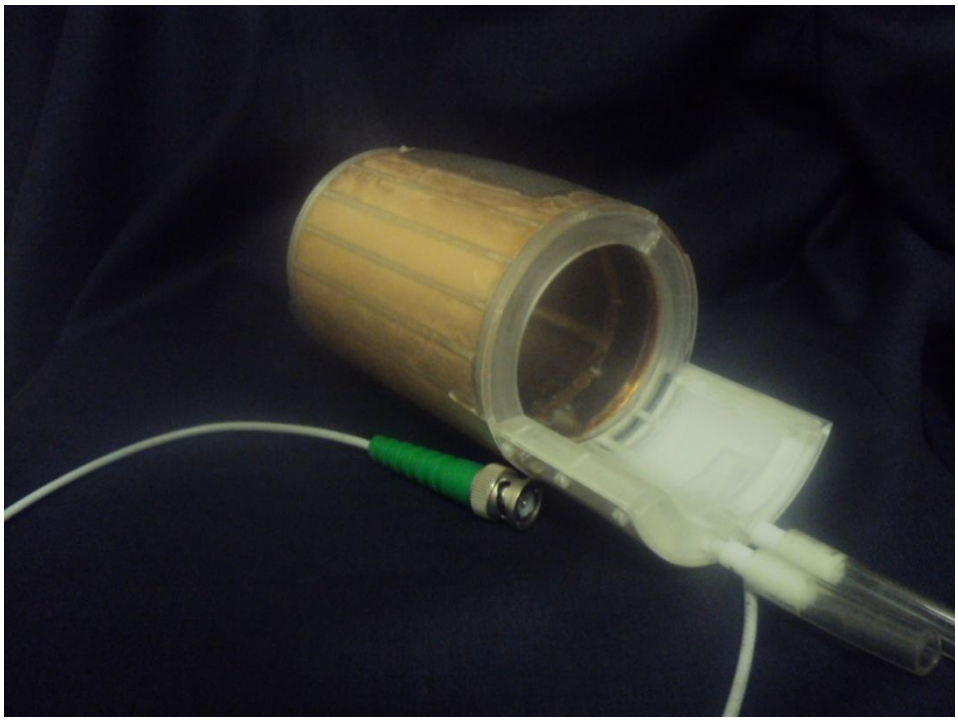

Figure 4.1: The 8cm internal diameter volume coil. The full animal was positioned within the coil (*cf.* the Surface coil - Figure 3.2)

4.2.2.1 Operative interventions in the MRI of peripheral nerve experiment

4.2.2.1.1 Unrepaired Sciatic Nerve Transection (MRI)

Rather than capping the ends of transected nerves in silicone and burying the nerve/cap construct in local muscle which may seriously distort local anatomy (*cf.* 2.2.1.1 – 2.2.1.3) a less invasive transection model was used in the sciatic nerve anatomical experiments. Following otherwise identical pre-operative preparation, a much more limited ≈5-8mm skin incision was made over the area of the hind limb which experience had taught would be directly above the upper border of the *rectus femoris* muscle. At this level the sciatic nerve was dissected free of its surrounding connective tissue and a 1mm segment excised by sharp dissection with no attempted repair. The skin was closed as described previously

4.2.2.1.2 Sciatic Nerve Crush

Anæsthesia and nerve exposure were identical to above, however rather than being divided the nerve was crushed using No 5a jeweller's forceps for two periods of ten seconds. Before closure, the nerve was inspected to ensure that there was no loss of continuity.

4.2.2.1.3 Intraneural Injection of manganese chloride

Manganese Chloride ($MnCl_2$) is a paramagnetic agent used as contrast media in MRI studies (Elster 1994) In biological neuronal systems it has been shown to be taken up by nervous tissue as an analogue of calcium and distributed along neuronal tracts (Natt *et al.*, 2002; Matsuda *et al.*, 2010). Following the protocol of Natt *et al.*, (2002) 120mMol solution of $MnCl_2$ (Sigma) in normal saline was injected into the sciatic nerve at the upper border of *rectus femoris* after standard anæsthesia and exposure. The contrast solution was delivered intraneurally by means of a micro-needle drawn from a glass tube after heating over a Bunsen flame. Accurate dispensation of contrast agent was achieved by securing the micro-needle with a short section of glass tubing onto a Hamilton syringe (Hamilton, Switzerland), with the join being sealed with molten paraffin wax. Manganese chloride solution was drawn up by evacuating the Hamilton syringe enough to fill the attached glass micro-needle and a segment of the pre-calibrated Hamilton syringe. 5μL of contrast was slowly introduced under the perineurium of the nerve under magnified vision, the needle held in place for ten minutes before extraction to minimise spillage of contrast solution from the nerve. Ten times greater volume of contrast was used than in the study of Natt *et al.,* (2002) due to the greater size of the sciatic nerve in relation to the optic tract. Thereafter wound closure and animal analgesia and recovery was following previously described methodology.

4.2.2.2 Study design

Literature suggests that segments of nerve undergoing Wallerian degeneration demonstrate signal changes on MRI, particularly using T_2 weighted sequences (Aagaard *et al.*, 2003; Bendszus *et al.*, 2004; Behr *et al.*, 2009). A series of experiments were designed to assess imaging of rat sciatic nerve using the 7T magnet and the custom built 2cm surface or 5.8cm volume coils. These included:

- Surface coil positioned over lateral aspect of a normal hind limb.
- Surface coil positioned over lateral aspect of a hind limb 7 days after sciatic nerve crush lesion. A time point at which Aagaard *et al.*, (2003) detects signal changes in injured nerve.
- Surface coil positioned over lateral aspect of a hind limb 7 days after sciatic nerve transection. A time point at which both Aagaard *et al.*, (2003) and Behr *et al.*, (2009) identify increases T_2 signal in distal nerve stumps.
- Surface coil positioned over lateral aspect of a hind limb 12 hours and 20 hours after intraneural injection with the paramagnetic contrast agent manganese chloride (5µl 120mM aqueous solution) (*cf.* Natt *et al.*, 2002).
- Volume coil surrounding full hind quarters of an animal with a normal nerve.
- Volume coil surrounding full hind quarters of an animal 7 days after sciatic nerve crush.
- Volume coil surrounding full hind quarters of an animal 7 days after sciatic nerve transection.
- Volume coil surrounding full hind quarters of an animal with a nerve injected with the paramagnetic contrast agent manganese chloride (12h and 20h post injection)

For each of these conditions a range of scanning sequences and parameters **(Appendix 2)** were used including proton density and T_1 weighted gradient echo sequences, T_2 weighted fast spin echo sequences, diffusion weighted and 3D gradient echo scans similar to that used in the DRG quantification. Images were first displayed on the SMIS console monitor, before being converted to *.tif* format for export.

4.2.3 EXPERIMENT THREE: High Frequency Ultrasound of the Rat Sciatic Nerve

4.2.3.1 Operative and Practical Techniques in the High Frequency Ultrasound Study

4.2.3.1.1 Unrepaired Sciatic Division (US)

For the ultrasound experiments, in order not to have dermal scar tissue overlying the nerve, which would potentially interfere with ultrasound transmission, a slightly larger more proximal skin and muscle incisions than those used for unrepaired sciatic nerve transection was utilised (*cf.* 4.2.2.1.1). Gentle retraction of these tissues still allowed easy access to the nerve, but offset the position of the final scar. As nerve regeneration was required for these experiments, the nerve was dissected free of its surrounding connective tissues and cleanly divided and the nerve stump ends put in close approximation to each other. Wound closure was not modified. Despite the larger incision required in this model no problems with wound breakdown were encountered.

4.2.3.1.2 Animals and pre-scan preparation

All animals used in the ultrasound studies were adult male Sprague Dawley rats, and were 'schedule one' killed prior to scanning. *Post mortem* the rump and hind leg was shaved, and further fur removal was facilitated by use of a commercial calcium thioglycolate depilatory cream (Veet® Hair removal cream, Reckitt Benckiser plc).

4.2.3.1.3 Ultrasound Scanning

All ultrasound imaging was performed using a VisualSonics® Vevo® 660 micro-imaging system, kindly loaned by Astra Zeneca UK **(Figure 4.2)**.

A single element, mechanically scanned, 3cm diameter 40MHz Real-Time Micro Visualization (RMV)-40A transducer was used to generate B-mode real time images of rat sciatic nerve on the integrated display monitor. Other parameters included a master gain of 21.00dB, 10x10mm field of view and 30 Hz frame rate. Commercial water based gel was used as a probe-skin interface (Parker Laboratories Inc, New Jersey). This system had a focal depth of 6mm generating high resolution images. Image capture and analysis were performed using the software accompanying the Vevo system.

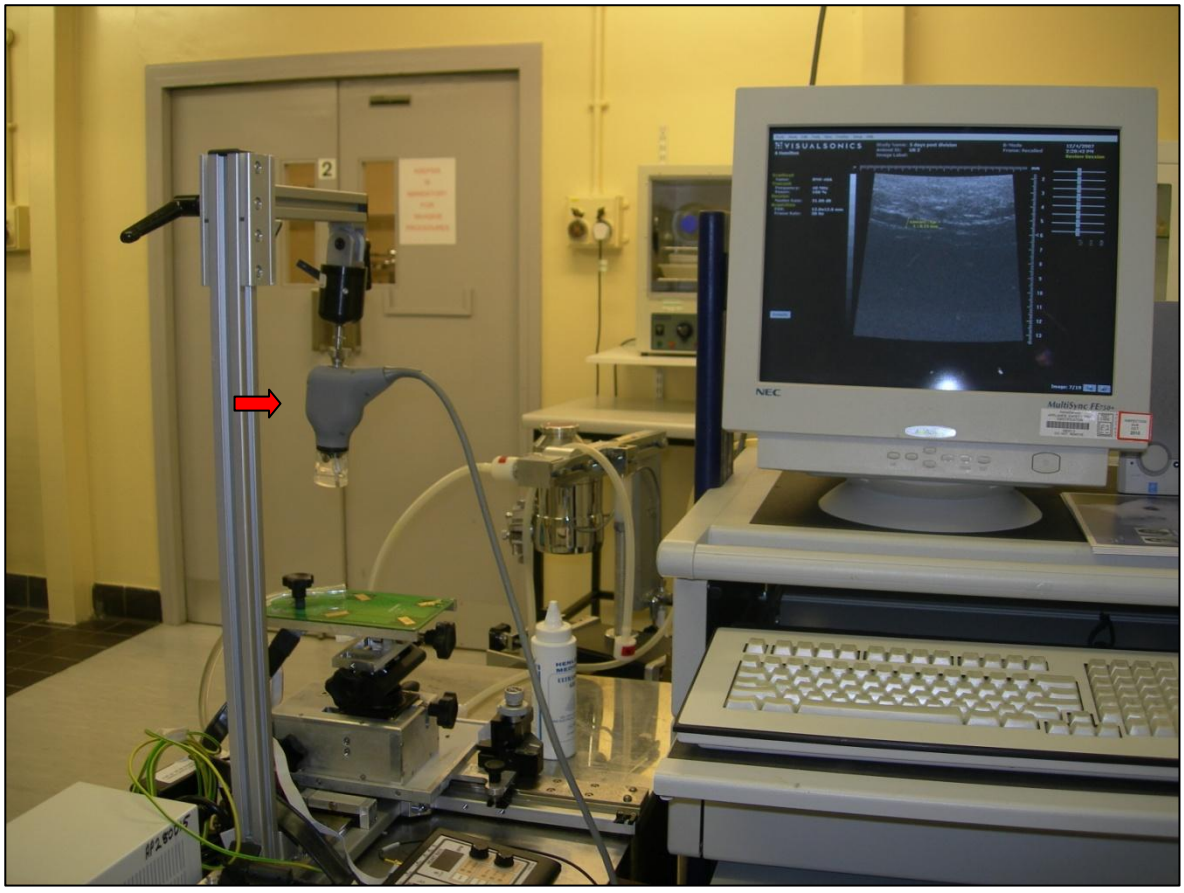

Figure 4.2: The VisualSonics Vevo 660 High frequency Ultrasound Scanner. The scan head (red arrow) is seen suspended from a holding gantry to the left of the picture, while the system casing and monitor are to the right.

4.2.3.2 Study Design

There was no previous literature suggesting that such an HFUS system had been used for nerve imaging using any animal model. The aim was to identify the intact rat sciatic nerve, the divided nerve and lesions in continuity. Additionally, it was unknown if the neuroinflammatory changes occurring during Wallerian degeneration would cause detectable change in the echogenicity of the distal stump after nerve transection.

The first pilot study was to scan a single normal animal to identify whether the HFUS system could visualise the sciatic nerve. Following this, two animals underwent identical unrepaired sciatic nerve transection operations in which the severed nerve ends were left in

close approximation but not coaptated. These animals were allowed to survive for 2 and 8 days respectively, before 'schedule one' termination and scanning allowing assessment of nerve response to injury and early regeneration. After scanning the course of the sciatic nerve was dissected under x3.8 loupe magnification (Surgical Acuity, Middleton, Wisconsin) to allow direct comparison of scanned images to gross appearance.

4.2.4 EXPERIMENT FOUR: High Frequency Ultrasound of the Human Digital Nerves

In this brief study the scan head of the Vevo 660 HFUS system was simply applied to the volar/ulnar aspect of the left index finger of three volunteers, using ultrasound transmission gel as an interface. Attempts were made to identify the components of the ulnar neurovascular bundle at the midpoint of the proximal and middle phalanges and the dorsal digital veins; common sites of injury.

4.3 RESULTS

4.3.1 EXPERIMENT ONE: *In Vivo* Volumetric L4 DRG MRI Scanning.

In vivo scanning of anæsthetised animals using the DRG imaging protocol had not been previously attempted. As a pilot study therefore, one animal was scanned alive under respiratory and temperature monitoring and again after 'schedule one' killing on the same day. The spinal cord and DRG could be distinguished in the live scan. Comparison with the images produced by *post mortem* scans **(Figure 4.3)** demonstrates that *in vivo* imaging gave lower signal-to-noise ratio, marked horizontal striation, 'smearing' of the image in the vertical axis and loss of signal toward the deeper areas of the animal in the scan taken from the live animal. In the *in vivo* scan, the signal is noted to deteriorate more markedly at the extremes of the sequence stack, and with distance from the surface coil (placed on the animals back) than in the *post mortem* images; the first and last few images of the

sequence, and the lower portion of each image appeared markedly degraded. It is interesting to note that blood vessels such as the abdominal aorta and paraspinal vessels are highlighted, presumably reflecting a time-of-flight angiography effect (Westbrook 2002). However, there does not seem to be any 'ghosting', possibly due to the 3D-gradient echo nature of the acquisition which is less affected by phase encoding artefact. Images from the two scans were analysed to measure the DRG volume as described previously (*cf.* 3.2.2.4). The results showed that the mean volume for the L4 ganglion was 4.5mm^3 in the *ex vivo* scan and 7.6mm^3 in the *in vivo* images.

4.3.2 EXPERIMENT TWO: Attempted MRI of the Rat sciatic Nerve

Despite interpretation of the resulting images by four observers cognisant of the pertinent neuroanatomy, the sciatic nerve could not be reliably identified using this technique. In many scans imaging the thigh longitudinally or obliquely (*cf.* Aagaard *et al.,* 2003), longitudinal structures were observed coursing parallel to the femur towards the popliteal fossa and thus following the topography of the nerve.

These structures would often display high intensity on T_2 weighed images; but when analysing the images as a sequence, they would be present in too great a number of slices to be consistent with the diameter of the nerve **(Figure 4.4)**.

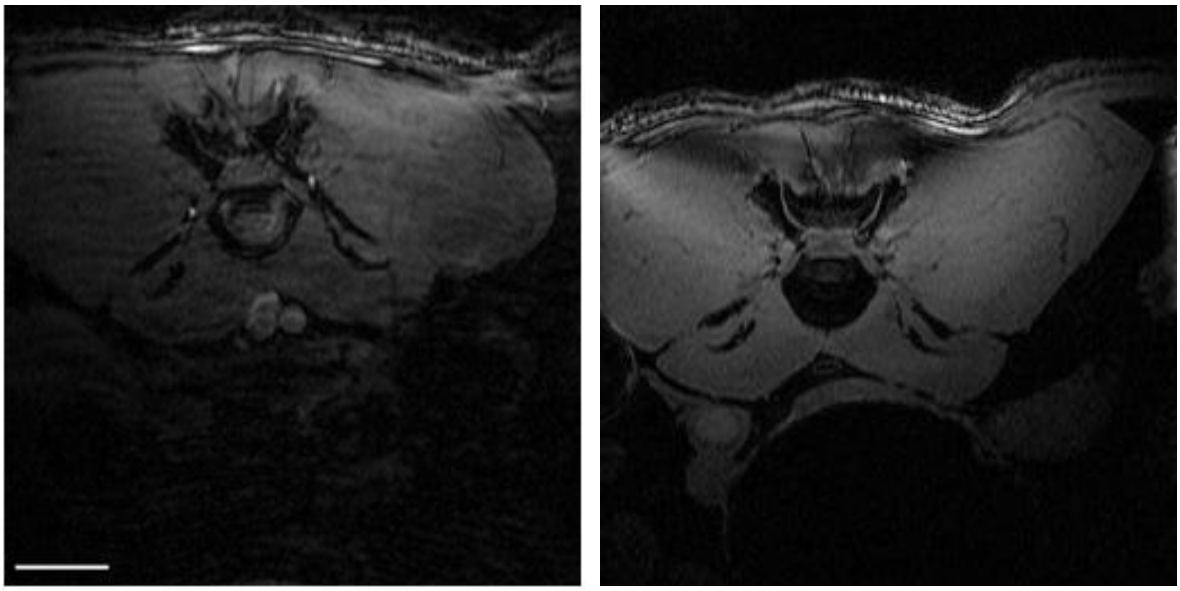

Figure 4.3: *In vivo* (left) and *ex vivo* (right) MR images of comparable sections of the same animal. Scale bar = 0.5cm.

This longitudinal structure is likely therefore to represent the intramuscular tissue plane deep to the gluteal muscles in which the sciatic nerve lies, rather than the nerve itself. Of interest, on fast spin echo T_2 weighted scans of animals which had undergone operations there was often diffuse signal hyperintensity in this region compared to the contralateral side **(Figure 4.5)**. However, again this structure was present at the same level in too many sections to be the sciatic nerve, and this hyperintensity was interpreted as more likely reflecting post traumatic œdema rather than any intrinsic neurophysiological phenomenon. In many of the post-operative or normal animals this region of interest would display marked T_2 hyperintensity bilaterally on fast spin echo images, **(Figure 4.4d, Figure 4.5)** a finding at odds with Behr *et al.,* (2009) who found un-operated nerve and its surrounding muscles to be isointense. Further, in scans transecting the thigh or leg distal to the knee joint in an axial plane (*cf.* Bendszus *et al.,* 2004; Behr *et al.,* 2009) no structures representing the three distal branches of sciatic nerve (tibial, popliteal and sural nerves) in cross section could be differentiated from the surrounding muscle tissue either post injury or using differing sequences **(Figure 4.6)**.

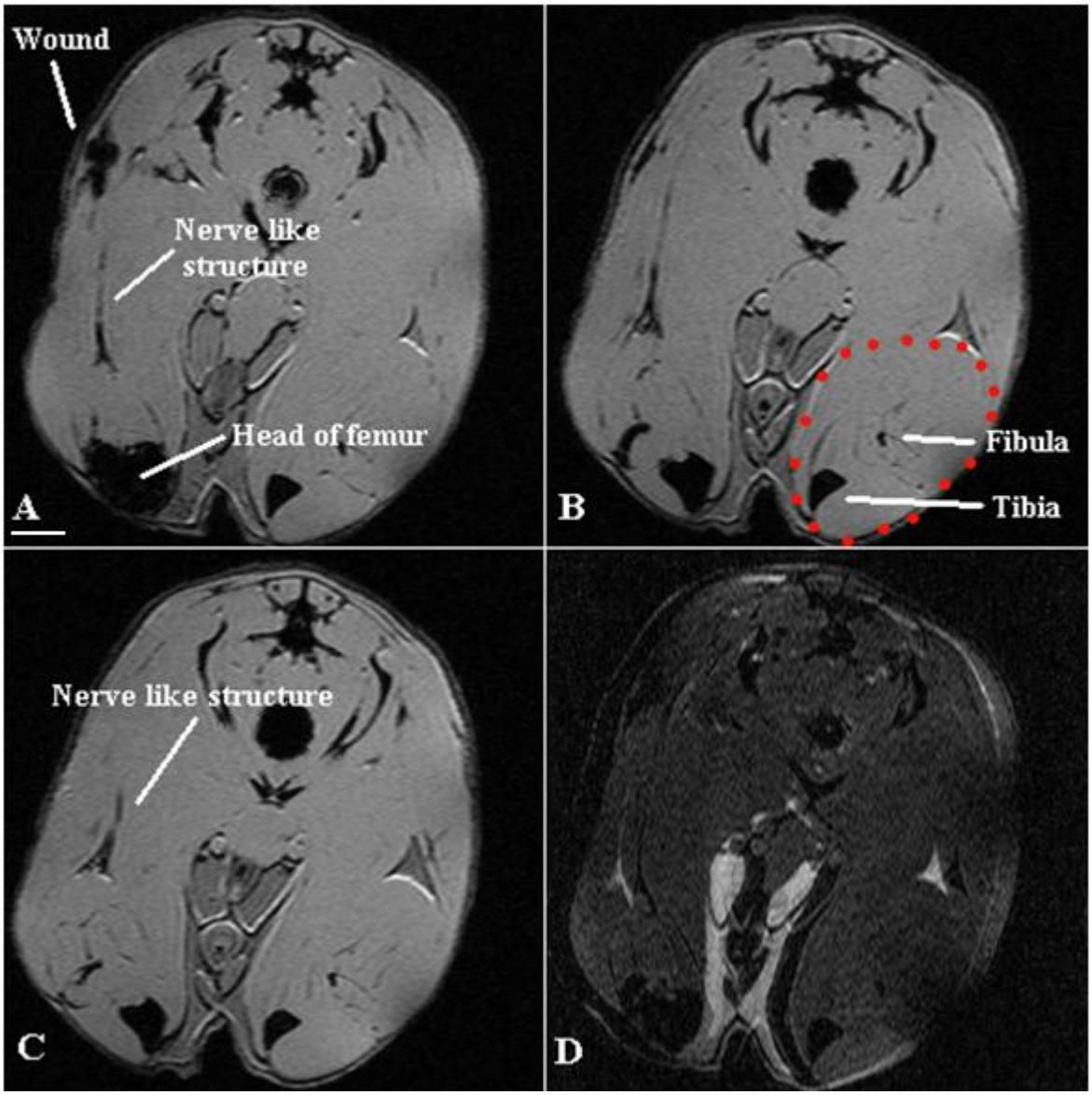

Figure 4.4: (A-C) Images from T_1-wighted gradient echo sequence of rat body and hind limbs around the region of the knee joint acquired using the volume coil. Animal had undergone sciatic crush 7 days previously. Image D is from a T_2-weighted fast spin echo sequence of the same animal; the higher level of noise is noted. The breach in the integrity of the superficial muscle layers at the level of the wound is noted. Running distally from beneath the wound is a longitudinal structure following the course of the nerve towards the popliteal fossa which is hyperintense on the T_2-weighted image. However, the same structure is also seen in slices B and C, at the same level; these slices are some 1cm distal to slice A, the structure cannot therefore be the 1mm diameter sciatic nerve. Further, in the more distal sections the leg below the knee has been cut in cross section (marked red in B), there is no evidence of any structure resembling the tibial or peroneal nerves visible in either sequence. Scale bar = 0.5cm.

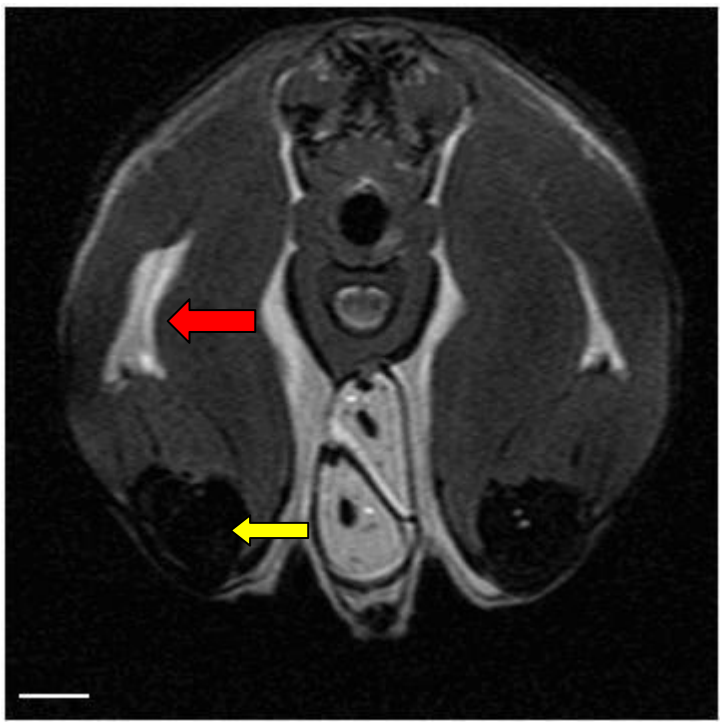

Figure 4.5: T_2 weighted axial fast spin echo sequence of rat hind limbs 7d after unilateral sciatic division. There is clearly greater enhancement in the area of the popliteal fossa and intramuscular plane on the operated side (left of picture, red arrow), but still a remarkably high signal intensity on the un-operated side. The femoral head is marked by the yellow arrow. Scale bar = 0.5cm.

Figure 4.6: Caption over.

Figure 4.6 (Previous page): T_2 weighted fast spin echo sequence transecting the distal legs in cross section just distal to the knee joint in an animal which was 7 days after left sided sciatic transection. The tibiae (red arrow) and fibulae (yellow arrow) are seen as dark areas bilaterally but no hyperintense areas that could represent the distal branches of the sciatic nerve can be identified. Scale bar = 0.5cm

Sans of animals in which the sciatic nerve had undergone intraneural injection with manganese chloride, similarly failed to demonstrate the sciatic nerve at the site of injection **(Figure 4.7)**, but rather occasionally demonstrated diffuse and non-specific T_1 signal gains appropriate sequenced images. Natt *et al.*, (2002) had described uptake and retrograde transport of $MnCl_2$ allowing tracing of neural pathways, but at neither time point at which injected nerves were imaged was any signal change in the DRG noted **(Figure 4.8)**.

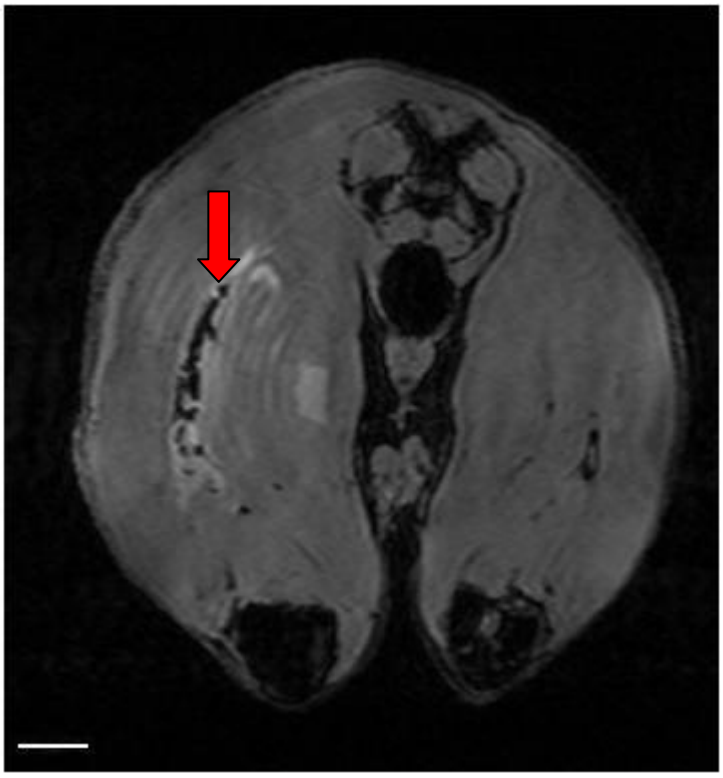

Figure 4.7: T_1 weighted high resolution oblique gradient echo sequence cutting through the thighs in a plane parallel to the femur 12h after intraneural injection of manganese chloride into the left sciatic nerve. Generalised disruption of the muscle planes caused by dissection is seen (red arrow), as is non-specific foci of signal increase, but no single structure traceable over multiple sections can be identified as the sciatic nerve. Scale bar = 0.5cm.

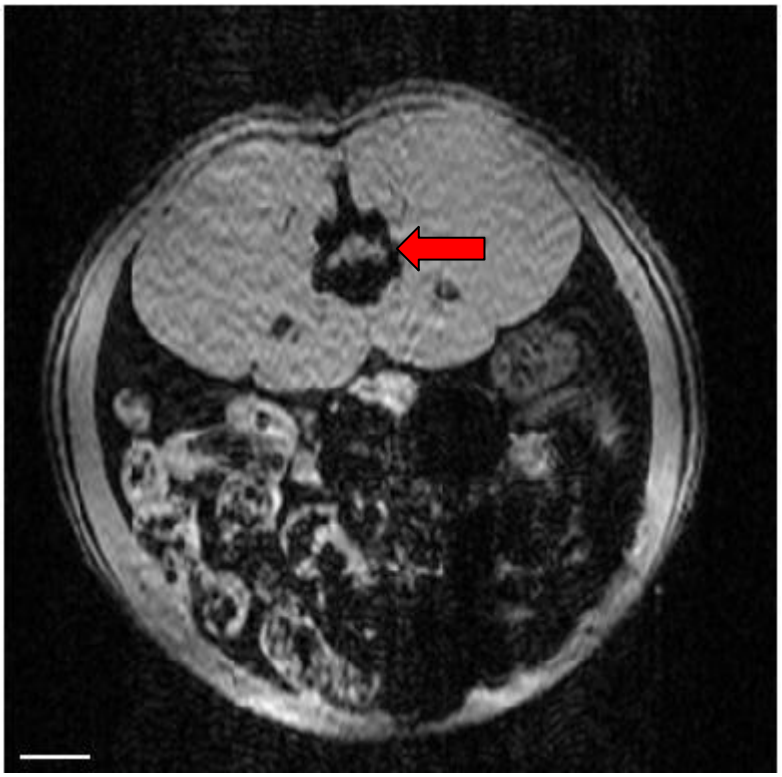

Figure 4.8 - T1 weighted high resolution axial gradient echo sequence at the level of the L4 DRG from an animal 20h after intraneural injection of manganese chloride into the left sciatic nerve. The DRG can be visualised each side of the spinal cord at the centre of the bulk of paraspinal muscles in the superior half of the image (red arrow marks right DRG). There is no convincing signal change between each side as would be expected after retrograde transport of paramagnetic contrast. Scale bar = 0.5cm.

4.3.3 EXPERIMENT THREE: High Frequency Ultrasound of the Rat Sciatic Nerve

4.3.3.1 Identification of the Sciatic Nerve

One normal adult male Sprague Dawley rat was scanned over the region of the sciatic nerve *post mortem*. The full course of the sciatic nerve was easily identifiable in both longitudinal and cross sectional axes from the emergence through the sciatic notch until its trifurcation **(Figure 4.9 & Figure 4.10)**. Further; the sural and peroneal branches were observable for the majority of their superficial course. The tibial nerve was not identifiable for its full course; being lost from view as it proceeded deeper into the cleft between the heads of gastocnemius muscle leaving the plane of penetration of the scan head **(Figure 4.11)**.

Figure 4.9 - HFUS image of the trunk of the rat sciatic nerve in longitudinal section (red arrow), emerging from under the echo impenetrable bone of the pelvis (dark crescent at the left hand side of image). The contrast of the hyperechoic epineurium and less bright neural tissue is appreciated

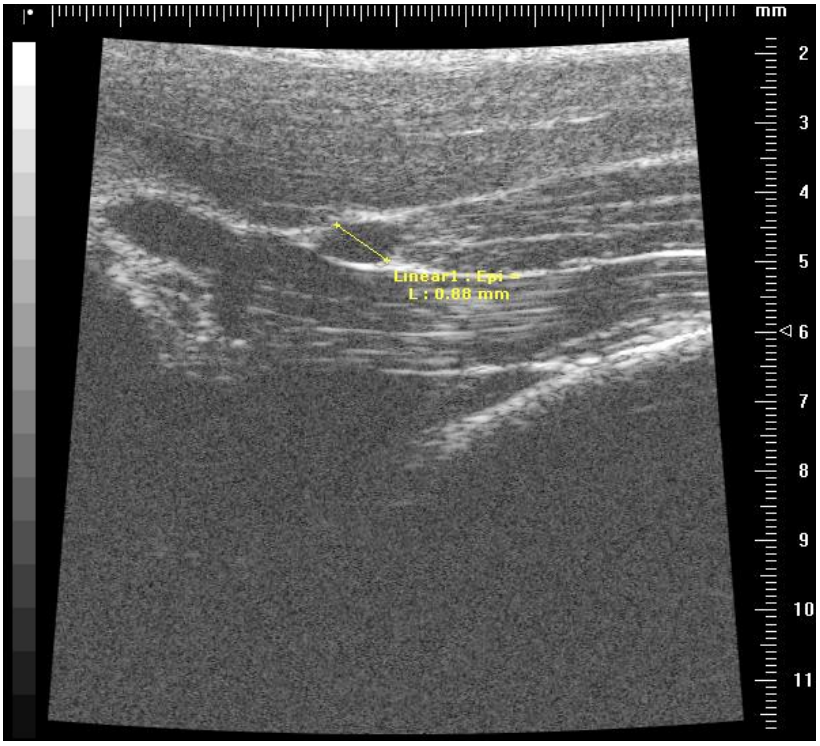

Figure 4.10 - HFUS image of the rat sciatic nerve in cross section, marked with real time measurement by the Vevo package (the cross sectional area being 0.89mm

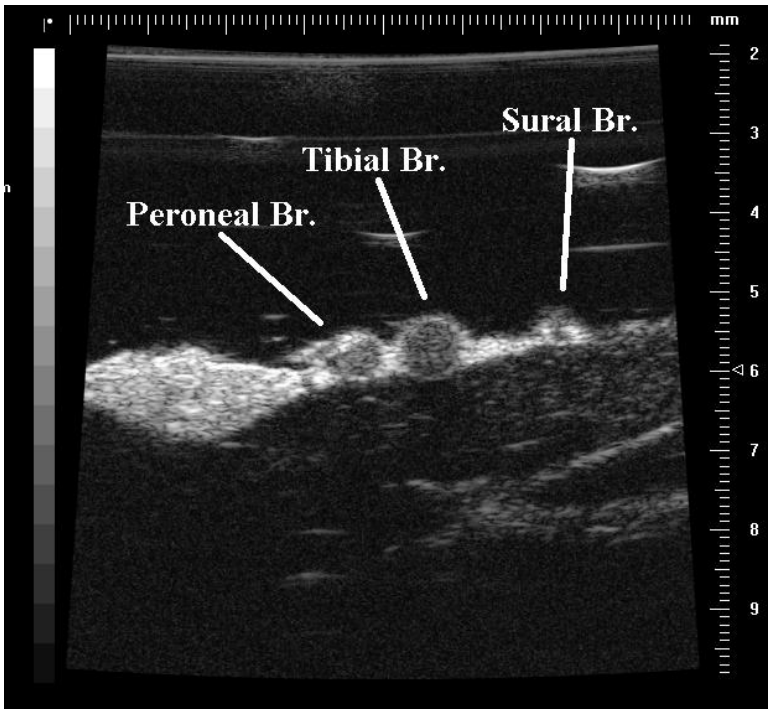

Figure 4.11 - HFUS image just distal to the trifurcation of the sciatic nerve in cross section,identifying the three branches.

4.3.3.2 Detection of injured Sciatic Nerve

To assess the ability of HFUS to detect differing degrees of nerve injury two animals underwent non-repaired sciatic nerve transection and were scanned *ex-vivo* after 2 and 8 days respectively. After 2 days an obvious gap in the continuity of the nerve was detected by HFUS, and verified on inspection **(Figure 4.12)**.

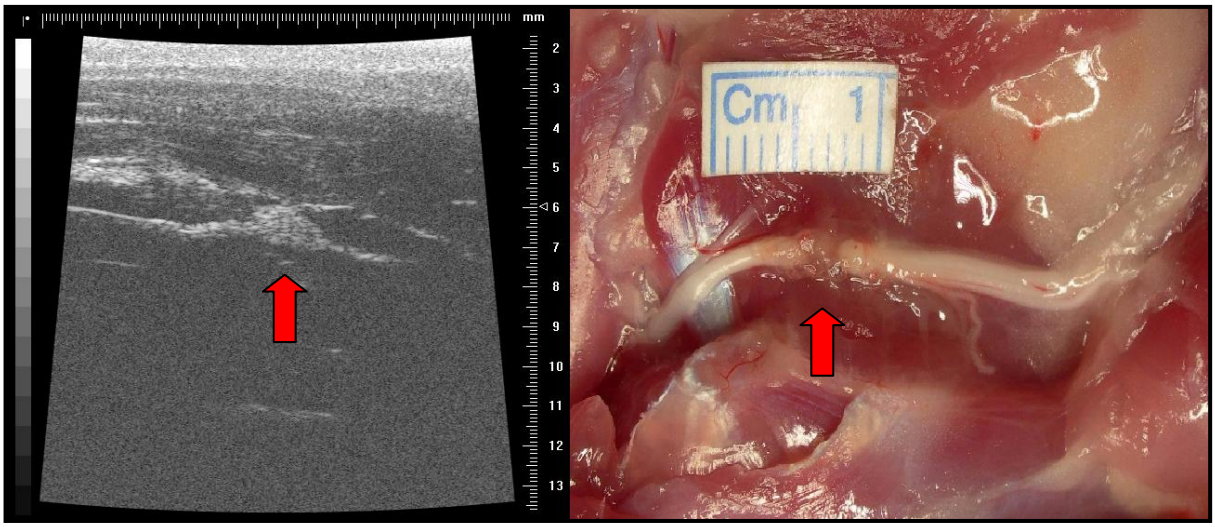

Figure 4.12: Comparison of HFUS image 2 days after sciatic nerve transection with gross appearance. An obvious gap at the site of injury can be seen of the HFUS image, which is verified by the dissection image (arrows).

At 8 days after injury a less marked disruption of the nerve architecture could be seen using ultrasound which corresponded to a partly regenerated lesion in continuity on visual examination **(Figure 4.13)**.

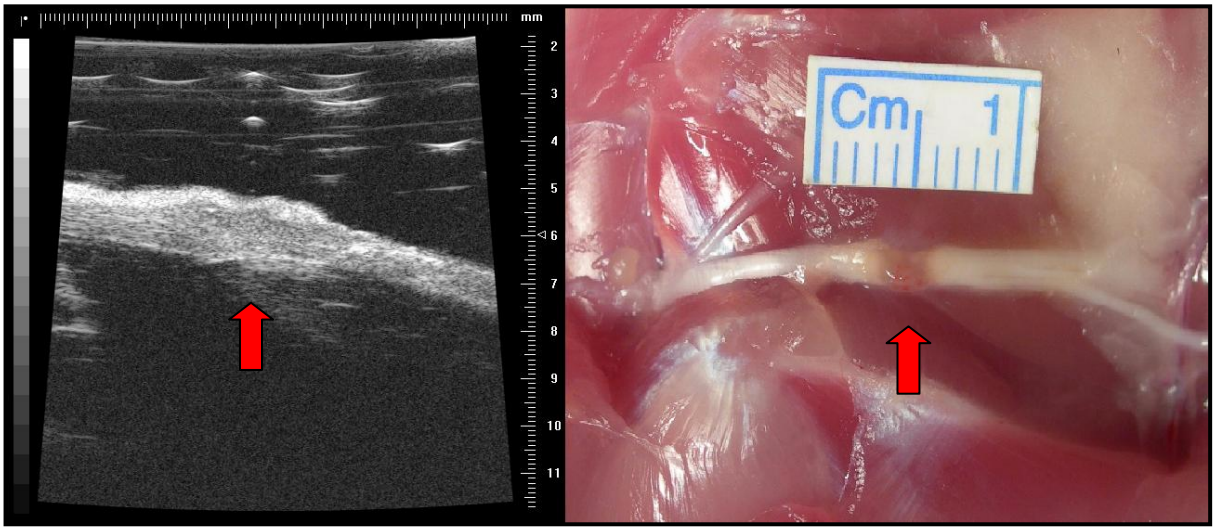

Figure 4.13: Comparison of HFUS image 8 days after sciatic nerve transection with gross appearance. While far from normal, the scanned image seems to demonstrate a continuity between the previously divided nerve ends. Gross appearance verified these findings, a confluent connective tissue bridge spanning the injury site. Injury sites marked by arrows.

At neither time point were any differences observable in the image signal from nerve segments proximal and distal to the injury, seeming to demonstrate that HFUS scanning shows purely anatomical features of regeneration rather than be affected by the underlying neuropathology.

4.3.4 EXPERIMENT FOUR: High Frequency Ultrasound of the Human Digital Nerves

Following the success of the animal sciatic HFUS scanning the ability of the unit to visualise the components of the human digital neurovascular bundle was assessed. In all three volunteers, both structures of the left index digital neurovascular bundle could be visualised at both the proximal and distal phalanx **(Figure 4.14)**. Using real time video

imaging, pulsatile motion of the digital artery and compressibility of the surrounding dorsal veins could be used to differentiate from the digital nerve. Locating the digital nerves was qualitatively slightly more difficult that identifying the sciatic branches in the rat despite their similar diameters, further, the quality of the human images was not as highly detailed, with a slightly greater signal to noise ratio presumably due to the thicker layer of keratinised epidermis and tough dermis on the volar aspect of the human hand compared to the flank of the rat.

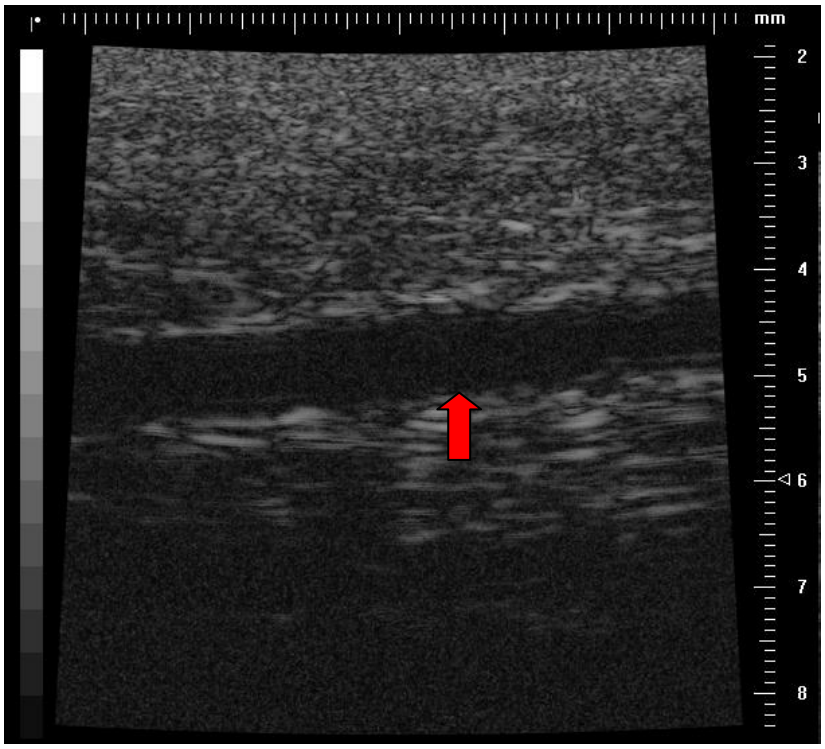

Figure 4.14: The human left index finger ulnar digital nerve (red arrow), visualised by HFUS at the midpoint of the proximal phalanx.

4.4 DISCUSSION

4.4. EXPERIMENT ONE: *In Vivo* Volumetric L4 DRG MRI Scanning

In vivo imaging presents a few logistical issues not encountered with dead animals; holding the surface coil in position securely over the rat's hind quarters without embarrassing the animal's respiration requires some compromise of coil security. Further, the animal cannot be seen when within the magnet bore, making assessment of depth of anæsthesia

more challenging. Comparison of the *in vivo* to *post mortem* scans (*cf.* Figure 4.3) demonstrates a number of artefacts, the signal-to-noise ratio is worse in the live animal images with a greater degree of 'unsharpness', there is marked horizontal striations with the image appearing 'smeared' in y-axis. This is most likely to reflect motion artefacts due large regular global movements such as the respiratory excursion and cardiac cycle, as smaller more local motion caused by pulsatile flow in medium and small blood vessels, and less predictable movements such as peristalsis in the abdominal viscera. Quantification of the DRG profiles obtained during the *in vivo* and *post mortem* scanning demonstrates a 69% increase in the measured mean volume of the DRG in the live scan. It is unlikely that a volume change of such magnitude could occur as a post-mortem artefact, and therefore this apparent enlargement must be substantially attributable to the reduced image quality produced *in vivo*. Such large artefactual effects on the apparent volume of the DRG were felt to be too great to allow further animals to be sacrificed in any more numerous studies of live scanning until solutions could be employed to improve the resolution of *in vivo* imaging.

Various possible strategies to compensate for the effect of motion artefact have been explored. Increasing the number of signal averages has been suggested (West *et al.*, 2007); however this greatly increases the scan time, which may become restrictive if imaging live animals. The increased time needed to optimally position the coil and shim the magnet encountered on the *in vivo* trial lead to the rat being anæsthetised for approximately 2.5h, and any significant further elongation of this period must be viewed with caution.

Navigator echoes are often used as a motion compensation device (Ehman & Felmlee, 1989; Wang *et al.*, 1996), this technique takes an additional line of non-phase encoded data

which, in k-space can be used to detect in-plane motion (Kadah *et al.,* 2004). Unfortunately no navigator echo enabled sequences were included in SMIS® parameter library, and despite extensive searching, no literature emerging from other groups using such techniques and translatable to our hardware could be found.

A third potential technique for reducing the effect of motion artefact is the use of respiratory and ECG gaiting (Burdett *et al.,* 1993; Weber *et al.,* 2006), in which a piezoelectric transducer and electrodes are used to externally monitor the animals respiratory motion and ECG respectively. This information is fed into the MRI hardware and the sequence is run only during set periods of the cardiac and respiratory cycles. This technique will also necessitate some lengthening of the image acquisition time, but is believed to be the most satisfactory option. After some delay, funding sources were identified for purchase of such equipment, and compatibility issues relating to both the scanner and SMIS hardware seem close to being resolved and which hopefully allow gaiting to be used in future experiments.

4.4.2 EXPERIMENT TWO: Attempted MRI of the Rat sciatic Nerve

The failure of numerous attempts to visualise the rat sciatic nerve with the 7T hardware using a variety of MRI sequences, coil conditions, increasingly severe nerve injury models and contrast enhancement is surprising, frustrating and disappointing. Image resolution is unlikely to be responsible for these difficulties as, in the DRG imaging protocols (amongst those used when attempting to locate the nerve) structures such as the paravertebral arteries, and joint space of the intervertebral facet joints could easily be identified, both of which are substantially smaller than the 0.8-1mm diameter sciatic nerve.

The difficulties most probably reflect lack of contrast between the neural structures and the surrounding muscle, despite the much higher lipid content of nerve in comparison to muscle. It is noted that DRG are surrounded predominantly by bone of the intervertebral foramina and the subdural space, explaining why these issues were not relevant in DRG imaging. The hardware used in the experiments of Aagaard *et al.,* (2003) and Bendszus *et al.,* (2004) were markedly different from our 7T scanner, both of the earlier studies using 1.5T clinical scanners, with wide diameter surface coils and access to complex sequences such as FLASH, short τ-inversion, turbo inversion recovery, fat suppressed T_1-weighting and double spin echo which were not available using the SMIS® parameter library being limited to T_1 and T_2 weighted gradient-, and spin-echo sequences. It is less easy to explain why the findings of Behr *et al.,* (2009) could not be mirrored, as the 4.7T research scanner used by this group seems to have had a limited number sequences available in its library (i.e. no complex sequences were used, or in fact mentioned in this group's paper), and yet multiple attempts over a significant time period assessed by this study could not localise the sciatic nerve with precision great enough to consider running a full experiment based on the technique. Further, our methodology consistently found T_2 signal hyperintensity in the area of the nerve on both sides after unilateral nerve injury and even in normal subjects.

4.4.3 EXPERIMENTS THEE AND FOUR: High Frequency Ultrasound of the Rat Sciatic Nerve and Human Digital Nerve

Ultrasound imaging of peripheral neural structures is becoming an increasingly recognised and useful clinical imaging modality (Khachi *et al.,* 2007), with applications including diagnosis of carpal tunnel and other compression neuropathies (Lee *et al.,* 1999), guiding regional anæsthesia blocks (Baldi *et al.,* 2007; Hadzic *et al.,* 2008) and investigation of nerve and nerve sheath tumours (Stelow *et al.,* 2004; Gruber *et al.,* 2007). Current clinical

scanners used for superficial tissue imaging, such as nerve, muscle, tendon, breast and testes tend to use frequencies in the range of 7-18MHz (http://www.medical.siemens.com), the Vevo system offers up to 40MHz which therefore offers higher resolution imaging, but at the cost of reduced beam penetration, the focal plane for the RMV-40 scan head used being only 6mm.

There have been both anatomical verification studies (Cartwright *et al.,* 2007) and clinical (Cokluk & Aydin, 2007) investigations of imaging transections of the major upper limb neural structures (brachial plexus, radial, median and ulnar nerves), but no published work describing imaging of structures as small as the manual digital nerves could be identified. Animal studies have described ultrasound imaging of neuromata in the rabbit peroneal nerve after transection (de Kool *et al.*, 2005).

Imaging the rat sciatic nerve was relatively easy and the full course from the sciatic notch to well beyond the trifurcation into the main branches could easily be demonstrated. Further, imaging of injured nerve was straight forward, but was hampered if the scar tissue from the skin incision was interposed. Although limited time availability with the scanner precluded investigating a wide range of time points, there was a clear difference in the images when comparing new and partly regenerating injuries corresponding to neurotmetic and axonotmetic grades of Sunderland's nerve injury classification (Sunderland 1951). HFUS clearly offers a new and powerful *in vivo* research tool potentially applicable for many applications in peripheral nerve research. The animal experiments described here were all performed *ex vivo* as the limited time available with the scanner precluded application for an amendment to the researcher's animal licence to allow ultrasound imaging of live animals. However, the HFUS scanning is entirely non-invasive, and because the images are generated and captured in real time there is no necessity for the

animal to lie still for prolonged time periods requiring anaesthesia. It might also be possible that HFUS scanning could be undertaken without any form of anaesthesia or sedation, an obvious boon in terms on animal welfare.

There is also an obvious potential for clinical translation of this technology, human digital nerves could be visualised, which does not seem to have been reported previously. The relative simplicity of use of the hardware has the potential to act as a valuable operative planning modality. The small 'footprint' and ease of training of the HFUS equipment could easily be implemented into a clinical setting where patients with digital injuries and equivocal clinical findings could be scanned to assess continuity of the digital neurovascular bundle, potentially reducing otherwise unnecessary 'exploratory' operations to explore a neuropraxic or axonotmetic nerve injury which need not have occurred. Such operations, presenting the surgeon with 'nothing to repair' inconvenience the patient, and have a significant health care cost associated with them. HFUS in the animal model discussed here appears to have the ability to differentiate between such grades of injury and physical nerve disruption and therefore holds the potential to significantly benefit patients.

CHAPTER 5

In Vitro Study of *N*-Acetylcysteine and Acetyl-*L*-Carnitine in Primary Sensory Neuronal Culture

5.1 BACKGROUND AND EXPERIMENTAL DESIGN

5.1.1 Development of DRG Neuronal Culture.

Cell or tissue culture of neuronal cells initially started during the first half of last century, with most research involving neuronal tissue isolated from central nervous system of embryonic or neonatal sources of tissue, (Harrison, 1907; Murray, 1965). It was not until later that cultures of adult peripheral nervous system neurons, initially sympathetic autonomic neurons, could be maintained **(Table 5.1)**.

TABLE 5.1: Landmarks in Development of Neuronal Tissue Culture

Cell Type	Tissue	Animal	Authors	Year
Unknown	Unknown	Chick Embryo	Roux (Cited in Hamburger 1997)	1885
Neurectoderm	Neural Tube	Frog Embryo	Harrison	1907
Autonomic Neuron	Sympathetic Ganglia (Thoracic or Lumbar sympathetic trunks)	Adult Human	Murray and Stout	1947
Primary Sensory Neuron	Dorsal Root Ganglion	Chick Embryo	Scott *et al.*,	1969
Primary Sensory Neuron	Dorsal Root Ganglion	Human Embryo	Scott	1971
Autonomic Neuron	Sympathetic Ganglia (Superior Cervical Ganglion)	Adult Rat	Silberstein *et al.*,	1972a 1972b
Autonomic Neuron	Sympathetic Ganglia (Thoracic or Lumbar sympathetic trunks)	Adult Frog	Hill and Burnstock	1975
Primary Sensory Neuron	Dorsal Root Ganglion	Adult Frog	Padjen *et al.*, (cited in Scott 1977)	1975
Primary Sensory Neuron	Dorsal Root Ganglion	Adult Mouse	Scott	1977

The DRG dissociation and culture methodology used in this study follow the modifications of Scott's technique by Lindsay (Lindsay *et al.,* 1988; Lindsay *et al.,* 1996), which includes final suspension and culturing of neuronal cells in modified Bottenstein and Sato's (B&S) medium. This has precisely controlled additives and therefore avoids the methodological uncertainty inherent in leaving serum present in the final culture. This method has been successfully used by members of our research group (Caddick *et al.,* 2006; Kingham *et al.,* 2007; Mahay *et al.,* 2008)

5.1.2 Effects of ALCAR/NAC in *In Vitro* systems.

To date there have been no published experiments investigating the effect of NAC in cultured primary sensory neurons, and only one paper in which ALCAR was used to treat dissociated DRG from aging animals as a model of Alzheimer's disease in which NGF or ALCAR at one dosage level, reduced neuron death over time (Manfridi *et al.,* 1992). However ALCAR was not shown to improve growth rate of 'axons' when assessing the same neurite bearing cells subsequently.

NAC is neuroprotective for neuroma cells after withdrawal of neurotrophic support (Ferrari *et al.,* 1995), prevents oligodendrocyte apoptosis after TNFα withdrawal (Mayer *et al.,* 1994) and reduces the response and expression of apoptotic markers in PC12 cells stressed with reactive oxygen species generated by a range of chemicals. The beneficial effect of NAC in PC12 survival experiments has been verified by other groups subjecting cells stressed by lead (Aykin Burns *et al.,* 2005), hydrogen peroxide (O'Loghlen *et al.,* 2006), and cyanide exposure (Satpute *et al.,* 2008). The prime aim of these experiments were to analyse the mitochondrial or signalling events occurring after stressing and antioxidant treatment and although cell survival assays are frequently cited, these studies do not discuss the effect of NAC on neurite production. It is through such *in vitro* methodologies that NAC was found to increase intracellular synthesis of glutathione;

suppress NGF-induced c-fos and MAPK signalling, but not Ras (Katama *et al.*, 1996) NAC ALSO up-regulates Ras-ERK pathway signalling (Yan *et al.*, 1995; Yan *et al.*, 1998) which in turn amplifies synthesis of the anti-apoptotic factor Bcl-2 mRNA (Hsiao *et al.*, 2008). NAC also offers protection from free radical induced apoptosis; this requires signalling through at least two MAPK independent signalling cascades (O'Loghlen *et al.*, 2006).

ALCAR has been demonstrated to prevent the normal decrease in expression of NGF receptors in cultures of aged animal forebrain (Angelucci *et al.,* 1988), and to up-regulate the response of cultured PC12 cells to NGF in terms of both survival and neurite outgrowth (Taglialatela *et al.,* 1991). Brain neurons from the cerebral cortex, striatum and thalamus treated with ALCAR after serum withdrawl derived a survival benefit and performed favorablly in a varity of tests of apoptosis (Ishi *et al.,* 2000). Survival of cultured forebrain neurons subjected to the neurotoxin N-methy-d-aspartate (NMDA) is partialty enhanced by ALCAR (Forloni *et al.,* 1994).

5.1.3 Aims

No studies could be found in which young adult DRG neurons had been exposed to NAC or ALCAR *in vitro,* giving rise to the possibility of studying the biological effects of these neuroprotective and regeneration promoting agents using methodology previously shown to be effective for DRG neuron culture.

Previous work investigating NAC or ALCAR in cell line culture systems had used molar doses with huge variation, differing by orders of magnitude, particularly in studies using ALCAR. Given that many neurite inducing agents demonstrate a bell shaped dose-effect curve (Calabresi, 2008), it was an initial aim to try to define high, medium and low doses of each agent that did not display detrimental effects on cell culture. Representative high,

medium and low doses from the range used in previously published studies up to this threshold were selected (1mM, 5mM and 10mM for NAC and 100μM, 1mM and 10mM for ALCAR).

The most interesting documented effects of these agents *in vivo* is to provide primary sensory neuronal neuroprotection post-axotomy and, at least for ALCAR, to enhance peripheral nerve regeneration (Hart *et al.*, 2002c, Wilson et al 2010). Hence an experiment was designed to assess axotomised cell survival in culture and neurite outgrowth analysis as equivalent measures of these two effects. Cell survival and neuritogenesis in developing sympathetic peripheral neurons and PC12 cells are enhanced by, if not dependent on, NGF, the interaction of its various receptors and their downstream signaling cascades (Green & Kaplan, 1995; Kaplan & Miller, 1997, 2000; Kaplan & Stephens, 1994; Miller & Kaplan, 2001a, 2001b, 2003, 2007; Goold & Gordon Weeks, 2005). NGF was therefore chosen to act as a control arm for this experiment.

5.2 MATERIALS AND METHODS

5.2.1 DRG Neuronal Culture and NAC/ALCAR Treatment

5.2.1.1 DRG harvest, dissemination, culture

Young adult male Sprague-Dawley rats (Harlan Sprague Dawley Inc, UK) (n=3) were killed by concussion and decapitation. The vertebral column and its surrounding paraspinal muscles were rapidly dissected free, placed in disinfected plastic Petri dishes before expedient transport to a laminar flow culture hood within the tissue culture laboratory.

Within the culture hood, and using surgical loupe magnification (x3.8, Surgical Acuity, Middleton, Wisconsin) the vertebral columns were split in the sagittal plane and the spinal

cord removed, revealing the spinal roots entering the intervertebral foramina. The DRG were carefully pulled from their fascial connections with jewellers forceps, and collected in a Petri dish containing F-12 Nutrient Mixture (Invitrogen, UK) with L-glutamine (Invitrogen, UK) supplemented with 5ml/l penicillin/streptomycin (Invitrogen, UK) at 37ºC. Nearly all of the rat's DRG could be harvested, giving 40-45 ganglia per animal. Once suspended in this medium further microdissection was performed to excise the root or spinal nerve segments and connective tissue, leaving only the neuron containing part of the DRG swelling. The clean ganglia were collected in a 35mm culture dish containing 1.8ml F-12 nutrient medium as described.

Isolation of neuronal cells from the DRG connective tissue was performed by chemical and physical dissociation, beginning with addition of 0.125% (v/v) collagenase type IV (Worthington, UK) to the F-12 medium This was incubated for 60 minutes at 37°C in 5% CO_2 after which the F12/collagenase mixture was removed with a sterile glass pipette (Poulten & Graf, Barking UK), and fresh F12 and collagenase added and incubated for a further hour. After removal of collagenase, fresh F12 with 0.2% (v/v) trypsin (Worthington, UK) was added and the suspension returned to the incubator for 30min. After this period the medium was then removed and 30% (v/v) foetal bovine serum (Invitrogen, UK) in F-12 was used to inactivate the trypsin. Ganglia were washed in F12 and then mechanically dissociated by gentle trituration using a sterile glass Pasteur pipette until no DRG tissue clumps could be macroscopically identified. This cell suspension was passed through a 70μm filter (BD Falcon, UK) to remove any residual clumps of cells as well as myelin and connective tissue fragments. The suspension was centrifuged (Centaur 2, MSE) at 200g for 5min and the medium aspirated from the pellet to remove dead cells and debris.

Tituration, resuspension and centrifugation steps were repeated at least twice to ensure adequate DRG dissolution. Following the final centrifugation, all but the last 500µl of the supernatant was removed from the cell bolus and the cells were re-suspended in the remaining supernatant fluid. This concentrated cell suspension was further separated from any residual debris by layering. A track of 2ml of 15%(v/v) bovine serum albumin (BSA, Sigma, UK) BSA was prepared running down the side of a 15ml conical polypropylene tube (Falcon), the remaining cell suspension was gently pipetted down this BSA track to be collected on top of the BSA layer. These tubes were centrifuged at 600rpm for 10min, after which all supernatant fluid and cell debris were gently removed to leave only the bolus of dissociated neurons.

The neurons were re-suspended in 1.9ml modified Bottenstein and Sato's medium (F12 medium supplemented with 0.1mg/ml transferrin, 20nM progesterone, 100µM putrescine, 30nM sodium selenite, 1mg/ml BSA, 0.01mM cytosine arabinoside and 10pM insulin (all Sigma-Aldrich) and made up to the required volume to fill two eight well chamber slides per animal. 1900µl of neuron suspension from each animal were plated onto two sterile 8-well chamber slides (Lab-Tek) pre-coated with LaminiN-1 (2µg/ml diluted in tissue culture water, Sigma-Aldrich), which had been applied to the slides and incubated at 37°C, 5% CO_2 for two hours before seeding the DRG neurons. Neurons from each experimental animal were kept separated at all times.

5.2.1.2 NAC, ALCAR and NGF Treatment

After seeding the neurons either further BS medium (for absolute control conditions) or NGF, NAC or ALCAR made up in BS medium to the required concentrations were added to each well respectively; additive concentration/dilution calculations were planned so that

a further 100µl of treatment containing medium were added to each well, ensuring a final medium volume of 2ml for each condition.

NAC and ALCAR were purchased as anhydrous crystals/powder (Sigma-Aldrich) which dissolved in BS medium and serially diluted to give appropriate molar concentrations whereby addition of 100µl of concentrate would give final culture concentrations of 1mM, 5mM and 10mM for NAC; and 100µM, 1mM and 10mM for ALCAR. As storage and weighing the NAC/ALCAR crystals cannot logistically be undertaken under sterile conditions each solution was passed through a 0.22µm pore syringe driven microbiological filter (Millipore) prior to final addition to the culture medium. NGF control conditions were made up to 150ng/ml, reconstituted in F-12 (NGF 2.5, from mouse submaxillary glands, Sigma, UK), a concentration previously documented to stimulate neurite formation in similar DRG cultures (Mahay *et al.,* 2008). Neurons from each animal were seeded over two eight well chamber slides with a final volume of 2000µl in each well, treatments were administered as demonstrated in **Figure 5.1**, and slides were then incubated undisturbed at 37°C with 5% CO_2 for 24h.

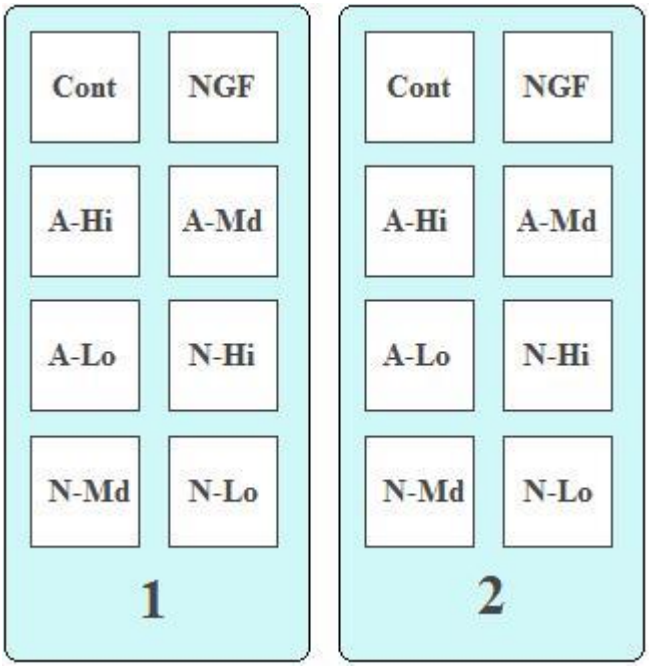

Figure 5.1: Schematic representation of the distribution and treatment of neurons seeded from each experimental animal. A final volume of 2000µl of BS medium, including additives was contained in each well. Treatment conditions were BS medium only (Cont), 150ng/ml NGF (NGF), 10mM ALCAR (A-Hi), 1mM ALCAR (A-Md), 100µM ALCAR (A-Lo), 10mM NAC (N-Hi), 5mM NAC (N-Md) and 1mM NAC (N-Lo). Culture duration was 24h at 37°C with 5% CO_2.

5.2.2 Culture Fixation, Histology and Image Analysis

5.2.2.1 Immunohistochemical Staining

After the 24h culture period, the BS medium was carefully removed by gentle pipetting not to disturbing adherent neurons; the cells were then fixed by addition of 1ml of 4% paraformaldehyde (Sigma-Aldrich, USA) in PBS at 4°C for 15 min. Each well was then washed three times in 1ml PBS for ten minutes, the cells permeabilised using 1ml of PBS with 0.2% (v/v) Triton X-100 for 20 min followed by a further three PBS washes. Neurons were 'blocked' by of addition of 2ml of 1% (w/v) normal horse serum (Sigma-Aldrich, USA) in antibody diluent for 1h in a humid chamber following which the cells were incubated overnight in 1ml of 0.1% (w/v) primary monoclonal antibody against $ß_{III}$ tubulin (Sigma-Aldrich, USA) in antibody diluent at 4°C.

The next day, after a PBS wash cells were incubated in flourescein isothiocyanate (FITC; λEx. 495nm, λEm. 519nm) conjugated horse-anti-mouse secondary antibody (Vector Laboratories, Peterborough, UK) at 1% (w/v) in antibody diluent for 2 hours at room temperature. After a final PBS wash, the plastic chamber construct was carefully removed from the underlying glass slide and coverslips mounted with Vectashield® mounting medium for fluorescence with 1.5 μm/ml 4',6-diamidino-2-phenylindole (DAPI, λEx. 345nm, λEm. 455nm, Vector Laboratories)

5.2.2.2 Image Analysis and Statistical Analysis

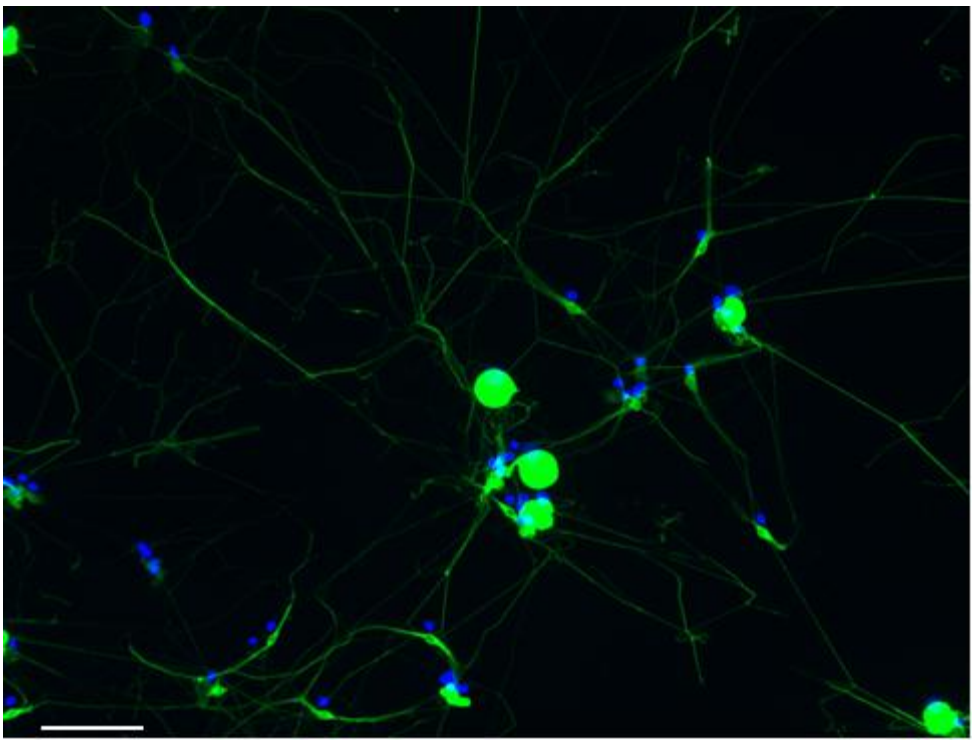

Figure 5.2: x10 view of cultured neurons with FITC (green) staining. The cell bodies and the extensive mesh of neurites can be seen. Scale bar = 50μm.

Slides were visualised under an Olympus BX60 fluorescent microscope using an appropriate FITC filter (Olympus, Japan), allowing visualisation of the green FITC staining of the neuronal cytoplasm in both the perikaryon and the neurites **(Figure 5.2)**.

Images were captured at x10 magnification using an Evolution QEi monochrome digital camera (Media Cybernetics, Bethesda, USA) using the same exposure time for all captures, and processed for export using Image-Pro Plus software (Media Cybernetics). The DRG culture experiment images were captured and analysed according to the principles of stereology (*cf.* 2.2.4). In contrast to previous studies which have analysed a 'random sample of representative' neurons (Caddick *et al.,* 2006; Gardiner *et al.,* 2005; Mahay *et al.,* 2008) care was taken to generate as close to a non-biased 'systematic random sample' as possible (West et al 1991). For each well of the plates, a corner was chosen at random, and working from that point a systematic series of fifteen images were taken from each well, giving a total of thirty samples per condition per animal.

Image analysis was performed using the Java based free-ware image processing software suite Image J (Abramoff *et al.,* 2004; Rasband, 2007-2009) and consisted of counting the number of adherent cells in each field, and the number of such cells bearing neurites at least one cell soma long. In line with non-biased quantification methodology, two edges of each field were designated as exclusion surfaces and neuron cell bodies crossing these were excluded from both counts. The mean number of adherent neurons and proportion of neurite bearing cells were pooled from both wells with the same conditions for each animal, and the results from each animal recorded to derive an n=3 mean and standard deviation statistics for each control and treatment condition. Comparison between different treatments was carried out by one-way ANOVA with Bonferonni post-hoc testing; all statistical comparisons were carried out using GraphPad Prism® (v 4.03) software.

5.3 RESULTS

After 24h of culture there was evidence of neuronal adherence to the laminin substrate in all treatment groups as well as in both the absolute and NGF control conditions. Further, there was a degree of neurite formation by some cells in all groups. The extent of adherence and neurite formation are summarised in **Table 5.2** and represented graphically in **Figures 5.3 and 5.4** with representative images of the neurons in **Figure 5.5**.

Table 5.2: Neuron Adherence and Percentage Neurite Formation

Condition	Neuron Adherence		Neurite Formation	
	Mean Number Adherent (Cells)	*Significance Vs. Control in ANOVA*	*Neurite Bearing Cells (%)*	*Significance Vs. Control in ANOVA*
Control	17.42 (1.49)	N/A	2.90 (1.27)	N/A
NGF	16.5 (6.21)	No ($p > 0.05$)	35.2 (3.46)	Yes ($p < 0.001$)
ALCAR High	10.68 (6.50)	No ($p > 0.05$)	1.30 (1.41)	No ($p > 0.05$)
ALCAR Med.	19.55 (7.52)	No ($p > 0.05$)	4.86 (6.39)	No ($p > 0.05$)
ALCAR Low	17.07 (5.05)	No ($p > 0.05$)	2.48 (1.38)	No ($p > 0.05$)
NAC High	10.57 (7.41)	No ($p > 0.05$)	4.63 (3.21)	No ($p > 0.05$)
NAC Med.	17.35 (8.51)	No ($p > 0.05$)	1.73 (1.15)	No ($p > 0.05$)
NAC Low	15.58 (9.25)	No ($p > 0.05$)	2.93 (2.34)	No ($p > 0.05$)

There were no significant differences in the mean number of adherent neurons between the control BS medium only group and any treatment group, including the NGF supplemented neurons, or between any two treatment groups ($p > 0.05$ for all possible pair-wise ANOVA analyses). Similarly, there was no significant difference in mean percentage of neurite bearing cells between the BS control group and the NAC or ALCAR treatment groups at any dose or between groups. However, neurons treated with NGF displayed a much higher degree of neurite formation with 5-12 times greater number of neurite bearing cells than the BS control or treatment groups ($p < 0.001$ in ANOVA in all possible pair-wise comparisons).

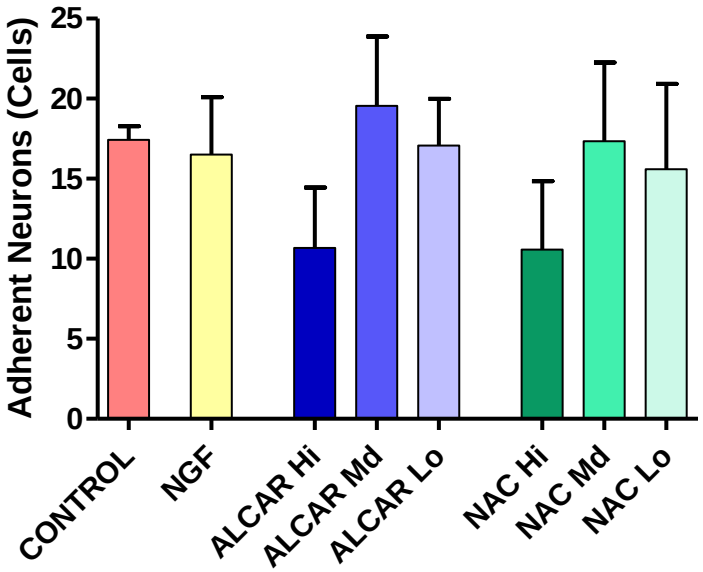

Figure 5.3: Effect of ALCAR or NAC treatment on number of neuronal cells adherent per x10 microscope field after 24h culture in BS medium only (Control), 150ng/ml NGF (NGF), 10mM ALCAR (A-Hi), 1mM ALCAR (A-Md), 100microM ALCAR (A-Lo), 10mM NAC (N-Hi), 5mM NAC (N-Md) and 1mM NAC (N-Lo). Plotted as mean per animal with SD, there are no significant differences between groups.

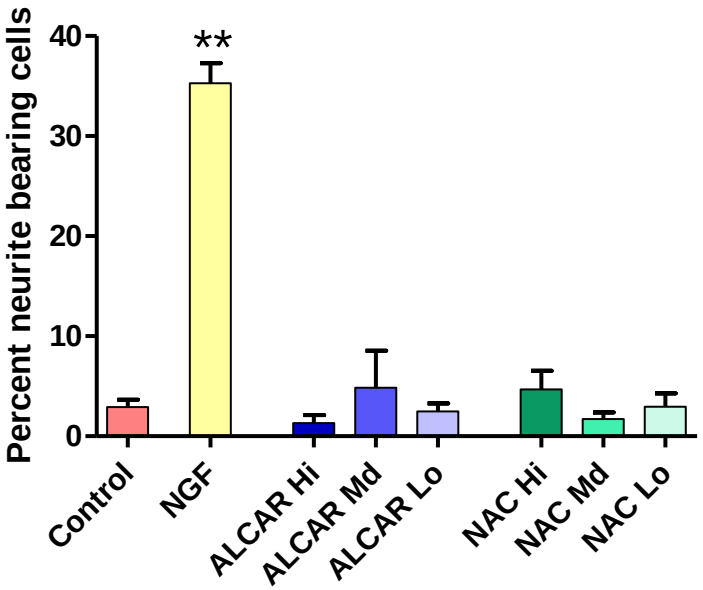

Figure 5.4: Effect of ALCAR or NAC treatment on percentage neurite bearing DRG neurons per x10 microscope field after 24h culture in BS medium only (Control), 150ng/ml NGF (NGF), 10mM ALCAR (A-Hi), 1mM ALCAR (A-Md), 100uM ALCAR (A-Lo), 10mM NAC (N-Hi), 5mM NAC (N-Md) and 1mM NAC (N-Lo). Plotted as mean per animal with SD, there are no significant differences between ALCAR or NAC groups and BS medium control; NGF treatment promotes significantly greater neurite formation (** = $p < 0.001$ Vs. all other groups in ANOVA)

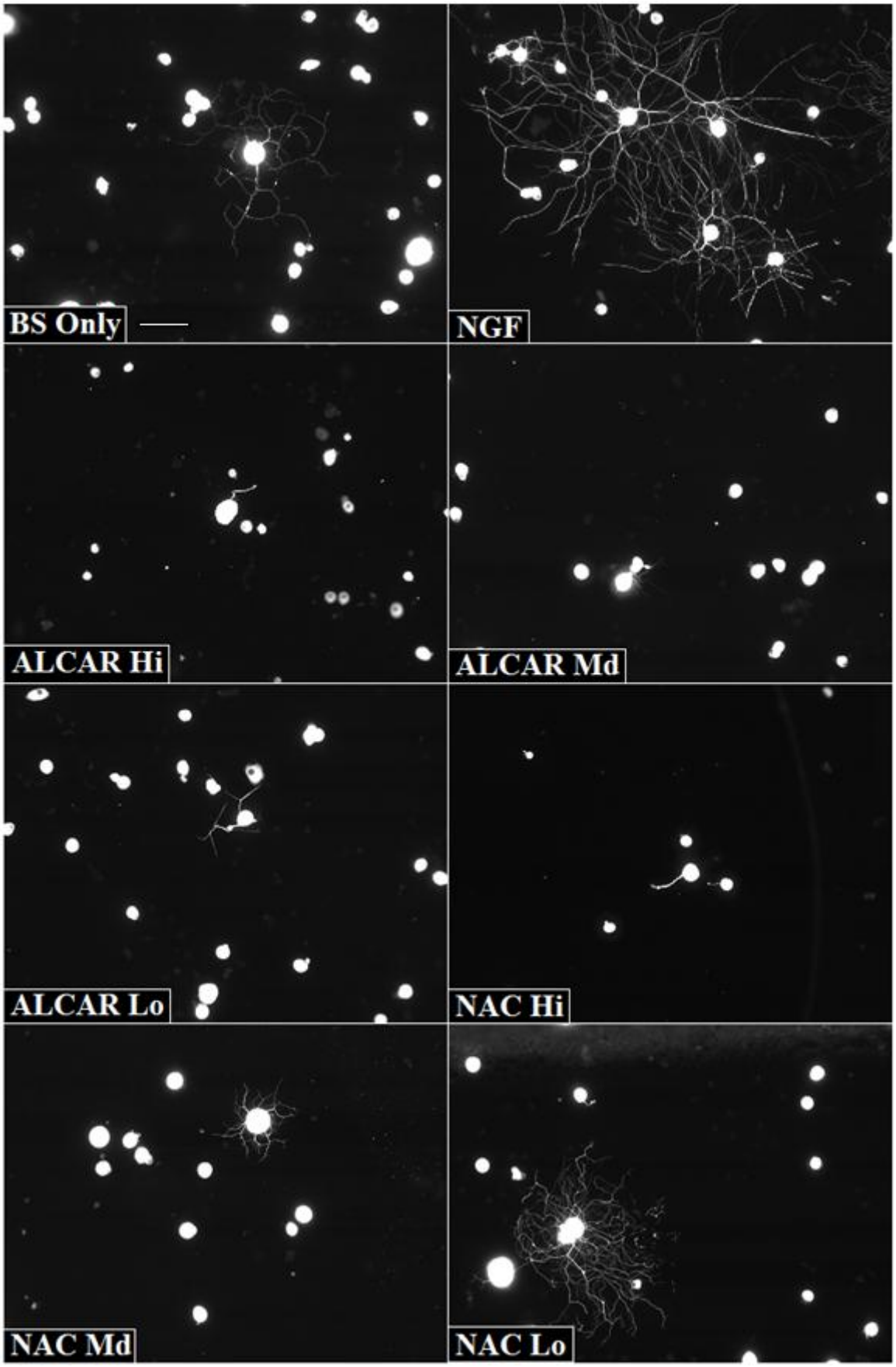

Figure 5.5: Caption over.

Figure 5.5 (Previous page): Representative images of x10 magnification fields of DRG neurons cultured for 24h with BS medium only (Cont), 150ng/ml NGF (NGF), 10mM ALCAR (A-Hi), 1mM ALCAR (A-Md), 100μM ALCAR (A-Lo), 10mM NAC (N-Hi), 5mM NAC (N-Md) and 1mM NAC (N-Lo). Adherent cells are present under all conditions but the proportion of neurite bearing cells is clearly larger in the NGF treated population. Scale bar = 50μm.

5.4 DISCUSSION

5.4.1 Methodology and Dosing Regime

The DRG dissociation and culture technique used in this experiment has been used successfully previously by our and other research groups (Lindsay *et al.*, 1988; Smith & Skene, 1997; Cafferty *et al.*, 2001; Gardiner *et al.*, 2005; Caddick *et al.*, 2006; Mahay *et al.*, 2008; Duran-Jimenez *et al.*, 2009). Laminin coating of glass slides as a growth interface and cellular adherence molecule has been shown not to influence either neuronal survival or secretion of trophic factors in culture (Lindsay *et al.*, 1988; Mahay *et al.*, 2008). Early DRG culture experiments suggested that untreated neuron will not extend neurites during the first 24h in culture, and that neuritogenesis is influenced by neurotrophic factors (Smith & Skene, 1997; Cafferty *et al.*, 2001). However, this study reproduces the results of others that a proportion of DRG neurons, in this case around 3%, can form neurites within this time frame in the absence of exogenous NGF; it has been hypothesized that this phenomenon can be attributable to soluble neurotrophic factors secreted from the neurons themselves in an autocrine fashion (Caddick *et al.*, 2006). In contrast, this and the above reports demonstrate that NGF treatment will stimulate extensive neuritogenesis within the first 24h in culture. This relatively early time point was chosen to maximize the likelihood of detecting a neurotrophic effect of ALCAR or NAC treatment.

Rather than quantifying a random selection of neurons, as is frequently cited, efforts have been made in this experiment to apply the principles of stereology to image capture and

neuron analysis, producing a systematic random sample. The exact number of neurons extracted and cultured from each animal will be different, both due to biological diversity and cell loss during the culture preparation. To account for the effect of such variability three separate animals were used, and each treatment condition cultured in two separate wells, therefore increasing the degree of sampling for each experimental condition. Further, consistent sampling rules were followed in cell counting aiming to ensure that each cultured neuron has the same chance of being counted (*cf.* 2.2.4.1 & 2.4.1.3). Although further repeats of the experiment to increase sample numbers would further reduce the coefficient of variation, it is unlikely that there would be a change in the overall results.

Choice of ALCAR and NAC dosage regime was difficult due to the huge variation of concentrations used in previous published in vitro studies; further, the finding that many neurite inducing agents follow a 'bell shaped' dose effect curve necessitated selecting a range of concentration for each agent (Calabresi, 2008). The doses selected are representative of those previously published up to the limit of 10mM, above which both ALCAR and NAC became cytotoxic in pilot studies, although higher doses that this have been cited in the literature. The finding of no significant differences in neuron adhesion between the control, ALCAR/NAC or NGF cultures wound suggest that the range selected does not have any detrimental effects on neuronal survival and could safely be used in future experimental protocols. A formal neuronal survival experiment, either with multiple quantification of the same active culture over time or multiple cultures fixed at different time points and quantified for neuron count and apoptosis detection could be used to further assess the putative in vitro neuroprotective effects, as suggested for ALCAR by Manfridi et al (1992).

The only assessment of neurite formation presented in this study is the proportion of neurite bearing cells. More sophisticated assessments, such as number of neurites per cell, length of longest neurite and neurite density are often used in neuronal culture experiments; however these were not carried out in this study because there were so few cells bearing neurites in the ALCAR/NAC groups and BS medium only control.

5.4.1 Effect of ALCAR and NAC

Both ALCAR and NAC have been demonstrated to prevent neuronal apoptosis after peripheral nerve injury (McKay Hart *et al.,* 2002b; Wilson *et al.,* 2003; Hart *et al.*, 2004a) and protect PC12 and embryonic CNS neurons from cell death induced by a wide range of chemical, oxidative and ischæmic insults *in vitro* (Ferrari *et al.,* 1995; Mayer *et al.*, 1994; Aykin Burns *et al.,* 2005; O'Loghlen *et al.,* 2006; Satpute *et al.,* 2008; Angelucci *et al.*, 1988; Ishi *et al.,* 2000; Forloni *et al.,* 1994). Further, ALCAR treatment in murine models of sciatic nerve injury increases the rate of peripheral nerve regeneration and target organ re-innervation (Hart *et al.,* 2002c; Wilson *et al.*, 2009).

Exact mechanisms by which these varying effects are expressed are incompletely understood and still under investigation, but they seem to fall into two overlapping 'spheres of activity'. Firstly the agents are antioxidant directly, and by products of their metabolism, such as up-regulation of glutathione by NAC (Hart *et al.*, 2004), may account for neuroprotective effects in culture with reactive oxygen species such as hydrogen peroxide and toxins which affect oxidative metabolism (O'Loghlen *et al.,* 2006; Aykin Burns *et al.,* 2005; Satpute *et al.,* 2008). Many of the elements of the effector limb of the apoptosis cascade involve generation of reactive oxygen species (*cf.* 1.2.4) and supplementing the intracellular antioxidant pool may partly explain the DRG neuronal survival effect of these agents in vivo. The second type of effects seem involve

interaction with the neurotrophin signalling pathways and involve modification of mRNA and protein expression, such as up-regulation of Ras (Yan *et al.,* 1995; Yan *et al.,* 1998), and Bcl-2 mRNA (Hsiao *et al.,* 2008). Such complex interactions contribute to post axotomy neuroprotection (Reid *et al.,* 2009), and seem likely to be responsible for the regeneration enhancing effects.

Given these neurotrophin like effects, this study was designed to asses if ALCAR or NAC could be a substitute for NGF which, along with BDNF, has been proposed as a main neurotrophin responsible for neurite outgrowth in DRG/Schwann cell co-culture experiments (Golz et al 2006; Mahay et al 2008). The findings of the initial experiment presented here show that such simple substitution does not stimulate axonal regeneration directly. There are many possible explanations for this negative finding *in vitro* when compared to the complexity of the neurobiological events of inflammation, Wallerian degeneration and guided regeneration that occurs in a live animal. Previous culture based experiments have suggested that ALCAR causes increased expression of neurotrophin receptors on PC12 cells, and to up-regulate cellular response to NGF i.e. cells would produce neurites when exposed to low dose NGF which did not affect control cells. ALCAR and or NAC may therefore amplify the effect of the reduced amount of neurotrophins received by axotomised neurons post injury. It would be useful in subsequent experiments to examine the effect of ALCAR/NAC when DRG neurons are exposed to a range of NGF doses. Further, there is little published data concerning the effects of ALCAR/NAC on Schwann cells and experiments using co-culture and SC pre-conditioned medium would be proposed.

In summary, this study is only the first of many possible experimental protocols. Nevertheless, an ALCAR/NAC dosage regime has been established which spans the range of previously published *in vitro* work and which does not appear detrimental to DRG

neurons in culture. Neither ALCAR nor NAC substitute for NGF intrinsically in this primary sensory neuron culture model, but many possibilities exist to further work.

CHAPTER 6

Overview & Proposals for Future Work

6.1 OVERVIEW

The existence of peripheral nerves was known to Hippocrates and Herophilus in the 4th and 3rd Centauries BBC respectively (Adams, 1849; Sunderland, 1991; Belen *et al.*, 2009). Recognition of the significance of nerve injury and discussion of nerve repair techniques have been credited to the Persian physicians Rahzes and Avicenna and to Galen in the 1st and 2nd Century's CE (Terzis *et al.*, 1997; Battiston *et al.*, 2009), nerve suturing was described by Paul von Aegina in the 7th Century (Streppel *et al.*, 2000) and refined by Gabriele Ferrara (1543-1627) working from Milan (Artico *et al.*, 1996). More recently, peripheral nerve surgery has been revolutionised by development of the operating microscope (Smith 1966; Terzis *et al.*, 1997). During the 2nd World War, Sir Herbert Seddon reported cases of primary and secondary nerve repair as well as describing nerve grafting, and subsequently Sir Sidney Sunderland examined the internal fascicular architecture of peripheral nerves, classifying nerve injury in order to rationalise surgical intervention strategies (Sunderland, 1984).

Despite these clinical advances, which have also been accompanied by exponential increase in the scientific understanding of the cellular and molecular basis of nerve response to injury and regeneration (*cf.* 1.2.2.2 - 1.2.2.4), sensory recovery after peripheral nerve injury is still far from satisfactory (Lundborg, 2000; Kline *et al.*, 2000); in fact "no adult with a major nerve transection has ever attained normal sensibility" (de Mendinaceli & Seaber, 1989) The ætiology of such disappointing outcomes is multifactorial, reflecting the neurobiological hurdles of nerve regeneration (Gordon *et al.*, 2003), peripheral target organ atrophy (Liss *et al.*, 1994; Zelena, 1982) and CNS somatotopic re-modelling (Lundborg, 2003). Of primary importance is the apoptotic death of primary sensory neurons in the dorsal root ganglia (DRG), which occurs over a two month period post nerve transection (McKay Hart *et al.*, 2002a), and accounts for loss of up to 50% of

neurons (Arvidsson *et al.,* 1986; Cheema *et al.,* 1994a & b; Degn *et al.,* 1999; Ekstrom, 1995; Groves *et al.,* 1997; Himes & Tessler, 1989; Liss *et al.,* 1994; Liss *et al.,* 1996; Ljungberg *et al.,* 1999; McKay Hart *et al.,* 2002a; Ranson, 1909; Rich *et al.,* 1987; Rich *et al.,* 1989; Tandrup *et al.,* 2000; Ygge 1989). As only surviving cells can regenerate, these neurons are lost from the regenerative pool (Fu & Gordon, 1997) and such cellular attrition will contribute to the reduced 'innervation density' of the skin after nerve trauma (Weiberg *et al.* 2003).

Two neuroprotective agents ALCAR and NAC have been identified which prevent post-axotomy neuronal apoptosis in murine models (McKay Hart *et al.* 2002b; Hart *et al.* 2004a.) These agents have a range of metabolic, antioxidant, signalling and translational activities, and the mechanism by which they exert their neuroprotective role remains under investigation (*cf.* 1.2.4). Translation of the potential clinical benefit of adjuvant ALCAR/NAC therapy into the clinic remains an obvious objective, and the studies reported here were designed to facilitate this process. The overarching aims of this thesis were to further study the activity and utility of these agents, and to investigate objective, non-invasive imaging techniques, MRI and HFUS which could be used to act as an index of neuronal population change or nerve regeneration, and would be applicable to human patients.

Key questions in establishing a clinical trial of the neuroprotective agents relate to the logistical considerations of therapy. Optimal doses for both agents have been identified (Wilson *et al.,* 2003; West *et al.,* 2007a), it has been shown that a short delay in commencing ALCAR or NAC therapy does not confer a detrimental effect on neuron survival (Zhang *et al.,* 2005; Wilson *et al.,* 2007). The NAC treatment duration study described in Chapter 2 addressed the issue of how long therapy should continue post

injury, and the results allow two main conclusions to be drawn. Firstly, all groups treated for less that the full duration of the experiment did show a degree of neuronal loss. However, the amount of apoptosis which occurred after cessation of treatment was notably less that occurring over the same time period in untreated animals as described in previous experiments. At one month after sciatic axotomy with no treatment there is loss of ≈22% of DRG neurons (McKay Hart *et al.*, 2002a), but after one month of NAC administration followed by a month of no treatment, there was only ≈5% neuronal death. The implication is that apoptosis does not resume at the normal rate after cessation of NAC therapy, and that approximately 17% of neurons which would have undergone apoptosis were saved by NAC treatment.

The second conclusion from the NAC treatment duration study is that one month treatment seems to preserve all but ≈5% of sensory neurons, and would appear to be a reasonable, clinically applicable duration of therapy.

Chapter three describes volumetric MRI of the L4 DRG of the animals in the NAC treatment duration study. Problems with existing clinical and neurophysiological tests of nerve regeneration (*cf.* 1.3.1) would potentially hamper monitoring and assessment of a clinical trial of ALCAR/NAC treatment; MRI measurement of changes in the DRG volume has been proposed as a non-invasive, objective test which may translate to a clinical outcome measure of neuronal population change (West *et al.*, 2007b). Previous work had suggested that DRG volume reduces in proportion with neuron loss (McKay Hart *et al.*, 2002a; Wilson *et al.*, 2003); and that in a pilot study, MRI assessment of L4 volume correlated with both histological DRG volume assessment and neuron loss (West *et al.*, 2007b). The results of this study verify that volumetric MRI has the ability to detect significant reduction in DRG volume under experimental conditions, and that these

correlate to neuronal loss. MRI measurement of DRG volume loss was shown however to have sensitivity restrictions, not being as precise as stereological neuronal counting and failing to detect small changes in volume. If cognisance of these limitations is applied to future experiments, volumetric MRI is proposed as a highly useful and time efficient assessment modality, potentially able to replace histological analysis in the murine model. The human DRG is much larger than that in the rat, and MRI measurement of human ganglion volume may present less methodological difficulties. Pilot studies (as yet unpublished) have demonstrated the possibility of imaging volunteer human brachial plexus DRG in cross section to facilitate volume measurement.

Other proposed applications of MRI were explored in Chapter three. Firstly, scanning of a live animal was performed, verifying that maintaining safe anæsthesia within the scanner was possible and identifying the particular challenges of *in vivo* imaging, such as movement of respiratory excursion and the and cardiac cycle. Various strategies to address these issues are discussed, such as use of respiratory gating or navigator echoes, which are predicted to enhance the resolving power of live scanning allowing multiple sequential imaging of animals, tracking DRG volume change over time.

Significant time was spent attempting to reproduce the findings of other groups studying human or rat nerve injury which suggest that detectable MRI signal changes occur in degenerating nerve, and that these changes resolve during axonal regrowth (Britz *et al.*, 1995; Britz *et al.*, 1996; Aagaard *et al.*, 2003; Bendszus *et al.*, 2004; Bher *et al.*, 2009). Disappointingly, despite systematic application of a wide variety of hardware and MRI sequence combinations, including intraneural injection of contrast media (*cf.* 4.2.2.2), the rat sciatic nerve could not be reliably identified on high resolution T_1 or diffusion weighted scans, nor could signal change corresponding to site of axotomy be detected on T_2

weighted images. The explanation for being unable to replicate the results of other groups is uncertain, but probably reflects differences in the hardware and sequence libraries available between researchers.

In contrast, a pilot study investigating the application of HFUS to peripheral nerve injury was highly successful. The rat sciatic nerve could easily be identified throughout its full extra-pelvic course, and even its three terminal branches were followed for some way distally. Ultrasound imaging at two time points after nerve transection demonstrated that HFUS was able to detect a physical breach in nerve continuity; neurotmetic grade injury in Sunderland's classification (Sunderland, 1951). After a period of healing, HFUS could still identify anatomical derangement in what has reviled to be a continuous nerve structure on direct observation, such epineural continuity is a feature of axonotmetic grade injury. As imaging of the human digital nerves was also demonstrated to be relatively easy, HFUS is proposed as being of potential diagnostic benefit in patients with finger lacerations threatening the digital neurovascular bundle, although clearly further verification studies are required.

Chapter 5 discusses establishment of an experimental protocol to investigate the effects of ALCAR and NAC administration in a cell culture system of primary sensory neurons. Acknowledging that the cellular dose response to many neuritogenic substances is non-linear (Calabresi, 2008), the first phase of this work was to select doses of the neuroprotective agents as used in previous *in vitro* experiments to take forward into future work. Representative high, medium and low doses for each agent were identified which did not have any detrimental effect on neuronal survival and laminin adherence compared to control conditions. NGF is the prototype neurotrophic factor (Green & Kaplan, 1995; Kaplan & Miller, 1994, 1997; Kaplan & Stephens, 1994; Miller & Kaplan, 2000, 2001a,

2001b, 2003, 2007; Gould & Gordon Weeks, 2005); the hypothesis that ALCAR or NAC exert their neuroprotective and pro-regenerative effects by substituting for NGF was tested. In isolation none of the tested neuroprotectant doses enhanced cell survival or neurite outgrowth after 24h in culture. So far, only these early and relatively simple investigations have been performed, and the scope for culture based systems to investigate the neuroprotective effects of ALCAR and NAC documented *in vivo* remains to be further explored.

6.2 PROPOSED FURTHER WORK

Future research efforts concerning the neuroprotective potential of ALCAR and NAC are likely to proceed along two parallel tracts. Firstly are those experiments designed to investigate the mechanisms by which the agents exert their effects, this would be anticipated to involve further *in vitro* work, such as examining whether NAC and ALCAR modify neuronal behavior in the presence of NGF or in co-culture with Schwann cells.

Recent work investigating neuronal apoptotic gene expression post axotomy using laser microdissection and quantitative real-time polymerase chain reaction has identified that NAC administration alters transcription of Bax, Bcl-2 and caspase-3 genes to promote mitochondrial stabilisation and hence survival rather than apoptosis in some DRG neuronal subpopulations (Reid *et al.*, 2009). This technique clearly offers much scope for investigation of signalling cascade modifications that follow axotomy and ALCAR/NAC neuroprotection.

The second group of experiments are those designed to facilitate clinical translation of ALCAR/NAC neuroprotection and investigate the logistics of such therapy, such as the NAC treatment duration study presented above. No murine study has yet investigated the

effectiveness of oral administration of either agent, which is anticipated to need large doses to overcome first pass hepatic metabolism (Olsson *et al.,* 1988). While there are two published experiments demonstrating that ALCAR increases peripheral nerve regeneration rate (McKay Hart *et al.,* 2002c; Wilson *et al.,* 2010) this has not to date been carried out for NAC treatment. Most patients with nerve injury do undergo nerve repair or grafting, such reconnection with neurotrophic factors in the distal stump confers an incomplete neuroprotective benefit (McKay Hart *et al.,* 2002a), an experiment designed to investigate duration of therapy needed to provide complete neuroprotection after sciatic nerve transection and repair may provide further information guiding clinical therapy.

Volumetric MRI scanning of the rat DRG has been shown to act as a proxy measure of neuronal population under experimental conditions, and the possibility of *in vivo* imaging has been established. Further refinements to the technique, such as use of respiratory or ECG gaiting may increase the resolution of live scanning sufficiently to allow repeated analyses of animals over time. Pilot MRI studies of human standardised DRG imaging facilitating volume measurement, controlled with cadaveric DRG stereological neuron counting are underway.

The potential to visualise the rat sciatic nerve response to transection, regeneration and neuroprotectant treatment with MRI remains unfulfilled. One potential avenue for exploration would be to more closely emulate the experimental protocols of other groups, which used human clinical scanners, with propriety surface coils and access to a large range of commercial pulse sequences (Aagaard *et al.,* 2003; Bendszus *et al.,* 2004). The HFUS pilot reported here was necessarily limited by only having a brief period of access to the unit. The next step in evaluation would by a blinded trial; with a group of animals undergoing sham, crush or transection operations with the researcher scanning the animals

(potentially *in vivo*) unaware of the operation each had received, to test the diagnostic sensitivity of the system.

In summary, the research described above brings a clinical trial of NAC/ALCAR sensory neuroprotection a step closer, suggesting that one month therapy post injury is likely to provide substantial clinical benefit and, for the first time demonstrates that NAC has the potential to save neurons after axotomy, rather than simply delay onset of apoptosis. MRI volumetry of the rat DRG has been verified to act as a sensitive proxy measure of neuron loss, and the potential for *in vivo* scanning explored. This technique will be applicable to future murine studies, as well as justifying establishment of a human volumetric MRI DRG imaging protocol. HFUS has been demonstrated to hold significant potential for further peripheral nerve imaging in animals and potential translation to investigating injury to small calibre superficial human nerves.

Establishment of an experimental protocol to further investigate the neurobiological effects of ALCAR and NAC *in vitro* will hopefully further elucidate the mechanisms by which these agents eliminate sensory neuronal apoptosis after peripheral nerve injury.

APPENDICES

APPENDIX 1: Miscellaneous Laboratory Materials & Equipment

1.1. REAGENTS ETC.

MATERIAL	MANUFACTURER	PRODUCT CODE
Cryostat	Leica Microsystems, Nussloch, D-69226, Germany	CM30505
DAKO Pen for Immunohistochemistry	DAKO, Glostrup, Denmark, DK-2600	S2002
DPX Mounting Medium	BDH Laboratory Supplies, Poole, BH15 1TD, England	-
Glass Coverslips (22x55mm)	Scientific Laboratory Supplies Ltd. www.scientific-labs.com	-
Paraformaldehyde	Sigma®, Sigma-Aldrich Co Ltd, www.sigma-aldrich.com	P6148
Potassium Phosphate	Sigma®, Sigma-Aldrich Co Ltd, www.sigma-aldrich.com	P-5379
Sodium Azide	Sigma®, Sigma-Aldrich Co Ltd, www.sigma-aldrich.com	S-2002
Sodium Chloride	AnalaR®, BDH Laboratory Supplies, Poole, BH15 1TD, England	10241AP
Sodium Phosphate	Sigma®, Sigma-Aldrich Co Ltd, www.sigma-aldrich.com	S-7907
Sucrose	AnalaR®, BDH Laboratory Supplies, Poole, BH15 1TD, England	102747E
Tissue-Tek® OCT Compound	Sakura Finetek	4583
Triton X-100 (*t*-ctylphenoxypolyethoxyethanol)	BDH Laboratory Supplies, Poole, BH15 1TD, England	306324N

Vectabond ™ Reagent	Vector Laboratories, Inc. 30 Ingold Rd, California, USA. www.vectorlabs.com	SP-1800
Vectashield® Mounting Medium with DAPI	Vector Laboratories, Inc. 30 Ingold Rd, California, USA. www.vectorlabs.com	H-1000
Manganese Chloride (anhydrous)	Sigma®, Sigma-Aldrich Co Ltd, www.sigma-aldrich.com	244589

1.2. PREPARATION OF SOLUTIONS

1.2.1. Phosphate Buffered Saline

For 10L: add 87.9g Sodium Chloride, 2.72g Potassium Phosphate and 113.5g of Sodium Phosphate to 7L distilled water. Magnetic stir for 3h, make up to 10L and adjust pH.

1.2.2. Paraformaldehyde (4%)

For 1L: (in fume hood) add 40g anhydrous Paraformaldehyde to 800ml PBS, heat until solution clears (max 60°C). Make solution up to 1L, store at 4°C, use within 24h.

1.2.3. PBS-Sucrose Solution (15%)

Add 150g sucrose and 1g sodium azide in 1L PBS, store at 4°C.

1.2.4. Antibody Diluent Solution (0.03% Triton X-100, 0.1% BSA, 0.1% Sodium Azide)

For 1L: dissolve 0.3ml Triton X-100, 1g Bovine Serum Albumin and 1g sodium azide in 1L PBS, store at 4°C.

1.2.5. Triton X-100 Permeabilisation Solution

For 1L: dissolve 20ml Triton X-100 in 9980ml PBS

APPENDIX 2: Surgical Materials

MATERIAL	MANUFACTURER	PRODUCT CODE
#15 & #23 Surgical Blade	Swan-Morton, Sheffield, England	0205 & 0210
Biogel sterile gloves	Williams Medical Supplies Ltd, UK	406A8
Buprenorphine Hydrochloride	Alstoe Animal Health, UK	00063/4000
Isoflourane BP 100% v/v	Rhodia Organique Fine Ltd, Avonmouth, Bristol, BS11 9YF	ISO-9001
Johnson's Cotton Buds x100	Johnson & Johnson Medical, UK	J3762856
Silicone Tubing (High grade, 1mm internal diameter)	Philip Harris International, Linchfield, Staffordshire, UK	T88-5420
10 µL Hamilton Syringe	Hamilton, Bonaduz, Switzerland	80357
3/0 Polypropyline suture (Prolene™)	Ethicon™, Johnson & Johnson Intl. www.ethicon.com	W8770
4/0 Vicryl TM	Ethicon™, Johnson & Johnson Intl.	W9825
6/0 Polypropyline suture (Prolene™)	Ethicon™, Johnson & Johnson Intl.	W8718
9/0 & 6/0 Ethilon	Ethicon™, Johnson & Johnson Intl	W2898
Chlorhexidine Gluconate 0.5% w/v	Preston Pharmaceuticals, UK	ML13460/01
Surgical Loupe Telescopes (x3.8)	Surgical Acuity, 3225 Deming Way Suite 190, Middleton, WI 53562	Custom

APPENDIX 3: *N*-acetylcysteine Treatment

MATERIAL	MANUFACTURER	PRODUCT CODE
0.9% w/v Sodium Chloride Intravenous Injection BP	Baxter Healthcare Ltd, UK	FKB1313G
1 ml syringe with needle (28 guage) Kendall Monoject ™, Tyco	Healthcare UK Ltd, Gosport, PO1 3AS, UK.	1100-601630
N-acetylcysteine 200mg/ml (Parvolex ®)	Parvolex, UCB Pharma Ltd, Slough, Berkshire, SL1 3WE. UK	PL 00039/0410

APPENDIX 4: Hoechst H33342 & Propidium Iodide Fluorescent Staining

4.1. MATERIALS AND REAGENTS

MATERIAL	WORKING DILUTION	MANUFACTURER	PRODUCT CODE
Bisbenzimide Hoechst 33342	1µg/ml	Fluka, Sigma®, Sigma-Aldrich Co Ltd, www.sigma-aldrich.com	14533
Propidium Iodide	1µg/ml	Fluka, Sigma®, Sigma-Aldrich Co Ltd, www.sigma-aldrich.com	81845

4.2. STAINING PROTOCOL

1. **Section:** Cut entire ganglion into serial 50µm sections onto Vectabond® coated slides.
2. DAKO pen around edges.
3. **Permeabilise:** 0.1% Triton X in PBS 15 minutes
4. **Wash:** PBS 5min × 2
5. **Stain:** Apply 1µg/ml Propidium iodide with 1µg/ml Hoechst 33342 in PBS (300µl) onto slide and incubate 10 min room temp.
6. **Wash:** PBS 5min × 2
7. **Mount:** Vectashield for fluorescence with glass cover slip
8. **Seal:** with DPX
9. **Store:** Light exclusion slide box at 4°C.

APPENDIX 5: Fluorescence Microscopy and Optical Dissection

MATERIAL	MANUFACTURER	PRODUCT CODE
Optical Microscope	Olympus Optical Co. Ltd, Japan	BX60
Optical Microscope	Olympus Co. Ltd, Japan	BX61
Digital Camera (Cooled, Monochrome 12-bit)	Media Cybernetics, Inc. 8484 Georgia Ave, Silverspring, MD, USA.	Evolution QEi 32-0074A-101
Digital Camera (Colour)	Olympus Optical Co. Ltd, Japan	U-SPT Optitronics
Fluorescent Lamp Burner Unit	Olympus Optical Co. Ltd, Japan	U-RFL-T
Motorised XY Microscope Stage (BioPrecision 3x2 Upright Stage)	Ludl Electronic Products Ltd (LEP)	99S000
Stage Controller	Ludl Electronic Products Ltd (LEP)	MAC 5000
Z-Focus Microcator Control Box	Olympus Optical Co. Ltd, Japan	BX-UCB

APPENDIX 6: MRI Scanning Hardware

MATERIAL	MANUFACTURER	PRODUCT CODE
7T actively shielded 15cm horizontal bore MRI scanner	Magnex UK Ltd, Abingdon	-
SMIS console software	Magnetic Resonance Research Systems, Guildford UK	-
2cm Surface Coil	Department of Imaging Science, University of Manchester, UK.	Custom
8cm Volume Coil	Department of Imaging Science, University of Manchester, UK.	Custom
Magnet Probes	Department of Imaging Science, University of Manchester, UK.	Custom
Tektronix 475 Oscilloscope	**Tektronix, Inc.** 14150 SW Karl Braun Drive, Beaverton, United States	-

APPENDIX 7: MRI SEQUENCE PARAMETERS

7.1 DRG Volumetry Protocol

7.1.1. Scout Images

TR (Time to repeat)	50ms
TE (Time to echo)	5ms
Number of Averages	4
Number of Samples	128
Number of Views	65
Flip Angle	30°
Field of View	100x100mm
Matrix	128x64
Block Size	64
Number of Slices	3
Slice Thickness/Separation	1mm/1mm
Scan Time	3 min

7.1.2. Sagittal Gradient Echo Sequence

TR	140ms
TE	5ms
Number of Averages	4
Number of Samples	128
Number of Views	64
Flip Angle	30°
Field of View	30x30mm
Matrix	128x64
Block Size	64
Number of Slices	8
Slice Thickness/Separation	1/1
Scan Time	3 min

7.1.3. Low Resolution Coronal Gradient Echo Sequence

TR	102ms
TE	6ms
Number of Averages	4
Number of Samples	128
Number of Views	64
Flip Angle	30°
Field of View	30x30mm
Matrix	128x64
Block Size	64
Number of Slices	6
Slice Thickness/Separation	0.5/0.5mm
Scan Time	3min

7.1.4. High Resolution Coronal Gradient Echo Sequence

TR	102ms
TE	6ms
Number of Averages	64
Number of Samples	256
Number of Views	128
Flip Angle	30°
Field of View	30x30mm
Matrix	256x128
Block Size	64
Number of Slices	6
Slice Thickness/Separation	0.5/0.5mm
Scan Time	14.88min

7.1.5. 3D Gradient Echo Sequence (Axial)

TR	17ms
TE	6ms
Number of Averages	32
Number of Samples	256
Number of Views	232
Flip Angle	Optimised (15-30°)
Field of View	30(w)x8(h)mm
Matrix	256x128
Block Size	64
Number of Slices	32
Slice Thickness/Separation	0.25mm
Scan Time	45min

7.2. Sciatic Nerve Imaging

7.2.1. Low Resolution Axial Gradient Echo Sequence (T_1 weighted)

TR	500ms
TE	6ms
Number of Averages	4
Number of Samples	128
Number of Views	64
Flip Angle	90°
Field of View	50x50mm
Matrix	128x64
Block Size	64
Number of Slices	30-50
Slice Thickness/Separation	0.5/0.5mm

7.2.2. Medium Resolution Axial Gradient Echo Sequence (T_1 weighted)

TR	800ms
TE	6ms
Number of Averages	4
Number of Samples	128
Number of Views	64
Flip Angle	60°
Field of View	30x30mm
Matrix	128x64
Block Size	64
Number of Slices	44
Slice Thickness/Separation	0.5/0.5mm

7.2.3. High Resolution Oblique Gradient Echo Sequence (T_1 weighted)

TR	500ms
TE	6ms
Number of Averages	32
Number of Samples	128
Number of Views	256
Flip Angle	90°
Field of View	50x50mm
Matrix	256x128
Block Size	64
Number of Slices	11
Slice Thickness/Separation	0.5/0.5mm

7.2.4. Axial Gradient Echo Sequence (diffusion weighted)

TR	1000ms
TE	60ms
Number of Averages	4
Number of Samples	128
Number of Views	64
Flip Angle	N/A
Field of View	050x50mm
Matrix	128x64
Block Size	64
Number of Slices	10
Slice Thickness/Separation	1/2mm
Diffusion Gradient	8ms
Diffusion Time	24ms

7.2.5. Medium Resolution Axial Fast Spin Echo Sequence (T_2 weighed)

TR	1000ms
TE	60ms
Number of Averages	4
Number of Samples	128
Number of Views	64
Flip Angle	N/A
Field of View	50x50mm
Matrix	256x128
Block Size	64
Number of Slices	8
Slice Thickness/Separation	1/1mm

7.2.6. Medium Resolution Coronal Fast Spin Echo Sequence (T2 weighted)

TR	2000ms
TE	32ms
Number of Averages	4
Number of Samples	256
Number of Views	128
Flip Angle	N/A
Field of View	24x24mm
Matrix	128x64
Block Size	64
Number of Slices	8
Slice Thickness/Separation	0.5/0.5mm

APPENDIX 8: High Frequency Ultrasound Scanning

MATERIAL	MANUFACTURER	PRODUCT CODE
Vevo 660 High frequency ultrasound scanner	VisualSonics Inc. 3080 Yonge Street Suite 6100, Box 66 Toronto, Ontario, Canada	660
40MHz RMV Ultrasound scan head	VisualSonics Inc. 3080 Yonge Street Suite 6100, Box 66 Toronto, Ontario, Canada	RMV-40A
Veet® Hair removal cream.	Reckitt Benckiser plc, Turner House 103-105 Bath Road, Slough, Berkshire, UK	-
Aquasonic® 100 Ultrasound Transmission Gel	Parker Laboratories Inc, New Jersey.	01-02

APPENDIX 9: Cell Culture Materials

MATERIAL	MANUFACTURER	PRODUCT CODE
Acetyl-*L*-carnitine	Sigma®, Sigma-Aldrich Co Ltd, www.sigma-aldrich.com	A6706
Bovine Serum Albumin	Invitrogen Ltd, 3 Fountain Drive Inchinnan Business Park, Paisley, Scotland.	15561020
Collagenase, Type IV.	Worthington Biochemical Corp. 730 Vassar Ave Lakewood, NJ, USA.	LS004186
Cytosine arabinoside	Sigma®, Sigma-Aldrich Co Ltd, www.sigma-aldrich.com	C1768
F-12 Nutrient Mixture (Ham), liquid	Invitrogen Ltd, 3 Fountain Drive Inchinnan Business Park, Paisley, Scotland.	21765037
Foetal Bovine Serum (Gamma-Irradiated)	Invitrogen Ltd, 3 Fountain Drive Inchinnan Business Park, Paisley, Scotland.	10109155
Insulin	Sigma®, Sigma-Aldrich Co Ltd, www.sigma-aldrich.com	I6634
Lab-Tek™ II 8 Chambered Coverglass	Nunc GmbH & Co. KG Robert-Bosch-Straße 1 D-63505 Langenselbold, Germany.	155409
LaminiN-1	Sigma®, Sigma-Aldrich Co Ltd, www.sigma-aldrich.com	L2020
Millex Syringe-driven filter unit (0.22µ mesh)	Millipore Corporate Headquarters: 290 Concord Road, Billerica, MA 01821, USA.	SLLGH04NL
N-acetylcysteine(cell culture tested, BioReagent)	Sigma®, Sigma-Aldrich Co Ltd, www.sigma-aldrich.com	A9165
Nerve Growth Factor-2.5S from murine submaxillary gland	Sigma®, Sigma-Aldrich Co Ltd, www.sigma-aldrich.com	N6009

Penicillin-Streptomycin, liquid (10,000 units penicillin;10,00µg streptomycin)	Invitrogen Ltd, 3 Fountain Drive Inchinnan Business Park, Paisley, Scotland.	15140163
Progesterone	Sigma®, Sigma-Aldrich Co Ltd, www.sigma-aldrich.com	P0130
Putrescine	Sigma®, Sigma-Aldrich Co Ltd, www.sigma-aldrich.com	P5780
Sodium selenite	Sigma®, Sigma-Aldrich Co Ltd, www.sigma-aldrich.com	S5261
Transferrin	Sigma®, Sigma-Aldrich Co Ltd, www.sigma-aldrich.com	T1408
Trypsin	Worthington Biochemical Corp. 730 Vassar Ave Lakewood, NJ, USA.	LS02120

APPENDIX 10: Immunofluorescent Staining

10.1 REAGENTS

MATERIAL	WORKING DILUTION	MANUFACTURER	PRODUCT CODE
1° Antibody Anti-ß$_{III}$-tubulin (mouse monoclonal)	1:1000	Sigma®, Sigma-Aldrich Co Ltd, www.sigma-aldrich.com	T8600
2° Antibody FITC-Conjugated Horse-anti-mouse. (IgG, H&L)	1:100	Vector Laboratories, Inc. 30 Ingold Rd, California, USA. www.vectorlabs.com	FI-2100
Blocking Serum Normal Horse Serum (2.5%)	1:100	Vector Laboratories, Inc. 30 Ingold Rd, California, USA. www.vectorlabs.com	S-2012

10.2. STAINING PROTOCOL

1. Aspirate cells growth medium
2. **Wash:** PBS - 5 min. RT
3. **Fix:** PFA 4% - 20 min. RT
4. **Wash:** PBS - 5 min. RT
5. **Permeabilise:** Triton X-100 - 30 min. RT
6. **Wash:** PBS - 5 min. RT
7. **Blocking:** NHS (1:100 - 5.4mg PBS + 60µl NHS) - 60 min. RT
8. **Primary Antibody:** Anti-ß$_{III}$-tubulin (1:1000: 1.2ml AbD + 12µl Ab) 16h 4°C
9. **Wash:** PBS - 5 min. RT
10. **Secondary antibody:** FITC Horse anti mouse (1:100: 5.4ml AbD + 60µl Ab) 2 hours. RT
11. **Wash:** PBS - 5 min. X 2 Times

12. **Mount:** Vectashield mounting medium with DAPI.

REFERENCES

Aagaard BD. Lazar DA. Lankerovich L. Andrus K. Hayes CE. Maravilla K. Kliot M. (2003) High-resolution magnetic resonance imaging is a non-invasive method of observing injury and recovery in the peripheral nervous system. Neurosurgery. 53(1):199-203.

Abate C. Patel L. Rauscher III FJ. Curran T. (1990) Redox regulation of fos and jun DNA-binding activity in vitro. Science 249:1157-1161.

Abramoff, M.D., Magelhaes, P.J., Ram, S.J. (2004) Image Processing with ImageJ. Biophotonics International 11(7): 36-42

Aitio ML. (2006) *N*-acetylcysteine - passe-partout or much ado about nothing? British Journal of Clinical Pharmacology. 61(1):5-15.

Al-Abdulla NA, Martin LJ. (1998) Apoptosis of retrogradely degenerating neurons occurs in association with the accumulation of perikaryal mitochondria and oxidative damage to the nucleus. Am. J. Pathol. 153: 447-456.

Ambron RT. Walters ET. (1996) Priming events and retrograde injury signals. A new perspective on the cellular and molecular biology of nerve regeneration. Molecular Neurobiology. 13(1):61-79.

Ames BN. Liu J. (2004) Delaying the mitochondrial decay of aging with acetylcarnitine. Annals of the New York Academy of Sciences. 1033:108-16.

Aminoff MJ. (2004) Electrophysiologic testing for the diagnosis of peripheral nerve injuries. Anesthesiology. 100(5):1298-303.

Andonian S. Coulthard T. Smith AD. Singhal PS. Lee BR. (2009) Real-time quantitation of renal ischemia using targeted microbubbles: in-vivo measurement of P-selectin expression. Journal of Endourology. 23(3):373-8

Angelucci L. Ramacci MT. Taglialatela G. Hulsebosch C. Morgan B. Werrbach-Perez K. Perez-Polo R. (1988) Nerve growth factor binding in aged rat central nervous system: effect of acetyl-L-carnitine. Journal of Neuroscience Research. 20(4):491-6.

Aota Y. Onari K. An HS. Yoshikawa K. (2001) Dorsal root ganglia morphologic features in patients with herniation of the nucleus pulposus: assessment using magnetic resonance myelography and clinical correlation. Spine. 26(19):2125-32.

Artico M. Cervoni L. Nucci F. Giuffre R. (1996) Birthday of peripheral nervous system surgery: the contribution of Gabriele Ferrara (1543-1627). Neurosurgery. 39(2):380-2; discussion 382-3.

Aruoma OI. Halliwell B. Hoey BM. Butler J. (1989) The antioxidant action of *N*-acetylcysteine: its reaction with hydrogen peroxide, hydroxyl radical, superoxide, and hypochlorous acid. Free Radical Biology & Medicine. 6(6):593-7.

Assuncao Guimaraes C. Linden R. (2004) Programmed cell deaths. Apoptosis and alternative deathstyles. European Journal of Biochemistry. 271(9):1638-50.

Aykin-Burns N. Franklin EA. Ercal N. (2005) Effects of *N*-acetylcysteine on lead-exposed PC-12 cells. Archives of Environmental Contamination & Toxicology. 49(1):119-23.

Baldassarri AM, Zetti G, Masson S, Gatti S, Albani AP, Ferla G, Boicelli AC. (1995) Magnetic resonance (MR) imaging and MR spectroscopy of nerve regeneration and target muscle energy metabolism in a model of prosthesis-guided reinnervation in rats. Acad Radiol. 2(2):128-34.

Baldi C. Bettinelli S. Grossi P. Fausto A. Sardanelli F. Cavalloro F. Allegri M. Braschi A. (2007) Ultrasound guidance for locoregional anesthesia: a review. Minerva Anestesiologica. 73(11):587-93.

Barazany D. Basser PJ. Assaf Y. (2009) In vivo measurement of axon diameter distribution in the corpus callosum of rat brain. Brain. 132(Pt 5):1210-20,

Barker PA. (2004) p75NTR is positively promiscuous: Novel partners and new insights. Neuron. 42:529-33.

Beal MF. (2000) Energetics in the pathogenesis of neurodegenerative diseases. Trends in Neurosciences. 23(7):298-304.

Behr B. Schnabel R. Mirastschijski U. Ibrahim B. Angenstein F. Schneider W. (2009) Magnetic resonance imaging monitoring of peripheral nerve regeneration following neurotmesis at 4.7 Tesla. Plastic & Reconstructive Surgery. 123(6):1778-88.

Belen D. Aciduman A. Er U. (2009) History of peripheral nerve repair: may the procedure have been practiced in Hippocratic School? Surgical Neurology 72(2):190-193.

Bendszus M. Koltzenburg M. (2001) Visualization of denervated muscle by gadolinium-enhanced MRI. Neurology. 57(9):1709-11.

Bendszus M. Koltzenburg M. (2002) Footdrop after peroneal nerve lesion.] Journal of Neurology, Neurosurgery & Psychiatry. 72(1):42.

Bendszus M. Koltzenburg M. Wessig C. Solymosi L.(2002) Sequential MR imaging of denervated muscle: experimental study. American Journal of Neuroradiology. 23(8):1427-31.

Bendszus M. Stoll G. (2003) Caught in the act: in vivo mapping of macrophage infiltration in nerve injury by magnetic resonance imaging. Journal of Neuroscience. 23(34):10892-6.

Bendszus M. Wessig C. Reiners K. Bartsch AJ. Solymosi L. Koltzenberg M. (2003) MR imaging in the differential diagnosis of neurogenic foot drop. American Journal of Neuroradiology. 24(7):1283-9.

Bendszus M. Wessig C. Schutz A. Horn T. Kleinschnitz C. Sommer C. Misselwitz B. Stoll G. (2005) Assessment of nerve degeneration by gadofluorine M-enhanced magnetic resonance imaging. Annals of Neurology. 57(3):388-95.

Bendszus M. Wessig C. Solymosi L. Reiners K. Koltzenburg M. (2004) MRI of peripheral nerve degeneration and regeneration: correlation with electrophysiology and histology. Experimental Neurology. 188(1):171-7.

Benn SC. Woolf CJ. (2004) Adult neuron survival strategies--slamming on the brakes. Nature Reviews Neuroscience. 5(9):686-700.

Bergman E. Fundin BT. Ulfhake B. (1999) Effects of aging and axotomy on the expression of neurotrophin receptors in primary sensory neurons. Journal of Comparative Neurology. 410(3):368-86.

Bergman E. Ulfhake B. (1998) Loss of primary sensory neurons in the very old rat: neuron number estimates using the dissector method and confocal optical sectioning. Journal of Comparative Neurology. 396(2):211-22.

Berman D. Rodin BE. (1982) The influence of housing condition on autotomy following dorsal rhizotomy in rats. Pain. 13(3):307-11.

Bilgen M. Heddings A. Al-Hafez B. Hasan W. McIff T. Toby B. Nudo R. Brooks WM. (2005) Microneurography of human median nerve. Journal of Magnetic Resonance Imaging. 21(6):826-30.

Blesch A. Tuszynski MH. (2004) Nucleus hears axon's pain. Nature Medicine. 10(3):236-7.

Blumenkopf B. Lipman JJ. (1991) Studies in autotomy: its pathophysiology and usefulness as a model of chronic pain. Pain. 45(2):203-9.

Bobinski M. de Leon MJ. Wegiel J. Desanti S. Convit A. Saint Louis LA. Rusinek H. Wisniewski HM. (2000) The histological validation of post mortem magnetic resonance imaging-determined hippocampal volume in Alzheimer's disease. Neuroscience. 95(3):721-5.

Borner C. (1996) Diminished cell proliferation associated with the death-protective activity of Bcl-2. Journal of Biological Chemistry. 271(22):12695-8.

Bothwell M. (1991) Keeping track of neurotrophin receptors. Cell. 65(6):915-8.

Bredesen DE. Rabizadeh S. (1997) p75NTR and apoptosis: Trk-dependent and Trk-independent effects. Trends in Neurosciences. 20(7):287-90.

Bremer J. (1990) The role of carnitine in intracellular metabolism. Journal of Clinical Chemistry & Clinical Biochemistry. 28(5):297-301.

Bremer J. (1990) The role of carnitine in intracellular metabolism. J Clin Chen Clin Biochem. 28(5):297-301

British National Formulary (BNF©) 60th Ed. (2010) British Medical Association and Royal Pharmaceutical Society of Great Britain.

Britz GW. Haynor DR. Kuntz C. Goodkin R. Gitter A. Kliot M. (1995) Carpal tunnel syndrome: correlation of magnetic resonance imaging, clinical, electrodiagnostic, and intraoperative findings. Neurosurgery. 37(6):1097-103.

Britz GW. Haynor DR. Kuntz C. Goodkin R. Gitter A. Maravilla K. Kliot M. (1996) Ulnar nerve entrapment at the elbow: correlation of magnetic resonance imaging, clinical, electrodiagnostic, and intraoperative findings. Neurosurgery. 38(3):458-65.

Brorson JR. Schumacker PT. Zhang H. (1999) Nitric oxide acutely inhibits neuronal energy production. The Committees on Neurobiology and Cell Physiology. Journal of Neuroscience. 19(1):147-58.

Brown GC. Borutaite V. (2001) Nitric oxide, mitochondria, and cell death. IUBMB Life. 52(3-5):189-95.

Burdett NG. Carpenter TA. Hall LD. (1993) A simple device for respiratory gating for the MRI of laboratory animals. Magnetic Resonance Imaging. 11(6):897-901.

Caddick J. Kingham PJ. Gardiner NJ. Wiberg M. Terenghi G. (2006) Phenotypic and functional characteristics of mesenchymal stem cells differentiated along a Schwann cell lineage. GLIA. 54(8):840-9.

Cafferty WB. Gardiner NJ. Gavazzi I. Powell J. McMahon SB. Heath JK. Munson J. Cohen J. Thompson SW. (2001) Leukemia inhibitory factor determines the growth status of injured adult sensory neurons. Journal of Neuroscience. 21(18):7161-70.

Calabrese EJ. (2008) Enhancing and regulating neurite outgrowth. Critical Reviews in Toxicology. 38(4):391-418.

Calabrese V. Giuffrida Stella AM. Calvani M. Butterfield DA. (2006) Acetylcarnitine and cellular stress response: roles in nutritional redox homeostasis and regulation of longevity genes. Journal of Nutritional Biochemistry. 17(2):73-88.

Cande C. Cohen I. Daugas E. Ravagnan L. Larochette N. Zamzami N. Kroemer G. (2002) Apoptosis-inducing factor (AIF): a novel caspase-independent death effector released from mitochondria. Biochimie. 84(2-3):215-22.

Carlstedt T. (2000) Approaches permitting and enhancing motoneuron regeneration after spinal cord, ventral root, plexus and peripheral nerve injuries. Current Opinion in Neurology. 13(6):683-6.

Cartwright MS. Chloros GD. Walker FO. Wiesler ER. Campbell WW. (2007) Diagnostic ultrasound for nerve transection. Muscle & Nerve. 35(6):796-9.

Castillo M. Mukherji SK. (1996) MRI of enlarged dorsal ganglia, lumbar nerve roots, and cranial nerves in polyradiculoneuropathies. Neuroradiology. 38(6):516-20.

Chan YM. Yick LW. Yip HK. So KF. Oppenheim RW. Wu W. (2003) Inhibition of caspases promotes long-term survival and reinnervation by axotomized spinal motoneurons of denervated muscle in newborn rats. Experimental Neurology. 181(2):190-203.

Chapman JR. (2004) Compliance: the patient, the doctor, and the medication? Transplantation. 77(5):782-6.

Cheema SS. Barrett GL. Bartlett PF. (1996) Reducing p75 nerve growth factor receptor levels using antisense oligonucleotides prevents the loss of axotomized sensory neurons in the dorsal root ganglia of newborn rats. Journal of Neuroscience Research. 46(2):239-45.

Cheema SS. Richards L. Murphy M. Bartlet PF. (1994a) Leukaemia inhibitory factor prevents the death of axotomised sensor nearons in the dorsal root ganglia of the neonatal rat. Journal of Neuroscience Research. 37:213-218

Cheema SS. Richards L. Murphy M. Bartlet PF. (1994b) Leukaemia inhibitory factor rescues motoneurons from axotomy-induced cell death. Neuroreport. 5:989-992.

Chierzi S. Ratto GM. Verma P. Fawcett JW. (2005) The ability of axons to regenerate their growth cones depends on axonal type and age, and is regulated by calcium, cAMP and ERK. European Journal of Neuroscience. 21(8):2051-62.

Ciancio G. Pollack A. Taupier MA. Block NL. Irvin GL 3rd. (1988) Measurement of cell-cycle phase-specific cell death using Hoechst 33342 and propidium iodide: preservation by ethanol fixation. Journal of Histochemistry & Cytochemistry. 36(9):1147-52.

Clavijo-Alvarez JA. Nguyen VT. Santiago LY. Doctor JS. Lee WP. Marra KG. (2007) Comparison of biodegradable conduits within aged rat sciatic nerve defects. Plastic & Reconstructive Surgery. 119(6):1839-51.

Cluzel M. Bousquet J. Daures JP. Renon D. Clauzel AM. Godard PH. Michel FB. (1990) Ambulatory long-term subcutaneous salbutamol infusion in chronic severe asthma. Journal of Allergy & Clinical Immunology. 85(3):599-606.

Coderre TJ. Grimes RW. Melzack R. (1986) Deafferentation and chronic pain in animals: an evaluation of evidence suggesting autotomy is related to pain. Pain. 26(1):61-84.

Cokluk C. Aydin K. (2007) Ultrasound examination in the surgical treatment for upper extremity peripheral nerve injuries: part I. Turkish Neurosurgery. 17(4):277-82.

Corcoran GB. Wong BK. (1986) Role of glutathione in prevention of acetaminopheN-induced hepatotoxicity by *N-a*cetyl-L-cysteine in vivo: studies with *N-a*cetyl-D-cysteine in mice. Journal of Pharmacology & Experimental Therapeutics. 238(1):54-61.

Cotgreave IA. (1997) *N*-acetylcysteine: pharmacological considerations and experimental and clinical applications. Advances in Pharmacology. 38:205-27.

Cotgreave IA. Berggren M. Jones TW. Dawson J. Moldeus P. (1987) Gastrointestinal metabolism of *N*-acetylcysteine in the rat, including an assay for sulfite in biological systems. Biopharmaceutics & Drug Disposition. 8(4):377-86.

Coulson EJ. Reid K. Murray SS. Cheema SS. Bartlett PF. (2000) Role of neurotrophin receptor p75NTR in mediating neuronal cell death following injury. Clinical & Experimental Pharmacology & Physiology. 27(7):537-41.

Cregan SP. MacLaurin JG. Craig CG. Robertson GS. Nicholson DW. Park DS. Slack RS. (1999) Bax-dependent caspase-3 activation is a key determinant in p53-induced apoptosis in neurons. Journal of Neuroscience. 19(18):7860-9.

Csernansky JG. Hamstra J. Wang L. McKeel D. Price JL. Gado M. Morris JC. (2004) Correlations between antemortem hippocampal volume and postmortem neuropathology in AD subjects. Alzheimer Disease & Associated Disorders. 18(4):190-5.

Cudlip SA. Howe FA. Griffiths JR. Bell BA. (2002) Magnetic resonance neurography of peripheral nerve following experimental crush injury, and correlation with functional deficit. Journal of Neurosurgery. 96(4):755-9.

Culver D. (2003) The Shameful Wrong That Must Be Righted. New York Times, Oct. 10, Pg A13

Curtis R. Scherer SS. Somogyi R. Adryan KM. Ip NY. Zhu Y. Lindsay RM. DiStefano PS. (1994) Retrograde axonal transport of LIF is increased by peripheral nerve injury: correlation with increased LIF expression in distal nerve. Neuron. 12(1):191-204.

Curtis R. Tonra JR. Stark JL. Adryan KM. Park JS. Cliffer KD. Lindsay RM. DiStefano PS. (1998) Neuronal injury increases retrograde axonal transport of the neurotrophins to spinal sensory neurons and motor neurons via multiple receptor mechanisms. Molecular & Cellular Neurosciences. 12(3):105-18.

Dagum AB. Peripheral nerve regeneration, repair, and grafting. (1998) Journal of Hand Therapy. 11(2):111-7.

Dailey AT. Tsuruda JS. Filler AG. Maravilla KR. Goodkin R. Kliot M. (1997) Magnetic resonance neurography of peripheral nerve degeneration and regeneration. Lancet. 350(9086):1221-2.

Damadian R. (1971) Tumor detection by nuclear magnetic resonance. Science. 171(976):1151-3.

Davies AM. (1995) The Bcl-2 family of proteins, and the regulation of neuronal survival. Trends in Neurosciences. 18(8):355-8.

De Felipe C. Hunt SP. (1994) The differential control of c-jun expression in regenerating sensory neurons and their associated glial cells. Journal of Neuroscience. 14(5 Pt 1):2911-23.

De Koning P. Brakkee JH. Gispen WH. (1986) Methods for producing a reproducible crush in the sciatic and tibial nerve of the rat and rapid and precise testing of return of sensory function. Beneficial effects of melanocortins. Journal of the Neurological Sciences. 74(2-3):237-46.

de Kool BS. van Neck JW. Blok JH. Walbeehm ET. Hekking I. Visser GH. (2005) Ultrasound imaging of the rabbit peroneal nerve. Journal of the Peripheral Nervous System. 10(4):369-74.

De Medinaceli L. Freed WJ. Wyatt RJ. (1982) An index of the functional condition of rat sciatic nerve based on measurements made from walking tracks. Experimental Neurology. 77(3):634-43.

De Mendinaceli L, Seaber AV. (1989) Experimental nerve reconnection: importance of initial repair. Microsurgery. 10(1): 56-70

Deckwerth TL. Easton RM. Knudson CM. Korsmeyer SJ. Johnson EM Jr. (1998) Placement of the BCL2 family member BAX in the death pathway of sympathetic neurons activated by trophic factor deprivation. Experimental Neurology. 152(1):150-62.

DeFelipe j. Jones EG. (1991) Cajal's Degeneration & Regeneration of the Nervous System. Oxford University Press, London.

Degn J. Tandrup T. Jakobsen J. (1999) Effect of nerve crush on perikaryal number and volume of neurons in adult rat dorsal root ganglion. J Comp Neurol. 412(1):186-92.

Devor M. Schonfeld D. Seltzer S. Wall PD. (1979) Two Modes of Cutaneous Reinnervation following Peripheral Nerve Injury. Journal of Comparitive Neurology 185: 211-220.

Dhitavat S. Ortiz D. Shea TB. Rivera ER. (2002) Acetyl-L-carnitine protects against amyloid-beta neurotoxicity: roles of oxidative buffering and ATP levels. Neurochemical Research. 27(6):501-5.

Does MD. Snyder RE. (1996) Multiexponential T2 relaxation in degenerating peripheral nerve. Magnetic Resonance in Medicine. 35(2):207-13.

Dorph-Petersen KA. (1999) Stereological estimation using vertical sections in a complex tissue. Journal of Microscopy. 195(Pt 1):79-86.

DuraN-Jimenez B. Dobler D. Moffatt S. Rabbani N. Streuli CH. Thornalley PJ. Tomlinson DR. Gardiner NJ. (2009) Advanced glycation endproducts in

extracellular matrix proteins contribute to the failure of sensory nerve regeneration in diabetes. Diabetes 58(1);12: 2893-2903.

Edstrom A. Ekstrom PA. (2003) Role of phosphatidylinositol 3-kinase in neuronal survival and axonal outgrowth of adult mouse dorsal root ganglia explants. Journal of Neuroscience Research. 74(5):726-35.

Ehman RL. Felmlee JP. (1989) Adaptive technique for high-definition MR imaging of moving structures. Radiology. 173(1):255-63.

Eisenberg HA. Hood DA. (1994) Blood flow, mitochondria, and performance in skeletal muscle after denervation and reinnervation. Journal of Applied Physiology. 76(2):859-66.

Ekström PA. (1995) Neurones and glial cells of the mouse sciatic nerve undergo apoptosis after injury in vivo and in vitro. Neuroreport. 6(7):1029-32.

ElShamy WM, Fridvall LK, Ernfors P. (1998) Growth arrest failure, G1 restriction point override, and S phase death of sensory precursor cells in the absence of neurotrophiN-3. Neuron; 21: 1003-1015.

Elster AD. (1994) Questions and Answers in Magnetic Resonance Imaging. Mosby-Year Book, Missouri.

Engelhorn T. Eyupoglu IY. Schwarz MA. Karolczak M. Bruenner H. Struffert T. Kalender W. Doerfler A. (2009) In vivo micro-CT imaging of rat brain glioma: a comparison with 3T MRI and histology. Neuroscience Letters. 458(1):28-31.

Estevez AG. Spear N. Manuel SM. Radi R. Henderson CE. Barbeito L. Beckman JS. (1998) Nitric oxide and superoxide contribute to motor neuron apoptosis induced by trophic factor deprivation. Journal of Neuroscience. 18(3):923-31.

Estus S. Zaks WJ. Freeman RS. Gruda M. Bravo R. Johnson EM Jr. (1994) Altered gene expression in neurons during programmed cell death: identification of c-jun as necessary for neuronal apoptosis. Journal of Cell Biology. 127(6 Pt 1):1717-27.

Farooki S. Ashman CJ. Yu JS. Abduljalil A. Chakeres D. (2002) In vivo high-resolution MR imaging of the carpal tunnel at 8.0 tesla. Skeletal Radiology. 31(8):445-50.

Fernandez E. Pallini R. Gangitano C. Del Fa A. Sangiacomo CO. Sbriccoli A. Ricoy JR. Rossi GF. (1989) Effects of L-carnitine, L-acetylcarnitine and gangliosides on the regeneration of the transected sciatic nerve in rats. Neurological Research. 11(1):57-62.

Ferrari G. Yan CY. Greene LA. (1995) *N*-acetylcysteine (D- and L-stereoisomers) prevents apoptotic death of neuronal cells. Journal of Neuroscience. 15(4):2857-66.

Ferrari G. Yan CY. Greene LA. (1995) *N*-acetylcysteine (D- and L-stereoisomers) prevents apoptotic death of neuronal cells. Journal of Neuroscience. 15(4):2857-66.

Filler AG. Howe FA. Hayes CE. Kliot M. Winn HR. Bell BA. Griffiths JR. Tsuruda JS. (1993) Magnetic resonance neurography. Lancet. 341(8846):659-61.

Fiskum G. (2004) Mechanisms of neuronal death and neuroprotection. Journal of Neurosurgical Anesthesiology. 16(1):108-10.

Fleckenstein JL. Watumull D. Conner KE. Ezaki M. Greenlee RG Jr. Bryan WW. Chason DP. Parkey RW. Peshock RM. Purdy PD. (1993) Denervated human skeletal muscle: MR imaging evaluation. Radiology. 187(1):213-8.

Forloni G. Angeretti N. Smiroldo S. (1994) Neuroprotective activity of acetyl-L-carnitine: studies in vitro. Journal of Neuroscience Research. 37(1):92-6.

Friedlander RM. Gagliardini V. Rotello RJ. Yuan J. (1996) Functional role of interleukin 1 beta (IL-1 beta) in IL-1 beta-converting enzyme-mediated apoptosis. Journal of Experimental Medicine. 184(2):717-24.

Fu SY. Gordon T. (1997) The cellular and molecular basis of peripheral nerve regeneration. Molecular Neurobiology. 14(1-2):67-116.

Gadeberg P. Gundersen HJ. Tagehoj F. (1999) How accurate are measurements on MRI? A study on multiple sclerosis using reliable 3D stereological methods. Journal of Magnetic Resonance Imaging. 10(1):72-9.

Gagliardini V. Fernandez PA. Lee RK. Drexler HC. Rotello RJ. Fishman MC. Yuan J. (1994) Prevention of vertebrate neuronal death by the crmA gene. Science. 263(5148):826-8. [erratum appears in Science 1994;264(5164):1388].

Ganong WF. (1997) Cutaneous, Deep & Visceral Sensation. In Review of Medical Physiology 18th Ed. Appleton & Lange. Connecticut

Gardiner NJ. Fernyhough P. Tomlinson DR. Mayer U. von der Mark H. Streuli CH. (2005) Alpha7 integrin mediates neurite outgrowth of distinct populations of adult sensory neurons. Molecular & Cellular Neurosciences. 28(2):229-40.

George EB. Glass JD. Griffin JW. (1995) Axotomy-induced axonal degeneration is mediated by calcium influx through ioN-specific channels. Journal of Neuroscience. 15(10):6445-52.

Gillardon F. Klimaschewski L. Wickert H. Krajewski S. Reed JC. Zimmermann M. (1996) Expression pattern of candidate cell death effector proteins Bax, Bcl-2, Bcl-X, and c-Jun in sensory and motor neurons following sciatic nerve transection in the rat. Brain Research. 739(1-2):244-50.

Gillen C. Jander S. Stoll G. (1998) Sequential expression of mRNA for proinflammatory cytokines and interleukiN-10 in the rat peripheral nervous system: comparison between immune-mediated demyelination and Wallerian degeneration. Journal of Neuroscience Research. 51(4):489-96.

Glickman LT. Mackinnon SE. (1990) Sensory recovery following digital replantation. Microsurgery. 11(3):236-42.

Golz G. Uhlmann L. Ludecke D. Markgraf N. Nitsch R. Hendrix S. (2006) The cytokine/neurotrophin axis in peripheral axon outgrowth. European Journal of Neuroscience. 24(10):2721-30.

Goold RG. GordoN-Weeks PR. (2005) The MAP kinase pathway is upstream of the activation of GSK3beta that enables it to phosphorylate MAP1B and contributes to the stimulation of axon growth. Molecular & Cellular Neurosciences. 28(3):524-34.

Gordon T. Sulaiman O. Boyd JG. (2003) Experimental strategies to promote functional recovery after peripheral nerve injuries. Journal of the Peripheral Nervous System. 8(4):236-50.

GordoN-Weeks PR. (2004) Microtubules and growth cone function. Journal of Neurobiology. 58(1):70-83.

GordoN-Weeks PR. (2004) Microtubules and growth cone function. Journal of Neurobiology. 58(1):70-83.

Gotoh T. Mori M. (2006) Nitric oxide and endoplasmic reticulum stress. Arteriosclerosis, Thrombosis & Vascular Biology. 26(7):1439-46.

Grant GA. Britz GW. Goodkin R. Jarvik JG. Maravilla K. Kliot M. (2002) The utility of magnetic resonance imaging in evaluating peripheral nerve disorders. Muscle & Nerve. 25(3):314-31.

Grant GA. Goodkin R. Kliot M. (1999) Evaluation and surgical management of peripheral nerve problems. Neurosurgery. 44(4):825-39.

Green B. (1998) Repair and grafting of the peripheral nerve. In: Green, ed. Plastic Surgery. 630-695.

Greene LA. Kaplan DR. (1995) Early events in neurotrophin signalling via Trk and p75 receptors. Current Opinion in Neurobiology. 5(5):579-87.

Groves MJ. Christopherson T. Giometto B. Scaravilli F. (1997) Axotomy-induced apoptosis in adult rat primary sensory neurons. Journal of Neurocytology. 26(9):615-24.

Gruber H. Glodny B. Bendix N. Tzankov A. Peer S. (2007) High-resolution ultrasound of peripheral neurogenic tumors. European Radiology. 17(11):2880-8.

Gudziol V. Buschhuter D. Abolmaali N. Gerber J. Rombaux P. Hummel T. (2009) Increasing olfactory bulb volume due to treatment of chronic rhinosinusitis--a longitudinal study. Brain. 132(Pt 11):3096-101.

Gundersen HJ. Bagger P. Bendtsen TF. Evans SM. Korbo L. Marcussen N. Moller A. Nielsen K. Nyengaard JR. Pakkenberg B. *et al.,* (1988a) The new stereological tools: disector, fractionator, nucleator and point sampled intercepts and their use in pathological research and diagnosis. Acta Pathologica, Microbiologica et Immunologica Scandinavica. 96(10):857-81.

Gundersen HJ. Bendtsen TF. Korbo L. Marcussen N. Moller A. Nielsen K. Nyengaard JR. Pakkenberg B. Sorensen FB. Vesterby A. *et al.*, (1998b) Some new, simple and efficient stereological methods and their use in pathological research and diagnosis. Acta Pathologica, Microbiologica et Immunologica Scandinavica. 96(5):379-94.

Gundersen HJ. Jensen EB. (1987) The efficiency of systematic sampling in stereology and its prediction. Journal of Microscopy. 147(Pt 3):229-63.

Hadzic A. Sala-Blanch X. Xu D. (2008) Ultrasound guidance may reduce but not eliminate complications of peripheral nerve blocks. Anesthesiology. 108(4):557-8.

Hagen TM. Liu J. Lykkesfeldt J. Wehr CM. Ingersoll RT. Vinarsky V. Bartholomew JC. Ames BN. (2002) Feeding acetyl-L-carnitine and lipoic acid to old rats significantly improves metabolic function while decreasing oxidative stress. Proceedings of the National Academy of Sciences of the United States of America. 99(4):1870-5.

Ham J. Babij C. Whitfield J. Pfarr CM. Lallemand D. Yaniv M. Rubin LL. (1995) A c-Jun dominant negative mutant protects sympathetic neurons against programmed cell death. Neuron. Vol. 14(5);927-939.

Hamanishi C. Tanaka S. (1993) Dorsal root ganglia in the lumbosacral region observed from the axial views of MRI. Spine. 18(13):1753-6.

Hamburger V. (1997) Wilhelm Roux: visionary with a blind spot. Journal of the history of biology. 30 (2): 229–38

Hamburger V. (1997) Wilhelm Roux: Visionary with a Blind Spot. Journal of the History of Biology 30: 229–238.

Han D. Sen CK. Roy S. Kobayashi MS. Tritschler HJ. Packer L. (1997) Protection against glutamate-induced cytotoxicity in C6 glial cells by thiol antioxidants. American Journal of Physiology. 273(5 Pt 2):R1771-8.

Hanz S. Perlson E. Willis D. Zheng JQ. Massarwa R. Huerta JJ. Koltzenburg M. Kohler M. vaN-Minnen J. Twiss JL. Fainzilber M. (2003) Axoplasmic importins enable retrograde injury signalling in lesioned nerve. Neuron. 40(6):1095-104.

Harding AJ. Halliday GM. Cullen K. (1994) Practical considerations for the use of the optical disector in estimating neuronal number. Journal of Neuroscience Methods. 51(1):83-9.

Harisson RG. (1907) Observations on living developing nerve fibers. Proc. Soc. Exp. Riol. Med. 4: 140-143.

Hart AM. Terenghi G. (2004b) FrozeN-section fluorescence microscopy and stereology in the quantification of neuronal death within dorsal root ganglia. Journal of Molecular Histology. 35(6):565-80.

Hart AM. Terenghi G. Kellerth JO. Wiberg M. (2004a) Sensory neuroprotection, mitochondrial preservation, and therapeutic potential of *N*-acetylcysteine after nerve injury. Neuroscience. 125(1):91-101,

Hart AM. Terenghi G. Wiberg M. (2008) Neuronal death after peripheral nerve injury and experimental strategies for neuroprotection. Neurol Res. 30(10):999-1011.

Hart AM. Wiberg M. Youle M. Terenghi G. (2002) Systemic acetyl-L-carnitine eliminates sensory neuronal loss after peripheral axotomy: a new clinical approach in the management of peripheral nerve trauma. Experimental Brain Research. 145(2):182-9.

Hart AM. Wilson AD. Montovani C. Smith C. Johnson M. Terenghi G. Youle M. (2004c) Acetyl-l-carnitine: a pathogenesis based treatment for HIV-associated antiretroviral toxic neuropathy. AIDS. 18(11):1549-60.

Hasegawa T. Mikawa Y. Watanabe R. An HS. (1996) Morphometric analysis of the lumbosacral nerve roots and dorsal root ganglia by magnetic resonance imaging. Spine. 21(9):1005-9.

Hayashi Y. Ikata T. Takai H. Takata S. Ishikawa M. Sogabe T. Koga K. (1997)Effect of peripheral nerve injury on nuclear magnetic resonance relaxation times of rat skeletal muscle. Investigative Radiology. 32(3):135-9.

He JW. Hirata K. Kuraoka A. Kawabuchi M. (2000) An improved method for avulsion of lumbar nerve roots as an experimental model of nitric oxide-mediated neuronal degeneration. Brain Research. Brain Research Protocols. 5(3):223-30.

Heales SJ. Bolanos JP. Stewart VC. Brookes PS. Land JM. Clark JB. (1999) Nitric oxide, mitochondria and neurological disease. Biochimica et Biophysica Acta. 1410(2):215-28.

Hedreen JC. (1998) What was wrong with the Abercrombie and empirical cell counting methods? A review. Anatomical Record. 250(3):373-80.

Herz RCG, Jonker M, Verheul HB, Hillen B, Versteeg DHG, de Wildt DJ. (1996) Middle Cerebral Artery Occlusion in Wistar and Fischer-344 Rats: Functional and Morphological Assessment of the Model. Journal of Cerebral Blood Flow & Metabolism. 16:296–302.

Hill CE. Burnstock G. (1975) Amphibian sympathetic ganglia in tissue culture. Cell & Tissue Research. 162(2):209-33.

Himes BT. Tessler A. (1989) Death of some dorsal root ganglion neurons and plasticity of others following sciatic nerve section in adult and neonatal rats. Journal of Comparative Neurology. 284(2):215-30.

Hoang NT. (2006) Hand replantations following complete amputations at the wrist joint: first experiences in Hanoi, Vietnam. Journal of Hand Surgery - British Volume. 31(1):9-17.

Hornfelt M. Edstrom A. Ekstrom PA. (1999) Upregulation of cytosolic phospholipase A2 correlates with apoptosis in mouse superior cervical and dorsal root ganglia neurons. Neuroscience Letters. 265(2):87-90.

Howard MJ. David G. Barrett JN. (1999) Resealing of transected myelinated mammalian axons in vivo: evidence for involvement of calpain. Neuroscience. 93(2):807-15.

Howe FA. Filler AG. Bell BA. Griffiths JR. (1992) Magnetic resonance neurography. Magnetic Resonance in Medicine. 28(2):328-38.

Hsiao YH. Chen PS. Yeh SH. Lin CH. Gean PW. (2008) *N*-acetylcysteine prevents beta-amyloid toxicity by a stimulatory effect on p35/cycliN-dependent kinase 5 activity in cultured cortical neurons. J.Neurosci.Res. 86:2685-2695.

Hu P. McLachlan EM. (2003) Selective Reactions of Cutaneous and Muscle Afferent Neurons to Peripheral Nerve Transection in Rats. Journal of Neuroscience. 23(33):10559-10567.

International Commission on Non-Ionizing Radiation Protection. (2004) ICNIRP statement related to the use of security and similar devices utilizing electromagnetic fields. Health Physics. 87(2):187-96.

Ishii T. Shimpo Y. Matsuoka Y. Kinoshita K. (2000) Anti-apoptotic effect of acetyl-l-carnitine and I-carnitine in primary cultured neurons. Japanese Journal of Pharmacology. 83(2):119-24.

Iyer RB. Fenstermacher MJ. Libshitz HI. (1996) MR imaging of the treated brachial plexus. AJR. American Journal of Roentgenology. 167(1):225-9.

Jacobs RE. Ahrens ET. Dickinson ME. Laidlaw D. (1999) Towards a microMRI atlas of mouse development. Computerized Medical Imaging & Graphics. 23(1):15-24.

Jacobs RE. Cherry SR. (2001) Complementary emerging techniques: high-resolution PET and MRI. Current Opinion in Neurobiology. 11(5):621-9.

Jacobs WB. Fehlings MG. (2003) The molecular basis of neural regeneration. Neurosurgery. 53(4):943-48.

Jahnke K. Muldoon LL. Varallyay CG. Lewin SJ. Brown RD. Kraemer DF. Soussain C. Neuwelt EA. (2009) Efficacy and MRI of rituximab and methotrexate treatment in a nude rat model of CNS lymphoma. Neuro-Oncology. 11(5):503-13.

Jander S. Lausberg F. Stoll G. (2001) Differential recruitment of CD8+ macrophages during Wallerian degeneration in the peripheral and central nervous system. Brain Pathology. 11(1):27-38.

Jander S. Pohl J. Gillen C. Stoll G. (1996) Differential expression of interleukiN-10 mRNA in Wallerian degeneration and immune-mediated inflammation of the rat peripheral nervous system. Journal of Neuroscience Research. 43(2):254-9.

Jaquet JB. Luijsterburg AJ. Kalmijn S. Kuypers PD. Hofman A. Hovius SE. (2001) Median, ulnar, and combined mediaN-ulnar nerve injuries: functional outcome and

return to productivity. Journal of Trauma-Injury Infection & Critical Care. 51(4):687-92.

Jenkins R. McMahon SB. Bond AB. Hunt SP. (1993) Expression of c-Jun as a response to dorsal root and peripheral nerve section in damaged and adjacent intact primary sensory neurons in the rat. European Journal of Neuroscience. 5(6):751-9.

Jerosch-Herold C. (2005) Assessment of sensibility after nerve injury and repair: a systematic review of evidence for validity, reliability and responsiveness of tests. Journal of Hand Surgery - British Volume. 30(3):252-64.

Jeulin C. Lewin LM. (1996) Role of free L-carnitine and acetyl-L-carnitine in post-gonadal maturation of mammalian spermatozoa. Human Reproduction Update. 2(2):87-102.

Johnson G. Wadghiri YZ. Turnbull DH. (1999) 2D multislice and 3D MRI sequences are often equally sensitive. Magnetic Resonance in Medicine. 41(4):824-8.

Jonas D. Conrad B. Von Einsiedel HG. Bischoff C. (2000) Correlation between quantitative EMG and muscle MRI in patients with axonal neuropathy. Muscle & Nerve. 23(8):1265-9.

Kadah YM. Abaza AA. Fahmy AS. Youssef AB. Heberlein K. Hu XP. (2004) Floating navigator echo (FNAV) for iN-plane 2D translational motion estimation. Magnetic Resonance in Medicine. 51(2):403-7.

Kamata H. Tanaka C. Yagisawa H. Matsuda S. Gotoh Y. Nishida E. Hirata H. (1996) Suppression of nerve growth factor-induced neuronal differentiation of PC12 cells. *N*-acetylcysteine uncouples the signal transduction from ras to the mitoge*N*-*a*ctivated protein kinase cascade. Journal of Biological Chemistry. 271(51):33018-25.

Kanaya F. Firrell JC. Breidenbach WC. (1996) Sciatic function index, nerve conduction tests, muscle contraction, and axon morphometry as indicators of regeneration. Plastic & Reconstructive Surgery. 98(7):1264-71.

Kaplan DR. Miller FD. (1997) Signal transduction by the neurotrophin receptors. Current Opinion in Cell Biology. 9(2):213-21.

Kaplan DR. Miller FD. (2000) Neurotrophin signal transduction in the nervous system. Current Opinion in Neurobiology. 10(3):381-91.

Kaplan DR. Stephens RM. (1994) Neurotrophin signal transduction by the Trk receptor. Journal of Neurobiology. 25(11):1404-17.

Kaplan DR. Miller FD. (1997) Signal transduction by the neurotrophin receptors. Current Opinion in Cell Biology. 9(2):213-21.

Kaplan DR. Miller FD. (2000) Neurotrophin signal transduction in the nervous system. Current Opinion in Neurobiology. 10(3):381-91.

Kauppila T. Correlation between autotomy-behavior and current theories of neuropathic pain. (198) Neuroscience & Biobehavioral Reviews. 23(1):111-29.

Keller JN. Kindy MS. Holtsberg FW. St Clair DK. Yen HC. Germeyer A. Steiner SM. Bruce-Keller AJ. Hutchins JB. Mattson MP. (1998) Mitochondrial manganese superoxide dismutase prevents neural apoptosis and reduces ischemic brain injury: suppression of peroxynitrite production, lipid peroxidation, and mitochondrial dysfunction. Journal of Neuroscience. 18(2):687-97.

Kelly EJ. Terenghi G. Hazari A. Wiberg M. (2005) Nerve fibre and sensory end organ density in the epidermis and papillary dermis of the human hand. British Journal of Plastic Surgery. 58(6):774-9.

Kenney AM. Kocsis JD. (1998) Peripheral axotomy induces long-term c-Jun amino-terminal kinase-1 activation and activator proteiN-1 binding activity by c-Jun and junD in adult rat dorsal root ganglia In vivo. Journal of Neuroscience. 18(4):1318-28.

Khachi G. Skirgaudes M. Lee WP. Wollstein R. (2007) The clinical applications of peripheral nerve imaging in the upper extremity. Journal of Hand Surgery - American Volume. 32(10):1600-4.

Kikkawa I. Sugimoto H. Saita K. Ookami H. Nakama S. Hoshino Y. (2001) The role of Gd-enhanced three-dimensional MRI fast low-angle shot (FLASH) in the evaluation of symptomatic lumbosacral nerve roots. Journal of Orthopaedic Science. 6(2):101-9.

Kikuchi Y. Nakamura T. Takayama S. Horiuchi Y. Toyama Y. (2003) MR imaging in the diagnosis of denervated and reinnervated skeletal muscles: experimental study in rats. Radiology. 229(3):861-7.

Kingham PJ. Kalbermatten DF. Mahay D. Armstrong SJ. Wiberg M. Terenghi G. (2007) Adipose-derived stem cells differentiate into a Schwann cell phenotype and promote neurite outgrowth in vitro. Experimental Neurology. 207(2):267-74.

Kirkland RA. Franklin JL. (2001) Evidence for redox regulation of cytochrome C release during programmed neuronal death: antioxidant effects of protein synthesis and caspase inhibition. Journal of Neuroscience. 21(6):1949-63.

Kline DG. (2000) Nerve surgery as it is now and as it may be. Neurosurgery. 46(6):1285-93.

Knight B. (1991) Forensic Pathology 2nd Ed. Oxford University Press.

Kobayashi J. Mackinnon SE. Watanabe O. Ball DJ. Gu XM. Hunter DA. Kuzon WM Jr. (1997) The effect of duration of muscle denervation on functional recovery in the rat model. Muscle & Nerve. 20(7):858-66.

Koliatsos VE. Price WL. Pardo CA. Price DL. (1994) Ventral root avulsion: an experimental model of death of adult motor neurons. Journal of Comparative Neurology. 342(1):35-44. [Erratum appears in J Comp Neurol 1994;344(1):160].

Koltzenburg M. Bendszus M. (2004) Imaging of peripheral nerve lesions. Current Opinion in Neurology. 17(5):621-6.

Kostelic JK. Haughton VM. Sether LA. (1991) Lumbar spinal nerves in the neural foramen: MR appearance. Radiology. 178(3):837-9.

Kouroku Y. Urase K. Fujita E. Isahara K. Ohsawa Y. Uchiyama Y. Momoi MY. Momoi T. (1998) Detection of activated Caspase-3 by a cleavage site-directed antiserum during naturally occurring DRG neurons apoptosis. Biochemical & Biophysical Research Communications. 247(3):780-4.

Krajewski S. Krajewska M. Ellerby LM. Welsh K. Xie Z. Deveraux QL. Salvesen GS. Bredesen DE. Rosenthal RE. Fiskum G. Reed JC. (1999) Release of caspase-9 from

mitochondria during neuronal apoptosis and cerebral ischemia. Proceedings of the National Academy of Sciences of the United States of America. 96(10):5752-7.

Kroemer G. (2003) Mitochondrial control of apoptosis: an introduction. Biochemical & Biophysical Research Communications. 304(3):433-5.

Kury P. Stoll G. Muller HW. (2001) Molecular mechanisms of cellular interactions in peripheral nerve regeneration. Current Opinion in Neurology. 14(5):635-9.

Larsson C. (2006) Protein kinase C and the regulation of the actin cytoskeleton. Cellular Signalling. 18(3):276-84.

Lawen A. (2003) Apoptosis-an introduction. Bioessays. 25(9):888-96.

Lazar DA. Ellegala DB. Avellino AM. Dailey AT. Andrus K. Kliot M. (1999) Modulation of macrophage and microglial responses to axonal injury in the peripheral and central nervous systems. Neurosurgery. 45(3):593-600.

Lee D. van Holsbeeck MT. Janevski PK. Ganos DL. Ditmars DM. Darian VB. (1999) Diagnosis of carpal tunnel syndrome. Ultrasound versus electromyography. Radiologic Clinics of North America. 37(4):859-72.

Lee M. Doolabh VB. Mackinnon SE. Jost S.FK (2000) 506 promotes functional recovery in crushed rat sciatic nerve. Muscle & Nerve. 23(4):633-40.

Levi-Montalcini R. (1998) The saga of the nerve growth factor. Neuroreport. 9(16):R71-83.

LewiN-Kowalik J. Marcol W. Larysz-Brysz M. Wolwender K. Pietrucha-Dutczak M. Gorka D. (2002) Pre-degenerated peripheral nerve extracts applied to the proximal stump of transected sciatic nerve enhance both regeneration and autotomic behavior in rats. Medical Science Monitor. 8(10):BR414-20.

Li H. Zhu H. Xu CJ. Yuan J. (1998) Cleavage of BID by caspase 8 mediates the mitochondrial damage in the Fas pathway of apoptosis. Cell. 94(4):491-501.

Li L. Oppenheim RW. Lei M. Houenou LJ. (1994) Neurotrophic agents prevent motoneuron death following sciatic nerve section in the neonatal mouse. Journal of Neurobiology. 25(7):759-66.

Li LY. Luo X. Wang X. (2001) Endonuclease G is an apoptotic DNase when released from mitochondria. Nature. 412(6842):95-9.

Lindholm D. Heumann R. Meyer M. Thoenen H. InterleukiN-1 regulates synthesis of nerve growth factor in non-neuronal cells of rat sciatic nerve. Nature. 330(6149):658-9, 1987 Dec 17-23.

Lindsay RM. (1988) Nerve growth factors (NGF, BDNF) enhance axonal regeneration but are not required for survival of adult sensory neurons. Journal of Neuroscience. 8(7):2394-2405.

Lindsay RM. (1996) Role of neurotrophins and trk receptors in the development and maintenance of sensory neurons: an overview. Philosophical Transactions of the Royal Society of London - Series B: Biological Sciences. 351(1338):365-73.

Liss AG. af Ekenstam FW. Wiberg M. (1994) Cell loss in sensory ganglia after peripheral nerve injury. An anatomical tracer study using lectiN-coupled horseradish peroxidase in cats. Scandinavian Journal of Plastic & Reconstructive Surgery & Hand Surgery. 28(3):177-88.

Liss AG. af Ekenstam FW. Wiberg M. (1996) Loss of neurons in the dorsal root ganglia after transection of a peripheral sensory nerve. An anatomical study in monkeys. Scandinavian Journal of Plastic & Reconstructive Surgery & Hand Surgery. 30(1):1-6.

Liu HM. Yang LH. Yang YJ. (1995) Schwann cell properties: 3. C-fos expression, bFGF production, phagocytosis and proliferation during Wallerian degeneration. Journal of Neuropathology & Experimental Neurology. 54(4):487-96.

Ljungberg C. Novikov L. Kellerth JO. Ebendal T. Wiberg M (1999) The neurotrophins NGF and NT-3 reduce sensory neuronal loss in adult rat after peripheral nerve lesion. Neurosci Lett. 26;262(1):29-32.

Lundborg G. (2000) A 25-year perspective of peripheral nerve surgery: evolving neuroscientific concepts and clinical significance. J Hand Surg. 25A: 391-414.

Lundborg G. Richard P. (2003) Bunge memorial lecture. Nerve injury and repair-a challenge to the plastic brain. Journal of the Peripheral Nervous System. 8(4):209-26.

Lundborg G. Rosen B. (2004) The two-point discrimination test--time for a re-appraisal. Journal of Hand Surgery - British Volume. 29(5):418-22.

Ma J. Novikov LN. Wiberg M. Kellerth JO. (2001) Delayed loss of spinal motoneurons after peripheral nerve injury in adult rats: a quantitative morphological study. Experimental Brain Research. 139(2):216-23.

Mahadevan SB. McKiernan PJ. Davies P. Kelly DA. (2006) Paracetamol induced hepatotoxicity. Archives of Disease in Childhood. 91(7):598-603.

Mahay D. Terenghi G. Shawcross SG. (2008) Schwann cell mediated trophic effects by differentiated mesenchymal stem cells. Experimental Cell Research. 314(14):2692-701.

Majdan M. Walsh GS. Aloyz R. Miller FD. (2001) TrkA mediates developmental sympathetic neuron survival in vivo by silencing an ongoing p75NTR-mediated death signal. Journal of Cell Biology. 155(7):1275-85.

Manfridi A. Forloni GL. Arrigoni-Martelli E. Mancia M. (1992) Culture of dorsal root ganglion neurons from aged rats: effects of acetyl-L-carnitine and NGF. International Journal of Developmental Neuroscience. 10(4):321-9.

Mant TG. Tempowski JH. Volans GN. Talbot JC. (1984) Adverse reactions to acetylcysteine and effects of overdose. British Medical Journal Clinical Research Ed. 289(6439):217-9.

Marion A. Aoudi W. Basarab A. Delachartre P. Vray D. (2010) Blood flow evaluation in high-frequency, 40 MHz imaging: a comparative study of four vector velocity estimation methods. Ultrasonics. 50(7):683-90.

Martin LJ. Kaiser A. Price AC. (1999) Motor neuron degeneration after sciatic nerve avulsion in adult rat evolves with oxidative stress and is apoptosis. Journal of Neurobiology. 40(2):185-201.

Marziali S. Gaudiello F. Bozzao A. Scire G. Ferone E. Colangelo V. Simonetti A. Boscherini B. Floris R. Simonetti G. (2004) Evaluation of anterior pituitary gland volume in childhood using three-dimensional MRI. Pediatric Radiology. 34(7):547-51.

Maser E. (2006) Neuroprotective role for carbonyl reductase?. Biochemical & Biophysical Research Communications. 340(4):1019-22.

Matsuda K. Wang HX. Suo C. McCombe D. Horne MK. Morrison WA. Egan GF. (2010) Retrograde axonal tracing using manganese enhanced magnetic resonance imaging. Neuroimage. 50(2):366-74.

Mattsson P. Meijer B. Svensson M. (1999) Extensive neuronal cell death following intracranial transection of the facial nerve in the adult rat. Brain Research Bulletin. 49(5):333-41.

Mayer M. Noble M. (1994) *N-a*cetyl-L-cysteine is a pluripotent protector against cell death and enhancer of trophic factor-mediated cell survival in vitro. Proceedings of the National Academy of Sciences of the United States of America. 91(16):7496-500.

Mazzoni IE. Said FA. Aloyz R. Miller FD. Kaplan D. (1999) Ras regulates sympathetic neuron survival by suppressing the p53-mediated cell death pathway. Journal of Neuroscience. 19(22):9716-27.

McDaniel B. Sheng H. Warner DS. Hedlund LW. Benveniste H. (2001) Tracking brain volume changes in C57BL/6J and ApoE-deficient mice in a model of neurodegeneration: a 5-week longitudinal micro-MRI study. Neuroimage. 14(6):1244-55.

McKay Hart A. Brannstrom T. Wiberg M. Terenghi G. (2002a) Primary sensory neurons and satellite cells after peripheral axotomy in the adult rat: timecourse of cell death and elimination. Experimental Brain Research. 142(3):308-18.

McKay Hart A. Wiberg M. Terenghi G. (2002b) Pharmacological enhancement of peripheral nerve regeneration in the rat by systemic acetyl-L-carnitine treatment. Neuroscience Letters. 334(3):181-5.

McKay Hart A. Wiberg M. Terenghi G. (2003) Exogenous leukaemia inhibitory factor enhances nerve regeneration after late secondary repair using a bioartificial nerve conduit. British Journal of Plastic Surgery. 56(5):444-50.

McVean A. Autotomy. (1975) Comparative Biochemistry & Physiology A-Comparative Physiology. 51(3):497-505.

Meyer M. Schreck R., Baeuerle PA. (1993) H2O2 and antioxidants have opposite effects on activation of NF-B and AP-1 in intact cells: AP-1 as secondary antioxidant-responsive factor. EMBO J 12:2005-2015.

Middleton G. Nunez G. Davies AM. (1996) Bax promotes neuronal survival and antagonises the survival effects of neurotrophic factors. Development. 122(2):695-701.

Mikko P. Laakso, Maarit Lehtovirta, Kaarina Partanen, Paavo J. RiekkinenSr., Hilkka Soininen. (2000) Hippocampus in Alzheimer's disease: a 3-year follow-up MRI study. Biological Psychiatry, 47(6): 557-561.

Miller FD Kaplan DR. (2001b) On Trk for retrograde signaling. euron. 32(5):767-70.

Miller FD. Kaplan DR. (2001a) Neurotrophin signalling pathways regulating neuronal apoptosis. Cellular & Molecular Life Sciences. 58(8):1045-53.

Miller FD. Kaplan DR. (2003) Signaling mechanisms underlying dendrite formation. Current Opinion in Neurobiology. 13(3):391-8.

Miller FD. Kaplan DR. (2007) o die or not to die: neurons and p63. Cell Cycle. 6(3):312-7.

Moats RA. VelaN-Mullan S. Jacobs R. Gonzalez-Gomez I. Dubowitz DJ. Taga T. Khankaldyyan V. Schultz L. Fraser S. Nelson MD. Laug WE. (2003) Micro-MRI at 11.7 T of a murine brain tumor model using delayed contrast enhancement. Molecular Imaging: Official Journal of the Society for Molecular Imaging. 2(3):150-8.

Mohamad N. Gutierrez A. Nunez M. Cocca C. Martin G. Cricco G. Medina V. Rivera E. Bergoc R. Mitochondrial apoptotic pathways. Biocell. 29(2):149-61.

Mohanna PN. Terenghi G. Wiberg M. (2005) Composite PHB-GGF conduit for long nerve gap repair: a long-term evaluation. Scandinavian Journal of Plastic & Reconstructive Surgery & Hand Surgery. 39(3):129-37.

Mohanna PN. Young RC. Wiberg M. Terenghi G. (2003) A composite poly-hydroxybutyrate-glial growth factor conduit for long nerve gap repairs. Journal of Anatomy. 203(6):553-65.

Morwood J. Taylor J. Eds. (2002) The Pocket Oxford Classical Greek Dictionary. Oxford.

Müller HW. Ignatius MJ. Hangen DH. Shooter EM. (1986) Expression of specific sheath cell proteins during peripheral nerve growth and regeneration in mammals. Journal of Cell Biology. 102(2):393-402.

Müller HW. Stoll G. (1998) Nerve injury and regeneration: basic insights and therapeutic interventions. Current Opinion in Neurology. 11(5):557-62.

Mulleman D. Mammou S. Griffoul I. Watier H. Goupille P. (2006) Pathophysiology of disk-related sciatica. I.--Evidence supporting a chemical component. Joint, Bone, Spine: Revue du Rhumatisme. 73(2):151-8.

Murphy M. Dutton R. Koblar S. Cheema S. Bartlett P. (1997) Cytokines which signal through the LIF receptor and their actions in the nervous system. Progress in Neurobiology. 52(5):355-78.

Murray MR. (1965) Nervous tissue in vitro. In: Cells and Tissues in Culture. E.N. Willmer, Ed. Academic Press, New York.

Murray RM. Stout AP. (1947) Adult human sympathetic ganglion cells cultivated in vitro. American Journal Of Anatomy. 80:225-273.

Nagata S. (2000) Apoptotic DNA fragmentation. Experimental Cell Research. 256(1):12-8.

Nagel S. Wagner S. Koziol J. Kluge B. Heiland S. (2004) Volumetric evaluation of the ischemic lesion size with serial MRI in a transient MCAO model of the rat: comparison of DWI and T1WI. Brain Research. Brain Research Protocols. 12(3):172-9.

Natt O. Watanabe T. Boretius S. Radulovic J. Frahm J. Michaelis T. (2002) High-resolution 3D MRI of mouse brain reveals small cerebral structures in vivo. Journal of Neuroscience Methods. 120(2):203-9.

Nemanic S. Alvarado MC. Price RE. Jackson EF. Bachevalier J. (2002) Assessment of locus and extent of neurotoxic lesions in monkeys using neuroimaging techniques: a replication. Journal of Neuroscience Methods. 121(2):199-209.

Nicholls DG. Budd SL. (2000) Mitochondria and neuronal survival. Physiological Reviews. 80(1):315-60.

Nobes CD. Tolkovsky AM. (1995) Neutralizing anti-p21ras Fabs suppress rat sympathetic neuron survival induced by NGF, LIF, CNTF and cAMP. Eur J Neurosci 7:344-350.

Norris DG. (2001) Implications of bulk motion for diffusioN-weighted imaging experiments: effects, mechanisms, and solutions. Journal of Magnetic Resonance Imaging. 13(4):486-95.

Novikov L. Novikova L. Kellerth JO. (1995) BraiN-derived neurotrophic factor promotes survival and blocks nitric oxide synthase expression in adult rat spinal motoneurons after ventral root avulsion. Neuroscience Letters. 200(1):45-8.

Novikov L. Novikova L. Kellerth JO. (1997) BraiN-derived neurotrophic factor promotes axonal regeneration and long-term survival of adult rat spinal motoneurons in vivo. Neuroscience. 79(3):765-74.

Nunez G. Del Peso L. (1998) Linking extracellular survival signals and the apoptotic machinery. Current Opinion in Neurobiology. Vol. 8(5):613-618.

Olausson H. Lamarre Y. Backlund H. Morin C. Wallin BG. Starck G. Ekholm S. Strigo I. Worsley K. Vallbo AB. Bushnell MC. (2002) Unmyelinated tactile afferents signal touch and project to insular cortex. Nature Neuroscience. 5(9):900-4.

O'Loghlen A. Perez-Morgado MI. Salinas M. Martin ME. (2006) *N*-acetylcysteine abolishes hydrogen peroxide-induced modification of eukaryotic initiation factor 4F activity via distinct signalling pathways. Cellular Signalling. 18(1):21-31.

Osechinskiy S. Kruggel F. (2009) Quantitative comparison of high-resolution MRI and myeliN-stained histology of the human cerebral cortex. Conference Proceedings: Annual International Conference of the IEEE Engineering in Medicine & Biology Society. 2009:85-9.

Park DS. Stefanis L. Yan CY. Farinelli SE. Greene LA. (1996) Ordering the cell death pathway. Differential effects of BCL2, an interleukiN-1-converting enzyme family protease inhibitor, and other survival agents on JNK activation in serum/nerve growth factor-deprived PC12 cells. Journal of Biological Chemistry. 271(36):21898-905.

Park DS. Stefanis L. Yan CYI. Farinelli SE. Greene LA. (1996) Ordering the cell death pathway. Differential effects of BCL2: an interleukiN-1-converting enzyme family protease inhibitor, and other survival agents on JNK activation in serum/nerve growth factor-deprived PC12 cells. J Biol Chem 271:21898-21905.

Perlson E. Hanz S. Medzihradszky KF. Burlingame AL. Fainzilber M. (2004) From snails to sciatic nerve: Retrograde injury signaling from axon to soma in lesioned neurons. Journal of Neurobiology. 58(2):287-94.

Pitts EV. Potluri S. Hess DM. Balice-Gordon RJ. (2006) Neurotrophin and Trk-mediated signalling in the neuromuscular system. International Anesthesiology Clinics. 44(2):21-76.

Polster BM. Fiskum G. (2004) Mitochondrial mechanisms of neural cell apoptosis. Journal of Neurochemistry. 90(6):1281-9.

Pover CM. Coggeshall RE. (1991) Verification of the disector method for counting neurons, with comments on the empirical method. Anatomical Record. 231(4):573-8.

Power C. Fanning N. Redmond HP. (2002) Cellular apoptosis and organ injury in sepsis: a review. Shock. 18(3):197-211.

Prabhu SS. Broaddus WC. Oveissi C. Berr SS. Gillies GT. (2000) Determination of intracranial tumor volumes in a rodent brain using magnetic resonance imaging, Evans blue, and histology: a comparative study. IEEE Transactions on Biomedical Engineering. 47(2):259-65.

Prescott LF. Donovan JW. Jarvie DR. Proudfoot AT. (1989) The disposition and kinetics of intravenous *N*-acetylcysteine in patients with paracetamol overdosage. European Journal of Clinical Pharmacology. 37(5):501-6.

Prescott LF. Illingworth RN. Critchley JA. Stewart MJ. Adam RD. Proudfoot AT. (1979) Intravenous *N-a*cetylcystine: the treatment of choice for paracetamol poisoning. British Medical Journal. 2(6198):1097-100.

Prunell GF. Troy CM. (2004) Balancing neuronal death. Journal of Neuroscience Research. 78(1):1-6.

Putcha GV. Johnson EM Jr. (2004) Men are but worms: neuronal cell death in C elegans and vertebrates. Cell Death & Differentiation. 11(1):38-48.

Puthalakath H. Huang DC. O'Reilly LA. King SM. Strasser A. (1999) The proapoptotic activity of the Bcl-2 family member Bim is regulated by interaction with the dynein motor complex. Molecular Cell. 3(3):287-96.

Qiu J. Cai D. Filbin MT. (2000) Glial inhibition of nerve regeneration in the mature mammalian CNS. GLIA. 29(2):166-74.

Ranson SW. (1906) Retrograde degeneration in the spinal nerves. Journal of Comparitive Neurology. 16:265-293.

Ranson SW. (1909) Alteration in the spinal ganglion cells following neurotomy. Journal of Comparitive Neurology and Psychology. 19:125-153.

Raphael DT. McIntee D. Tsuruda JS. Colletti P. Tatevossian R. (2005) Frontal slab composite magnetic resonance neurography of the brachial plexus: implications for infraclavicular block approaches. Anesthesiology. 103(6):1218-24.

Rasband WS. (1997-2009) ImageJ. US National Institutes of Health, Bethesda, Maryland, USA. http://rsb.info.nih.gov/ij/.

Ratan RR. Murphy TH. Baraban JM. (1994) Oxidative stress induces apoptosis in embryonic cortical neurons. Journal of Neurochemistry. 62(1):376-9.

Rebouche CJ. (2004) Kinetics, pharmacokinetics, and regulation of L-carnitine and acetyl-L-carnitine metabolism. Annals of the New York Academy of Sciences. 1033:30-41.

Reid AJ. Shawcross SG. Hamilton AE. Wiberg M. Terenghi G. (2009) *N*-acetylcysteine alters apoptotic gene expression in axotomised primary sensory afferent subpopulations. Neuroscience Research. 65(2):148-55.

Reynolds ML. Woolf CJ. (1993) Reciprocal Schwann cell-axon interactions. Current Opinion in Neurobiology. 3(5):683-93.

Riccardi C. Nicoletti I. (2006) Analysis of apoptosis by propidium iodide staining and flow cytometry. Nature Protocols. 1(3):1458-61.

Rich KM. Disch SP. Eichler ME. (1989) The influence of regeneration and nerve growth factor on the neuronal cell body reaction to injury. J Neurocytol. 18(5):569-76.

Rich KM. Luszczynski JR. Osborne PA. Johnson EM Jr. (1987) Nerve growth factor protects adult sensory neurons from cell death and atrophy caused by nerve injury. Journal of Neurocytology. 16(2):261-8.

Risling M. Aldskogius H. Hildebrand C. Remahl S. (1983) Effects of sciatic nerve resection on L7 spinal roots and dorsal root ganglia in adult cats. Experimental Neurology. 82(3):568-80.

Rosberg HE. Carlsson KS. Hojgard S. Lindgren B. Lundborg G. Dahlin LB. (2005) Injury to the human median and ulnar nerves in the forearm--analysis of costs for treatment and rehabilitation of 69 patients in southern Sweden. Journal of Hand Surgery - British Volume. 30(1):35-9.

Rosen B. Lundborg G. (1998) A new tactile gnosis instrument in sensibility testing. Journal of Hand Therapy. 11(4):251-7.

Rosenfeld J. Cook S. James R. (1997) Expression of superoxide dismutase following axotomy. Experimental Neurology. 147(1):37-47.

Sahly I. Khoutorsky A. Erez H. Prager-Khoutorsky M. Spira ME. (2006) ON-line confocal imaging of the events leading to structural dedifferentiation of an axonal segment into a growth cone after axotomy. Journal of Comparative Neurology. 494(5):705-20.

Sardesai AM. Patel R. Denny NM. Menon DK. Dixon AK. Herrick MJ. Harrop-Griffiths AW. (2006) Interscalene brachial plexus block: can the risk of entering the spinal

canal be reduced? A study of needle angles in volunteers undergoing magnetic resonance imaging. Anesthesiology. 105(1):9-13.

Sasaki K. (1995) Magnetic resonance imaging findings of the lumbar root pathway in patients over 50 years old. European Spine Journal. 4(2):71-6.

Sato J. Morimae H. Takanari K. Seino Y. Okada T. Suzuki M. Mizumura K. (2000) Effects of lowering ambient temperature on paiN-related behaviors in a rat model of neuropathic pain. Experimental Brain Research. 133(4):442-9.

Satpute RM. Hariharakrishnan J. Bhattacharya R. (2008) Alpha-ketoglutarate and *N-a*cetyl cysteine protect PC12 cells from cyanide-induced cytotoxicity and altered energy metabolism. Neurotoxicology. 29(1):170-8.

Schenker M. Burstedt MK. Wiberg M. (2006) Johansson RS. Precision grip function after hand replantation and digital nerve injury. Journal of Plastic, Reconstructive & Aesthetic Surgery: JPRAS. 59(7):706-16.

Schild HH. (1990) MRI made easy (...well Almost). Schering AG, Berlin.

Schmalbruch H. (1987a) Loss of sensory neurons after sciatic nerve section in the rat. Anatomical Record. 219(3):323-9.

Schmalbruch H. (1987b) The number of neurons in dorsal root ganglia L4-L6 of the rat. Anatomical Record. 219(3):315-22.

Schmidt H-M. Lanz U. (2004) Surgical Anatomy of the Hand. 1st Ed. Thieme, Stuttgart.

Schmitt AB. Breuer S. Liman J. Buss A. Schlangen C. Pech K. Hol EM. Brook GA. Noth J. Schwaiger FW. (2003) Identification of regeneratio*N-a*ssociated genes after central and peripheral nerve injury in the adult rat. BMC Neuroscience. 4:8.

Schoenwaelder SM. Burridge K. (1999) Bidirectional signaling between the cytoskeleton and integrins. Current Opinion in Cell Biology. 11(2):274-86.

Scott BS. (1971) Effect of potassium on neuron survival in cultures of dissociated human nervous tissue. Exp. Neurol. 30:297-308.

Scott BS. (1977) Adult Mouse Dorsal Root Ganglia Neurons in Cell Culture. Journal of Neurobiology. 8(5):417-427.

Scott BS. Engelbert VE. Gelbert VE. Fisherk C. (1969) Morphological and electrophysiological characteristics of dissociated chick embryonic spinal ganglion cells in culture. Exp. Neurol. 23:230-248.

Seaton TA. Cooper JM. Schapira AH. (1997) Free radical scavengers protect dopaminergic cell lines from apoptosis induced by complex I inhibitors. Brain Research. 777(1-2):110-8.

Seitz RJ. Reiners K. Himmelmann F. Heininger K. Hartung HP. Toyka KV. (1989) The blood-nerve barrier in Wallerian degeneration: a sequential long-term study. Muscle & Nerve. 12(8):627-35.

Sekharam M. Trotti A. Cunnick JM. Wu J. (1998) Suppression of fibroblast cell cycle progression in G1 phase by *N*-acetylcysteine. Toxicology & Applied Pharmacology. 149(2):210-6.

Shabas D. Gerard G. Rossi D. (1987) Magnetic resonance imaging examination of denervated muscle. Computerized Radiology. 11(1):9-13.

Shen J. Wang HY. Chen JY. Liang BL. (2006) Morphologic analysis of normal human lumbar dorsal root ganglion by 3D MR imaging. American Journal of Neuroradiology. 27(10):2098-103.

Shenaq JM. Shenaq SM. Spira M. (1989) Reliability of sciatic function index in assessing nerve regeneration across a 1 cm gap. Microsurgery. 10(3):214-9.

Shepherd AJ. Downing JE. Miyan JA. (2005) Without nerves, immunology remains incomplete -in vivo veritas. Immunology. 116(2):145-63.

Shimizu S. Matsuoka Y. Shinohara Y. Yoneda Y. Tsujimoto Y. (2001) Essential role of voltage-dependent anion channel in various forms of apoptosis in mammalian cells. Journal of Cell Biology. 152(2):237-50.

Shubayev V. I and Robert R. Myers. (2000) Upregulation and interaction of TNFa and gelatinases A and B in painful peripheral nerve injury. Brain Research 855: 83-89.

Silberstein SD. Brimijoin S. Molinoff PB. Lemberger L. (1972b) Induction of dopamine-hydroxylase in rat superior cervical ganglia in organ culture. Journal of Neurochemistry. 19(3):919-21.

Silberstein SD. Johnson DG. Hanbauer I. Bloom FE. Kopin IJ. (1972a) Axonal sprouts and (3H)norepinephrine uptake by superior cervical ganglia in organ culture. Proceedings of the National Academy of Sciences of the United States of America. 69(6):1450-5.

Singer P. Mehler S. (1986) Glucose and leucine uptake in the hypoglossal nucleus after hypoglossal nerve transaction with and without prevented regeneration in the Sprague-Dawley rat. Neuroscience Letters. 67(1):73-7.

Skene JH. (1989) Axonal growth-associated proteins. Annual Review of Neuroscience. 12:127-156

Smith JW. (1966) Microsurgery: review of the literature and discussion of micro-techniques. Plastic and Reconstructive Surgery. 37(3): 227-245.

Snider WD. Zhou FQ. Zhong J. Markus A. (2002) Signaling the pathway to regeneration. Neuron. 35(1):13-6.

Spira ME. Oren R. Dormann A. Gitler D. (2003) Critical calpaiN-dependent ultrastructural alterations underlie the transformation of an axonal segment into a growth cone after axotomy of cultured Aplysia neurons. Journal of Comparative Neurology. 457(3):293-312.

Sprawls P. (1988) Spatial characteristics of the MR image. In Magnetic Resonance Imaging. Stark DD & Bradley WG Ed. The CV Mosby Company, St. Louis

Stanisz GJ. Midha R. Munro CA. Henkelman RM. (2001) MR properties of rat sciatic nerve following trauma. Magnetic Resonance in Medicine. 45(3):415-20.

Staples B. Bravender T. (2002) Drug compliance in adolescents: assessing and managing modifiable risk factors. Paediatric Drugs. 4(8):503-13.

Stelow EB. Lai R. Bardales RH. Linzie BM. Mallery S. Stanley MW. (2004) Endoscopic ultrasound-guided fine-needle aspiration cytology of peripheral nerve-sheath tumors. Diagnostic Cytopathology. 30(3):172-7.

Stoll G. Griffin JW. Li CY. Trapp BD. (1989) Wallerian degeneration in the peripheral nervous system: participation of both Schwann cells and macrophages in myelin degradation. Journal of Neurocytology. 18(5):671-83.

Stoll G. Jander S. (1999) The role of microglia and macrophages in the pathophysiology of the CNS. Progress in Neurobiology. 58(3):233-47.

Stoll G. Jander S. Myers RR. (2002) Degeneration and regeneration of the peripheral nervous system: from Augustus Waller's observations to neuroinflammation. Journal of the Peripheral Nervous System. 7(1):13-27.

Stoll G. Trapp BD. Griffin JW. (1989) Macrophage function during Wallerian degeneration of rat optic nerve: clearance of degenerating myelin and Ia expression. Journal of Neuroscience. 9(7):2327-35.

Stoll G. Wesemeier C. Gold R. Solymosi L. Toyka KV. Bendszus M. (2004) In vivo monitoring of macrophage infiltration in experimental autoimmune neuritis by magnetic resonance imaging. Journal of Neuroimmunology. 149(1-2):142-6.

Strasser A. O'Connor L. Dixit VM. (2000) Apoptosis signaling. Annual Review of Biochemistry. 69:217-45.

Streppel M. Heiser T. Stennert E. (2000) Historical development of facial nerve surgery with special reference to hypoglossal-facial nerve anastomosis. HNO. 48:801–808.

Sulaiman OA. Gordon T. (2000) Effects of short- and long-term Schwann cell denervation on peripheral nerve regeneration, myelination, and size. GLIA. 32(3):234-46.

Sullivan JC. Wang B. Boesen EI. D'Angelo G. Pollock JS. Pollock DM. (2009) Novel use of ultrasound to examine regional blood flow in the mouse kidney. American Journal of Physiology - Renal Physiology. 297(1):F228-35

Sunderland S. (1951) A classification of peripheral nerve injuries producing loss of function. Brain. 74(4):491-516.

Sunderland SS. (1984) Nerve Repair (Editorial). American Journal of Hand Surgery. 9A: 1-3.

Sutter A. Riopelle RJ. Harris-Warrick RM. Shooter EM. (1979) Nerve growth factor receptors. Characterization of two distinct classes of binding sites on chick embryo sensory ganglia cells. J. Biol. Chem. 254: 5972-5982.

Suzuki H. Oyanagi K. Takahashi H. Kono M. Yokoyama M. Ikuta F. (1993) A quantitative pathological investigation of the cervical cord, roots and ganglia after long-term amputation of the unilateral upper arm. Acta Neuropathologica. 85(6):666-73. [Erratum appears in Acta Neuropathol 1993;86(5):546]

Suzuki R. Dickenson AH. (2000) Neuropathic pain: nerves bursting with excitement ... Neuroreport. 11(12):R17-21.

Swett JE. Torigoe Y. Elie VR. Bourassa CM. Miller PG. (1991) Sensory neurons of the rat sciatic nerve. Experimental Neurology. 114(1):82-103.

Taglialatela G. Angelucci L. Ramacci MT. Werrbach-Perez K. Jackson GR. Perez-Polo JR. (1991) Acetyl-L-carnitine enhances the response of PC12 cells to nerve growth factor. Brain Research. Developmental Brain Research. 59(2):221-30.

Tandrup T. (1993) A method for unbiased and efficient estimation of number and mean volume of specified neuron subtypes in rat dorsal root ganglion. Journal of Comparative Neurology. 329(2):269-76.

Tandrup T. (2004) Unbiased estimates of number and size of rat dorsal root ganglion cells in studies of structure and cell survival. Journal of Neurocytology. 33(2):173-92.

Tandrup T. Woolf CJ. Coggeshall RE. (2000) Delayed loss of small dorsal root ganglion cells after transection of the rat sciatic nerve. Journal of Comparative Neurology. 422(2):172-80.

Terenghi G, Calder JS, Birch R, Hall SM. (1998) A morphological study of Schwann cells and axonal regeneration in chronically transected human peripheral nerves. The Journal of Hand Surgery: Journal of the British Society for Surgery of the Hand. 23(5):583-587.

Terenghi G. (1999) Peripheral nerve regeneration and neurotrophic factors. J Anat. 194(Pt 1):1-14.

Terzis JK. Sun DD. Thanos PK. (1997) Historical and basic science review: Past, present and future of nerve repair, J. Reconstr. Microsurg. 13:215–225.

Tews DS. Goebel HH. Schneider I. Gunkel A. Stennert E. Neiss WF. (1997) DNA-fragmentation and expression of apoptosis-related proteins in experimentally denervated and reinnervated rat facial muscle. Neuropathology & Applied Neurobiology. 23(2):141-9.

Theiler K. (1989) The House Mouse: Atlas of Embryonic Development. NY: Springer-Verlag

The Nobel Assembly (2003) The Nobel Prize in Physiology or Medicine Press Release 6th October 2003. Available oN-line at: http://nobelprize.org/nobel_prizes/medicine/laureates/2003/press.html

Tofts PS. Silver NC. Barker GJ. Gass A. (2005) Object strength--an accurate measure for small objects that is insensitive to partial volume effects. Magma. 18(3):162-9.

Tonge DA. Aaronson OS. Golding JP. Jaggers D. (1996) Cellular migration and axonal outgrowth from adult mammalian peripheral nerves in vitro. Journal of Neurobiology. 29(2):151-64.

Tonge DA. Golding JP. Edbladh M. Kroon M. Ekstrom PE. Edstrom A. (1997) Effects of extracellular matrix components on axonal outgrowth from peripheral nerves of adult animals in vitro. Experimental Neurology. 146(1):81-90.

Tonra JR. Curtis R. Wong V. Cliffer KD. Park JS. Timmes A. Nguyen T. Lindsay RM. Acheson A. DiStefano PS. (1998) Axotomy upregulates the anterograde transport and expression of braiN-derived neurotrophic factor by sensory neurons. J Neurosci. 18(11):4374-83.

Torigoe K. Tanaka HF. Takahashi A. Awaya A. Hashimoto K. (1996) Basic behavior of migratory Schwann cells in peripheral nerve regeneration. Experimental Neurology. 137(2):301-8.

Ullmann JF. Cowin G. Kurniawan ND. Collin SP. (2010) A three-dimensional digital atlas of the zebrafish brain. Neuroimage. 51(1):76-82,

United States Patent and Trademark Office. (1974) United States Patent #3789832 Apparatus and Method for Detecting Cancer in Tissue. Available oN-line at http://patents.uspto.gov/

Van De Water TR. Lallemend F. Eshraghi AA. Ahsan S. He J. Guzman J. Polak M. Malgrange B. Lefebvre PP. Staecker H. Balkany TJ. (2004) Caspases, the enemy within, and their role in oxidative stress-induced apoptosis of inner ear sensory cells. Otology & Neurotology. 25(4):627-32.

Varejao AS. Meek MF. Ferreira AJ. Patricio JA. Cabrita AM. (2001) Functional evaluation of peripheral nerve regeneration in the rat: walking track analysis. Journal of Neuroscience Methods. 108(1):1-9.

Verhagen AM. Silke J. Ekert PG. Pakusch M. Kaufmann H. Connolly LM. Day CL. Tikoo A. Burke R. Wrobel C. Moritz RL. Simpson RJ. Vaux DL. (2002) HtrA2 promotes cell death through its serine protease activity and its ability to antagonize inhibitor of apoptosis proteins. Journal of Biological Chemistry. 277(1):445-54.

Vestergaard S. Tandrup T. Jakobsen J. (1997) Effect of permanent axotomy on number and volume of dorsal root ganglion cell bodies. Journal of Comparative Neurology. 388(2):307-12.

Virmani MA. Biselli R. Spadoni A. Rossi S. Corsico N. Calvani M. Fattorossi A. De Simone C. Arrigoni-Martelli E. (1995) Protective actions of L-carnitine and acetyl-L-carnitine on the neurotoxicity evoked by mitochondrial uncoupling or inhibitors. Pharmacological Research. 32(6):383-9.

Wang Y. Grimm RC. Felmlee JP. Riederer SJ. Ehman RL. (1996) Algorithms for extracting motion information from navigator echoes. Magnetic Resonance in Medicine. 36(1):117-23.

Weber AR. Proctor WH. Warner MR Verheyden CN. (1993) Autotomy and the Sciatic Functional Index. Microsurgery. 14:323-327.

Weber T. Vroemen M. Behr V. Neuberger T. Jakob P. Haase A. Schuierer G. Bogdahn U. Faber C. Weidner N. (2006) In vivo high-resolution MR imaging of neuropathologic changes in the injured rat spinal cord. American Journal of Neuroradiology. 27(3):598-604.

Welin D. Novikova LN. Wiberg M. Kellerth JO. Novikov LN. (2008) Survival and regeneration of cutaneous and muscular afferent neurons after peripheral nerve injury in adult rats. Exp Brain Res. 186(2):315-23.

Wessig C. Koltzenburg M. Reiners K. Solymosi L. Bendszus M. Muscle magnetic resonance imaging of denervation and reinnervation: correlation with electrophysiology and histology. Experimental Neurology. 185(2):254-61, 2004 Feb.

West CA. Davies KA. Hart AM. Wiberg M. Williams SR. Terenghi G. (2007b) Volumetric magnetic resonance imaging of dorsal root ganglia for the objective quantitative assessment of neuron death after peripheral nerve injury. Experimental Neurology - in press

West CA. Hart AM. Terenghi G. Wiberg M. (2007a) Analysis of the dose-response of *N*-acetylcysteine in the prevention of sensory neuronal loss after peripheral nerve injury. Acta Neurochirurgica - Supplement. 100:29-31.

West GA. Haynor DR. Goodkin R. Tsuruda JS. Bronstein AD. Kraft G. Winter T. Kliot M. (1994) Magnetic resonance imaging signal changes in denervated muscles after peripheral nerve injury. Neurosurgery. 35(6):1077-85.

West MJ. (1993) New stereological methods for counting neurons. Neurobiology of Aging. 14(4):275-85.

West MJ. (1999) Stereological methods for estimating the total number of neurons and synapses: issues of precision and bias. Trends in Neurosciences. 22(2):51-61.

Westbrook C. (2002) MRI at a Glance. Blackwell Science, Oxford.

Westling G. Johansson RS. (1984) Factors influencing the force control during precision grip. Experimental Brain Research. 53(2):277-84.

Wiberg M. Hazari A. Ljungberg C. Pettersson K. Backman C. Nordh E. Kwast-Rabben O. Terenghi G. (2003) Sensory recovery after hand reimplantation: a clinical, morphological, and neurophysiological study in humans. Scandinavian Journal of Plastic & Reconstructive Surgery & Hand Surgery. 37(3):163-73.

Wilson AD. Hart A. Wiberg M. Terenghi G. (2010) Acetyl-l-carnitine increases nerve regeneration and target organ reinnervation - a morphological study. J Plast Reconstr Aesthet Surg. 63(7):1186-95.

Wilson AD. Hart AM. Brannstrom T. Wiberg M. Terenghi G. (2003) Primary sensory neuronal rescue with systemic acetyl-L-carnitine following peripheral axotomy. A dose-response analysis. British Journal of Plastic Surgery. 56(8):732-9

Wilson AD. Hart AM. Brannstrom T. Wiberg M. Terenghi G. (2007) Delayed acetyl-L-carnitine administration and its effect on sensory neuronal rescue after peripheral nerve injury. Journal of Plastic, Reconstructive & Aesthetic Surgery. 60(2):114-8.

Wolf OT. Dyakin V. Vadasz C. de Leon MJ. McEwen BS. Bulloch K. (2002) Volumetric measurement of the hippocampus, the anterior cingulate cortex, and the retrosplenial granular cortex of the rat using structural MRI. Brain Research. Brain Research Protocols. 10(1):41-6.

Woolf CJ. (2003) No Nogo: now where to go? Neuron. 38(2):153-6.

Wullner U. Seyfried J. Groscurth P. Beinroth S. Winter S. Gleichmann M. Heneka M. Loschmann P. Schulz JB. Weller M. Klockgether T. (1999) Glutathione depletion and neuronal cell death: the role of reactive oxygen intermediates and mitochondrial function. Brain Research. 826(1):53-62.

Xia Z. Dickens M. Raingeaud J. Davis RJ. Greenberg ME. (1995) Opposing effects of ERK and JNK-p38 MAP kinases on apoptosis. Science 270:1326-1331.

Yakovlev AG. Knoblach SM. Fan L. Fox GB. Goodnight R. Faden AI. (1997) Activation of CPP32-like caspases contributes to neuronal apoptosis and neurological dysfunction after traumatic brain injury. Journal of Neuroscience. 17(19):7415-24.

Yan CY. Ferrari G. Greene LA. (1995) *N*-acetylcysteine-promoted survival of PC12 cells is glutathione-independent but transcriptioN-dependent. Journal of Biological Chemistry. 270(45):26827-32.

Yan CY. Greene LA. (1998) Prevention of PC12 cell death by *N*-acetylcysteine requires activation of the Ras pathway. Journal of Neuroscience. 18(11):4042-9.

Yeh ET. (1997) Life and death in the cardiovascular system. Circulation. 95(4):782-6.

Ygge J. (1989) Neuronal loss in lumbar dorsal root ganglia after proximal compared to distal sciatic nerve resection: a quantitative study in the rat. Brain Research. 478(1):193-5.

Yin Q. Kemp GJ. Frostick SP. (1998) Neurotrophins, neurones and peripheral nerve regeneration. Journal of Hand Surgery - British Volume. 23(4):433-7.

Yoneda A. Couchman JR. (2003) Regulation of cytoskeletal organization by syndecan transmembrane proteoglycans. Matrix Biology. 22(1):25-33.

Yoshimoto M. Kawaguchi S. Takebayashi T. Isogai S. Nonaka S. Kosukegawa I. Yamashita T. (2008) Morphological changes of the dorsal root ganglion in a patient with herpes zoster seen by magnetic resonance imaging. Journal of Orthopaedic Science. 13(4):383-6.

You S. Petrov T. Chung PH. Gordon T. (1997) The expression of the low affinity nerve growth factor receptor in long-term denervated Schwann cells. GLIA. 20(2):87-100.

Young RC. Wiberg M. Terenghi G. (2002) Poly-3-Hyrdoxybutrate (PHB): A resorbable conduit for long-gap repair in peripheral nerves. British Journal of Plastic Surgery. 55:235-240.

Zanelli SA. Solenski NJ. Rosenthal RE. Fiskum G. (2005) Mechanisms of ischemic neuroprotection by acetyl-L-carnitine. Annals of the New York Academy of Sciences. 1053:153-61.

Zarow C. Vinters HV. Ellis WG. Weiner MW. Mungas D. White L. Chui HC. (2005) Correlates of hippocampal neuron number in Alzheimer's disease and ischemic vascular dementia. Annals of Neurology. 57(6):896-903.

Zelena J. (1982) Survival of Pacinian corpuscles after denervation in adult rats. Cell & Tissue Research. 224(3):673-83.

Zha J. Harada H. Yang E. Jockel J. Korsmeyer SJ. (1996) Serine phosphorylation of death agonist BAD in response to survival factor results in binding to 14-3-3 not BCL-X(L). Cell. 87(4):619-28.

Zhang CG. Welin D. Novikov L. Kellerth JO. Wiberg M. Hart AM. (2005) Motorneuron protection by *N*-acetylcysteine after ventral root avulsion and ventral rhizotomy. British Journal of Plastic Surgery. 58(6):765-73.

Zimmermann M. Pathobiology of neuropathic pain. (2001) European Journal of Pharmacology. 429(1-3):23-37.

Zinkel S. Gross A. Yang E. (2006) BCL2 family in DNA damage and cell cycle control. Cell Death & Differentiation. 13(8):1351-9.

Zou H. Henzel WJ. Liu X. Lutschg A. Wang X. (1997) Apaf-1, a human protein homologous to C. elegans CED-4, participates in cytochrome c-dependent activation of caspase-3. Cell. 90(3):405-13